UNIVERSITY OF CALIFORNIA,
IRVINE

Modeling *SCN1A* Epilepsy with Dual Isogenic Pairs of Human iPSC-derived Neurons

DISSERTATION

submitted in partial satisfaction of the requirements
for the degree of

DOCTOR OF PHILOSOPHY

in Biological Sciences

by

Yunyao Xie

Dissertation Committee:
Professor Diane K. O'Dowd, Chair
Professor Edwin S. Monuki
Associate Professor Maksim V. Plikus
Assistant Professor Robert F. Hunt
Professor Xiangmin Xu

2019

DEDICATION

This dissertation is wholeheartedly dedicated to my thesis advisor, Dr. Diane O'Dowd for her great support and guidance in research and mentoring endeavors; my husband, Longwen Huang for his love and inspiration in neuroscience, and last but not least, my parents for their endless love and support.

TABLE OF CONTENTS

LIST OF FIGURES

LIST OF TABLES

ACKNOWLEDGMENTS

I would like to express the gratitude to my thesis advisor, Dr. Diane O'Dowd, who kindly provided me with great opportunities in my doctoral training. Her faith in me becoming a good scientist from the beginning was crucial to my personal and professional development. Her excitement in teaching and mentoring improved my understanding on the importance of passing down knowledge to the next generation of scientists. Without her guidance and persistent support this dissertation would not have been completed.

I would like to thank my committee members, Drs. Edwin Monuki, Maksim Plikus, Robert Hunt and Xiangmin Xu for their helpful advice on my thesis project and manuscript revision. Their guidance has been very important for my development as a scientist.

In addition, a thank you to all the current and past members in the O'Dowd lab, especially Nathan Ng for his hard work and dedication, Ryan Schutte for his patience and guidance in electrophysiology, and Olga Safrina and Dr. Martin Smith for their contribution to the project.

Thank you to my family and friends for their support, love and understanding throughout the journey. In particular, I would like to recognize my parents for their support, love and trust in me to let me chase my dream abroad, and my husband Longwen Huang for inspiring me with exciting neuroscience research and encouraging me when my electrophysiology rig broke down.

Finally, I would like to acknowledge my financial support provided by the National Institute of Health R01 grant NS083009 (O'Dowd) and Otto W. Shaler Scholarship.

CURRICULUM VITAE

Yunyao Xie

Education

2015 - 2019 **Doctor of Philosophy** in Biological Sciences
Department of Developmental and Cell Biology
University of California-Irvine, Irvine, CA
Thesis advisor: Diane K. O'Dowd, Ph.D.

2013 - 2015 **Master of Science** in Biotechnology with Stem Cell Emphasis
Department of Molecular Biology & Biochemistry
University of California-Irvine, Irvine, CA

2009 - 2013 **Bachelor of Science** in Biotechnology and Its Application
School of Life Sciences
Sun Yat-sen University, China

Research Experience

2014 - 2019 **Graduate student**
Department of Developmental and Cell Biology, UC Irvine, CA
Advisor: Diane K. O'Dowd, Ph.D.
- *Modeling SCN1A epilepsy in neurons derived from human isogenic iPSCs*

2012 - 2013 **Undergraduate researcher**
School of Biological Sciences, Sun Yat-sen University, China
Advisor: Zhumei He Ph.D.
- *Epigenetic regulation of gallic acid on aflatoxin synthesis*

Publications

1. **Xie Y,** Ng NN, Safrina OS, Ramos CM, Ess K, Schwartz PH, Smith MA, O'Dowd DK. Isogenic human iPSC pairs reveal a neuronal subtype-specific and genetic background-independent mechanism of *SCN1A* epilepsy. Under review.

2. Das A, **Xie Y**, Schutte SS, Neumann JC, MacGregor GR, Hunt RF, and O'Dowd DK. A CRISPR/Cas9 generated mouse model of *Scn1a* associated K1270T GEFS+ exhibits heat-induced seizures and reduced firing in GABAergic interneurons. In preparation.

3. Schutte RJ*, **Xie Y***, Ng NN*, Figueroa P, Pham AT, and O'Dowd DK. Generation of astrocyte enriched, neuron-free mouse feeder layers that support differentiation of functionally active networks of human iPSC-derived neurons. 2018. *J. Neurosci. Methods*. 294: 91-101.

4. **Xie Y***, Schutte RJ*, Ng NN*, Ess K, Schwartz PH, and O'Dowd DK. Reproducible and efficient generation of functionally active neurons from human iPSCs for preclinical disease modeling. 2018. *Stem Cell Res*. 26: 84-94.

5. Zhi Q, **Xie Y**, and He Z. Genome Mining for Aflatoxin Biosynthesis. *Fungal Genom Biol*, 2013, 3(1).

*** represents equal contributions**

Abstracts

1. **Xie Y**, Ng NN, Safrina OS, Ramos CM, Ess K, George AL Jr. Schwartz PH, O'Dowd DK. A CRISPR/Cas9-generated isogenic iPSC model reveals a neuronal subtype-specific mechanism of *SCN1A* epilepsy (2019). UCI Annual EpiCenter Symposium.

2. **Xie Y**, Ng NN, Safrina OS, Ramos CM, Ess K, George AL Jr. Schwartz PH, O'Dowd DK. A GEFS+*SCN1A* mutation causes cell type-specific and temperature-dependent defects in neurons derived from isogenic hiPSC pairs. Program No. 366.19. 2018 Neuroscience Meeting Planner. San Diego, CA: Society for Neuroscience, 2018. Online.

3. **Xie Y,** Ng NN, Safrina OS, Konopelski SE, Stover AE, Ess K, George AL Jr. Schwartz PH, O'Dowd DK. Cell type-specific defects in sodium channel functions in an isogenic human iPSC model of genetic epilepsy with febrile seizures plus. Program No. 203.09. 2017 Neuroscience Meeting Planner. Washington, DC: Society for Neuroscience, 2017. Online.

4. **Xie Y**, Ng NN, Safrina OS, Konopelski SE, Schutte RJ, Amoozadeh SA, Schutte SS, Stover AE, Ess K, George AL Jr., Smith MA, Schwartz PH, O'Dowd DK. Modeling *SCN1A*-associated epilepsy in human iPSC-derived neurons (2017). Translational Science Day, Institute of Clinical and Translational Science, UC Irvine.

5. **Xie Y**, Ng NN, Safrina OS, Konopelski SE, Schutte RJ, Amoozadeh SA, Schutte SS, Stover AE, Ess K, George AL Jr., Smith MA, Schwartz PH, O'Dowd DK. Modeling *SCN1A*-associated epilepsy in human iPSC-derived neurons. Program No. 582.09. 2016 Neuroscience Meeting Planner. San Diego, CA: Society for Neuroscience, 2016. Online.

6. **Xie Y**, Schutte RJ, Ng NN, Pham AT, Schutte SS, Banuelos MG, Stover AE, Ess K, George AL Jr., Smith MA, Schwartz PH, and O'Dowd DK. Functional differentiation of active neural networks from human iPSCs for neurological disease modeling (2016). UCI Annual EpiCenter Symposium.

7. **Xie Y**, Schutte RJ, Ng NN, Pham AT, Schutte SS, Banuelos MG, Stover AE, Ess K, George AL Jr., Smith MA, Schwartz PH, and O'Dowd DK. Functional differentiation of active neural networks from human iPSCs for neurological disease modeling. Program No. 665.25. 2015 Neuroscience Meeting Planner. Chicago, IL: Society for Neuroscience, 2015. Online.

Invited and Selected Talks

2019 Department of Developmental and Cell Biology, UC Irvine

2018 Annual EpiCenter Symposium, UC Irvine
2018 Department of Developmental and Cell Biology, UC Irvine
2016 Department of Anatomy and Neurobiology, UC Irvine
2016 Department of Neurobiology and Behavior, UC Irvine

Honors and Awards

2019 Otto W. Shaler Scholarship, UC Irvine
2018 Travel Award, Dept of Dev & Cell, UC Irvine
2018 Fine Science Tools Travel Award, School of Bio Sci, UC Irvine
2017 Invited for full proposal submission of Predoctoral Research Fellowship, American Epilepsy Society
2017 Travel Award, Dept of Dev & Cell, UC Irvine
2016 Travel Award, Dept of Dev & Cell, UC Irvine
2014 Graduate Fellowship, Dept of MB&B, UC Irvine
2013 Bachelor's degree with distinction
2012 National Scholarship, awarded by the Ministry of Education, China
2012 The First-class Scholarship, Sun Yat-sen University
2011 The First-class Scholarship, Sun Yat-sen University
2011 Techpool Bio-Pharma Co., Ltd Scholarship
2011 Li & Fung Scholarship, Victor and William Fung Foundation
2010 The First-class Scholarship, Sun Yat-sen University
2010 National Scholarship, awarded by the Ministry of Education, China

Teaching Experience

2018 Teaching assistant. Applied Human Anatomy (undergraduate course). UC Irvine
2017 Teaching assistant. Applied Human Anatomy (undergraduate course). UC Irvine
2015 Teaching assistant. Stem Cell Lab (graduate course). UC Irvine
2015 Teaching assistant. Molecular Biology (undergraduate course). UC Irvine
2015 Teaching assistant. Biochemistry (undergraduate course). UC Irvine
2015 Teaching assistant. Microbiology Lab (undergraduate course). UC Irvine

ABSTRACT OF THE DISSERTATION

Modeling *SCN1A* Epilepsy with Dual Isogenic Pairs of Human iPSC-derived Neurons

By

Yunyao Xie

Doctor of Philosophy in Biological Sciences

University of California, Irvine, 2019

Professor Diane O'Dowd, Chair

Over 1250 mutations in *SCN1A,* the Nav1.1 voltage-gated sodium channel gene, are associated with a variety of seizure disorders including Dravet syndrome (DS) and genetic epilepsy with febrile seizure plus (GEFS+). Individuals with *SCN1A* genetic epilepsy exhibit a broad range of seizure phenotypes and many of them are not well controlled by conventional anti-convulsant therapy. How specific mutations alter sodium channel function in a way that contributes to seizure generation is still largely unexplored. An understanding of cellular mechanisms is important for future studies targeted at developing more effective patient-specific therapies.

Previous studies in models including *Xenopus* oocytes, human embryonic kidney cells, mouse, *Drosophila* and zebrafish have provided some important insights into functional changes in sodium currents and firing properties associated with a number of *SCN1A* mutations. However, they also reveal that the same mutation can have distinct effects in the different models. By combining recent advances in stem cell reprogramming technology and gene editing tools it is now possible explore how specific gene mutations alter activity in human neurons. To evaluate changes in neuronal activity associated with a

specific mutation, independent of genetic background, we generated two pairs of isogenic human iPSC lines by CRISPR/Cas9 editing. One pair is a control line from an unaffected sibling, and the mutated control homozygous for the GEFS+ K1270T *SCN1A* mutation. The second pair is a GEFS+ patient line heterozygous for the K1270T mutation, and the corrected patient line.

To detect mutation-associated changes by comparing electrophysiological properties between cell lines, it is necessary to differentiate iPSC into neurons that could both fire action potentials and form synaptic connections. While there were a number of protocols for differentiation of iPSCs into neurons in the literature, there was a lot of variability in the time course and degree of differentiation even from plating to plating within one cell line. Starting with the published protocols we identified conditions that support robust reproducible differentiation from plating to plating and between iPSCs lines into cultures with GABAergic and glutamatergic neurons. The iPSC-derived neuronal cultures from both isogenic pairs of iPSCs that we generated contained a similar proportion of GABAergic and glutamatergic neurons. By comparing the electrophysiological properties in inhibitory and excitatory iPSC-derived neurons from these pairs, we found the K1270T mutation causes gene dosage-dependent and cell type-specific alterations in evoked firing and sodium currents that result in hyperactive neural networks. We also identified differences associated with genetic background and interaction between the mutation and genetic background. Dual isogenic iPSC-derived neuronal cultures provide an efficient strategy to evaluate the causality of a single gene mutation independent of genetic background and to develop patient-specific anti-seizure therapies.

Chapter I

Introduction

1.1. Introduction

Epilepsy is a common neurological disorder affecting 1.2% of the U.S. population that is characterized by recurrent seizures as a consequence of hyperexcitable and hypersynchronous neural networks[1–3]. The classifications of etiologies of epilepsies can be divided into four groups[4]. (1) Symptomatic: defined as epilepsies that are acquired through brain injury and diseases with structural abnormalities in brain; (2) Idiopathic: defined as epilepsies with genetic or presumed genetic causes and no neuroanatomical and pathological abnormalities. (3) Provoked: defined as epilepsies caused by specific systemic or environmental factors that are not associated with neuroanatomical and pathological abnormalities; (4) Cryptogenic: defined as epilepsies in presumed symptomatic nature with causes unidentified. The idiopathic generalized epilepsies are the most common epilepsies, accounting for 30% of seizure disorders[5,6]. 10% of genes identified in this broad group of epilepsies code for neurotransmitter receptors including NMDA, $GABA_A$ and nACh receptors, while 17% encode voltage-gated ion channels that are selectively permeable to each of the ions, sodium, potassium and calcium[7]. A myriad of mutations in voltage-gated sodium channels (Nav) that play an important role in electrical excitability confer genetic epilepsies. However, how specific mutations cause dysfunctional ion channels, disrupt neuronal activity and overall network activity, and give rise to seizures remains elusive.

In excitable cells, voltage-gated sodium channels are activated in response to membrane depolarization with sodium ions moving into cells to initiate action potential firing[8]. This is followed by inactivation that stops the flow of sodium ions and decrease the membrane potential to the rest state. Voltage-gated sodium channels have nine isoforms, each with distinct expression location and biophysical properties. Nav1.1, Nav1.2, Nav1.3

and Nav1.6 are the major isoforms expressed in the central nervous system[9]. Nav1.1 and Nav1.3 are located at the cell bodies of neurons, Nav1.2 in unmyelinated axons and dendrites, and Nav1.6 in myelinated axons and dendrites[10]. Due to the large number of mutations identified, Nav1.1 encoded by the *SCN1A* gene is the most common Nav in relevance to genetic epilepsy[11].

Similar to all other isoforms, Nav1.1 has two main components, a large α subunit and auxiliary β subunits[12] (**Figure I.1**). The α subunit are composed of four homologous domains (I-IV), each with six α-helical transmembrane segments (S1-S6)[13]. S1-S4 segments form the voltage-sensing domain and the S4 segment acts as a voltage sensor with positively charged residues residing in the transmembrane region that undergoes an outward movement upon depolarization of membrane potential[14,15]. S5 and S6 segments form the pore and the electronegative extracellular loop between S5 and S6 determines the sodium ion selectivity[14]. Conformational change of S4 is coupled to the movement of S4-S5 linker which pulls the S5 and S6 outward to open the pore, allowing sodium ions to move along the central pore[14]. The cytoplasmic loop between domain III and IV functions as the inactivation gate[16,17]. The β subunits are transmembrane segments and associated with the α subunit in a complementary manner with β1 or β3, and β2 or β4[18–20]. They play an important role in regulating the kinetics, voltage dependence of gating and cell adhesion of Nav[21,22].

Over 1200 mutations throughout the entire *SCN1A* gene are associated with a wide spectrum of epilepsies[23] (**Figure I.1**). 10% of *SCN1A* mutations are associated with genetic epilepsy with febrile seizure plus (GEFS+), while 85% accounts for Dravet syndrome (DS)[24,25]. GEFS+ is a mild form of epilepsy, characterized by febrile seizures in early

childhood that persist beyond 6 years of age[26]. DS patients have seizures at elevated body temperature in the first year of life and often progress to afebrile seizures and development of co-morbidities such as psychomotor delay, ataxia and cognitive impairment[27,28]. The heterogeneity of disease phenotypes not only arises from different mutations in the same gene, but also from the same mutation between individuals. There are multigenerational families in which individuals with the same *SCN1A* mutation exhibit a wide range of seizure phenotypes[29,30]. This complicates the understanding of the underlying cellular mechanisms of *SCN1A* epilepsy and the prescription of anti-epileptic drugs to epilepsy patients.

Several model systems have been used to map the links between individual *SCN1A* mutations and their functional consequences, facilitating the development of anti-epileptic therapeutics[31]. Heterologous expression systems including *Xenopus* oocytes, human embryonic kidney cells, or Chinese hamster ovary cells were used in the earliest work to demonstrate the biophysical effects of *SCN1A* mutations associated with epilepsy[32–36]. Exogenous sodium channel genes are cloned and expressed in these non-excitable cells which do not express endogenous voltage-gated sodium channels. These systems have the advantage of being able to establish good voltage control over the membrane potentials which allows for accurate measurement of the biophysical properties of the channels. However, it fails to reveal a consistent pathogenesis of *SCN1A* mutations that predisposes patients to hyperactive neural networks and seizure behaviors, due to the lack of the diversity of Nav channels and neuronal subtypes as *in vivo*[9,32,35,37,38]. Mouse models have been widely used to investigate *SCN1A* epilepsy. A variety of tools for genetic manipulations are available for generating transgenic mice with knock-in or knock-out mutations. The heterogeneity of cell types in mouse central nervous systems allows for

examination of the effect of *SCN1A* mutations in different cell types that underlie the alterations in circuitry and behaviors *in vivo*[39,40]. Although the similarity in the mouse and human genomes makes mice a useful model for neurological disorders, challenges of informing human health with mouse experimentation remain[41,42].

With the advent of induced pluripotent stem cells (iPSCs), patient iPSC-derived neurons have become a promising tool to study the cellular mechanism of epilepsy-associated *SCN1A* mutations and to develop personalized anti-epileptic therapeutics[43,44]. To understand disease-associated changes in neuronal function, it requires the iPSC-derived neurons do not only have neuronal morphology, but they are also capable of firing action potentials and forming functional synapses[45]. In contrast to plating iPSC-derived neural progenitors onto biochemical substrates, co-culturing with mouse astroglial feeder layers supports the maturation of excitability and synaptic activity in the derived neurons[46–48]. Prevailing methods of using primary mouse astrocytes are likely to cause contamination of primary mouse neurons that complicates distinguishing human iPSC-derived neurons and mouse neurons during live recording. Additionally, mouse primary astrocyte cultures have an unpredictable timeline of growth and recovery, making it difficult to coordinate with the plating of iPSC-derived neural progenitors. To overcome these issues, a reproducible and reliable method of generating astroglial feeder layers from cryopreserved mouse primary astrocyte cultures was developed to support the functional maturation of human iPSC-derived neurons, as described in Chapter 1 of the dissertation.

A common approach to model neurological disorders with human iPSCs is to use a large cohort of control and patient lines. To identify subtle alterations between control and patient lines, it is important to use a differentiation protocol that can consistently generate

functionally active neurons. Although many protocols can produce neurons that express neuronal markers and fire action potentials[49–51], there is limited discussion on the reproducibility in terms of the rate and degree of maturation in excitability and synaptic activity between individual platings and between independent cell lines. Large variability and low efficiency of protocols are likely to mask the small changes caused by the mutation in the patient line. In addition, it remains elusive on how the differentiation propensity of stem cells at different stages affect the functional maturation of the derived neurons. Many studies used neural stem cells, an expandable population of cells as the starting materials of neuronal differentiation[50,52,53], while some directly differentiate human iPSCs into neurons without the intermediate stage of expanding neural stem cells[51,54–60]. In Chapter 2 of the dissertation, the efficiency of the two protocols with or without using expandable neural stem cells was compared, and the direct differentiation protocol was modified by including the use of mouse astroglial feeder layers[49,61]. The reproducibility of the direct differentiation protocol was examined by tracking the rate and degree of maturation of neurons derived from multiple platings and two control cell lines over a time course of 5 weeks.

Using multiple control and patient lines can help understand the contribution of mutations to disease phenotypes. However, transcriptomic analysis in a number of iPSC lines reveals that genetic background variation accounts for differences between lines[62,63]. The genetic background variation was also manifested in multigenerational families in which individuals with the same *SCN1A* mutation exhibit a broad range of seizure phenotypes[29,30]. Differences in genetic background can also influence the underlying cellular phenotypes[64–66]. Therefore, subtle differences in cellular phenotypes might be

masked by multiple unrelated control and patient lines due to large variation in genetic background within each group[67]. Also, this strategy does not allow for studying the causality of genetic mutations to disease phenotypes. As epilepsy is associated with dysfunction of a variety of molecules that affect biophysical properties of neurons, and thus is susceptible to variations in genetic background, using dual isogenic pairs of control and mutant iPSC lines provides an efficient strategy to evaluate the causality of a single gene mutation independent of genetic background[67–71]. Comparison of electrophysiological properties of neurons within and between isogenic pairs can identify alterations that are possibly caused by one of the three factors: mutation alone, genetic background alone, or interaction between the mutation and the background. In Chapter 3, I aim to understand the causality of a missense *SCN1A* mutation to the etiology of epilepsy. Using CRISPR/Cas9 editing, dual isogenic pairs of iPSCs were generated: 1a) control (unaffected sibling), 1b) mutated control, and 2a) patient with *SCN1A* mutation (patient sibling), 2b) corrected patient. Electrophysiological properties were compared in inhibitory and excitatory neurons between and within the isogenic pairs to identify cell type-specific alterations caused by the mutation and/or genetic background.

In sum, the aims of my dissertation are to generate mouse astroglial feeder layers and functionally active human iPSC-derived neurons using reproducible and efficient protocols, and to determine the cellular effect of a *SCN1A* mutation in different neuronal subtypes derived from dual pairs of isogenic iPSCs. In Chapter 1, we developed a method using cryopreserved primary mouse astroglia to generate neuron-free and astrocyte-enriched feeder layers that promote the development of functional neural network in the human iPSC-derived neuronal cultures. In Chapter 2, we identified a direct differentiation

protocol that can reproducibly generate neuronal cultures from iPSCs in which the majority of cells not only have neuronal morphology and express neuronal markers, but they can also fire action potentials and form functional synaptic connections. The rate and degree of functional maturation is similar between two control lines. In Chapter 3, by comparing the electrophysiological properties in inhibitory and excitatory neurons from the dual isogenic pairs of iPSCs, we found the K1270T mutation causes gene dosage-dependent and cell type-specific alterations in sodium current density and evoked firing, resulting in hyperactive neural networks. We also identified differences associated with genetic background and interaction between the mutation and genetic background.

Human iPSC-derived neuronal cultures prepared using these protocols will facilitate identification of cellular defects in excitability and synaptic activity associated with neurological disorders that confer imbalance of excitation and inhibition. Furthermore, dual isogenic pairs of human iPSC-derived neurons cultures provide an efficient strategy to evaluate the causality of a single gene mutation independent of genetic background and a novel platform for developing patient-specific anti-seizure therapies.

Figure I.1 Mutations in Nav1.1 confer a broad spectrum of epilepsies. The Nav1.1 α subunit is composed of four homologous domains, each with six transmembrane segments. The S4 segments (gray) function as voltage sensors. Epilepsy-associated *SCN1A* mutations are represented as circles throughout the channel, with DS mutations in red and GEFS+ mutations in blue.

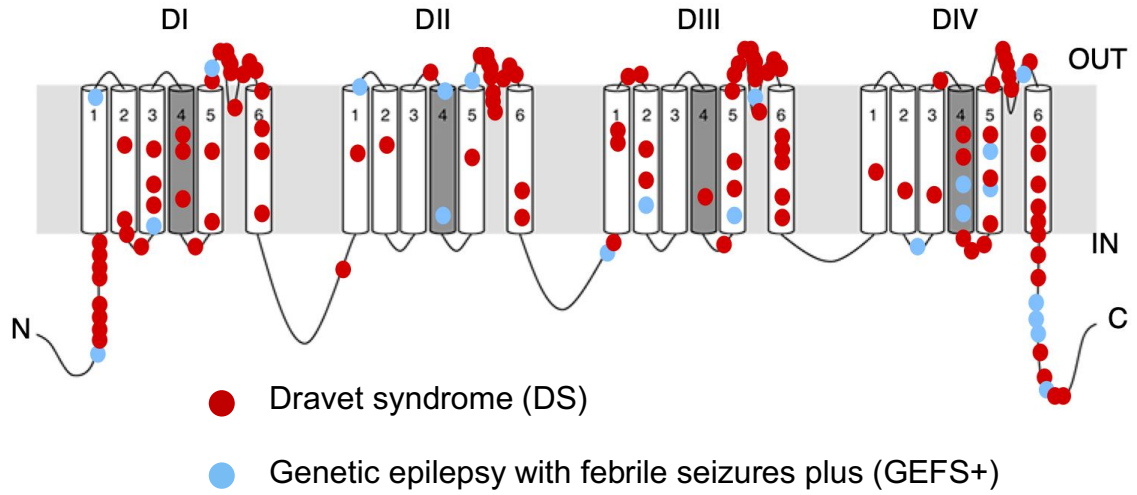

1.2. Bibliography

1. Fiest, K. M. *et al.* Prevalence and incidence of epilepsy: A systematic review and meta-analysis of international studies. *Neurology* **88**, 296–303 (2017).
2. Zack, M. M. & Kobau, R. National and State Estimates of the Numbers of Adults and Children with Active Epilepsy - United States, 2015. *MMWR. Morb. Mortal. Wkly. Rep.* **66**, 821–825 (2017).
3. Uhlhaas, P. J. & Singer, W. Neural Synchrony in Brain Disorders: Relevance for Cognitive Dysfunctions and Pathophysiology. *Neuron* **52**, 155–168 (2006).
4. Shorvon, S. D. The etiologic classification of epilepsy. *Epilepsia* **52**, 1052–1057 (2011).
5. Scheffer, I. E. *et al.* ILAE classification of the epilepsies: Position paper of the ILAE Commission for Classification and Terminology. *Epilepsia* **58**, 512–521 (2017).
6. Marini, C., King, M. A., Archer, J. S., Newton, M. R. & Berkovic, S. F. Idiopathic generalised epilepsy of adult onset: clinical syndromes and genetics. *J. Neurol. Neurosurg. & Psychiatry* **74**, 192 LP – 196 (2003).
7. Oyrer, J. *et al.* Ion Channels in Genetic Epilepsy: From Genes and Mechanisms to Disease-Targeted Therapies. *Pharmacol. Rev.* **70**, 142–173 (2018).
8. Hodgkin, A. L. & Huxley, A. F. A quantitative description of membrane current and its application to conduction and excitation in nerve. *J. Physiol.* **117**, 500–544 (1952).
9. Escayg, A. & Goldin, A. L. Sodium channel SCN1A and epilepsy: mutations and mechanisms. *Epilepsia* **51**, 1650–1658 (2010).
10. Catterall, W. A. Ion channel voltage sensors: structure, function, and pathophysiology. *Neuron* **67**, 915–928 (2010).
11. Oliva, M., Berkovic, S. F. & Petrou, S. Sodium channels and the neurobiology of epilepsy. *Epilepsia* **53**, 1849–1859 (2012).
12. Beneski, D. A. & Catterall, W. A. Covalent labeling of protein components of the sodium channel with a photoactivable derivative of scorpion toxin. *Proc. Natl. Acad. Sci. U. S. A.* **77**, 639–643 (1980).
13. Noda, M. *et al.* Primary structure of Electrophorus electricus sodium channel deduced from cDNA sequence. *Nature* **312**, 121–127 (1984).
14. Payandeh, J., Scheuer, T., Zheng, N. & Catterall, W. A. The crystal structure of a voltage-gated sodium channel. *Nature* **475**, 353–358 (2011).
15. Yarov-Yarovoy, V. *et al.* Structural basis for gating charge movement in the voltage sensor of a sodium channel. *Proc. Natl. Acad. Sci.* **109**, E93 LP-E102 (2012).
16. Vassilev, P. M., Scheuer, T. & Catterall, W. A. Identification of an intracellular peptide segment involved in sodium channel inactivation. *Science* **241**, 1658–1661 (1988).
17. West, J. W. *et al.* A cluster of hydrophobic amino acid residues required for fast Na(+)-channel inactivation. *Proc. Natl. Acad. Sci.* **89**, 10910 LP – 10914 (1992).
18. Isom, L. L., De Jongh, K. S. & Catterall, W. A. Auxiliary subunits of voltage-gated ion channels. *Neuron* **12**, 1183–1194 (1994).
19. Morgan, K. *et al.* beta 3: an additional auxiliary subunit of the voltage-sensitive sodium channel that modulates channel gating with distinct kinetics. *Proc. Natl. Acad. Sci. U. S. A.* **97**, 2308–2313 (2000).
20. Yu, F. H. & Catterall, W. A. Overview of the voltage-gated sodium channel family. *Genome Biol.* **4**, 207 (2003).

21. Isom, L. L. *et al.* Primary structure and functional expression of the beta 1 subunit of the rat brain sodium channel. *Science* **256**, 839–842 (1992).
22. Isom, L. L. *et al.* Structure and function of the beta 2 subunit of brain sodium channels, a transmembrane glycoprotein with a CAM motif. *Cell* **83**, 433–442 (1995).
23. Meng, H. *et al.* The SCN1A mutation database: updating information and analysis of the relationships among genotype, functional alteration, and phenotype. *Hum. Mutat.* **36**, 573–580 (2015).
24. Lossin, C. A catalog of SCN1A variants. *Brain Dev.* **31**, 114–130 (2009).
25. Claes, L. R. F. *et al.* The SCN1A variant database: a novel research and diagnostic tool. *Hum. Mutat.* **30**, E904-20 (2009).
26. Scheffer, I. E., Zhang, Y.-H., Jansen, F. E. & Dibbens, L. Dravet syndrome or genetic (generalized) epilepsy with febrile seizures plus? *Brain Dev.* **31**, 394–400 (2009).
27. Oguni, H., Hayashi, K., Awaya, Y., Fukuyama, Y. & Osawa, M. Severe myoclonic epilepsy in infants--a review based on the Tokyo Women's Medical University series of 84 cases. *Brain Dev.* **23**, 736–748 (2001).
28. Dravet, C. The core Dravet syndrome phenotype. *Epilepsia* **52 Suppl 2**, 3–9 (2011).
29. Abou-Khalil, B. *et al.* Partial and generalized epilepsy with febrile seizures plus and a novel SCN1A mutation. *Neurology* **57**, 2265–2272 (2001).
30. Goldberg-Stern, H. *et al.* Broad phenotypic heterogeneity due to a novel SCN1A mutation in a family with genetic epilepsy with febrile seizures plus. *J. Child Neurol.* **29**, 221–226 (2014).
31. Schutte, S. S., Schutte, R. J., Barragan, E. V & O'Dowd, D. K. Model systems for studying cellular mechanisms of SCN1A-related epilepsy. *J. Neurophysiol.* **115**, 1755–1766 (2016).
32. Spampanato, J., Escayg, A., Meisler, M. H. & Goldin, A. L. Functional effects of two voltage-gated sodium channel mutations that cause generalized epilepsy with febrile seizures plus type 2. *J. Neurosci.* **21**, 7481–7490 (2001).
33. Spampanato, J., Escayg, A., Meisler, M. H. & Goldin, A. L. Generalized epilepsy with febrile seizures plus type 2 mutation W1204R alters voltage-dependent gating of Na(v)1.1 sodium channels. *Neuroscience* **116**, 37–48 (2003).
34. Spampanato, J. *et al.* A Novel Epilepsy Mutation in the Sodium Channel SCN1A Identifies a Cytoplasmic Domain for β Subunit Interaction. *J. Neurosci.* **24**, 10022 LP – 10034 (2004).
35. Lossin, C., Wang, D. W., Rhodes, T. H., Vanoye, C. G. & George Jr., A. L. Molecular Basis of an Inherited Epilepsy. *Neuron* **34**, 877–884 (2002).
36. Lossin, C. *et al.* Epilepsy-associated dysfunction in the voltage-gated neuronal sodium channel SCN1A. *J. Neurosci.* **23**, 11289–11295 (2003).
37. Tang, B. *et al.* A BAC transgenic mouse model reveals neuron subtype-specific effects of a Generalized Epilepsy with Febrile Seizures Plus (GEFS+) mutation. *Neurobiol. Dis.* **35**, 91–102 (2009).
38. Martin, M. S. *et al.* Altered function of the SCN1A voltage-gated sodium channel leads to gamma-aminobutyric acid-ergic (GABAergic) interneuron abnormalities. *J. Biol. Chem.* **285**, 9823–9834 (2010).
39. Dutton, S. B. *et al.* Preferential inactivation of Scn1a in parvalbumin interneurons increases seizure susceptibility. *Neurobiol. Dis.* **49**, 211–220 (2013).
40. Tai, C., Abe, Y., Westenbroek, R. E., Scheuer, T. & Catterall, W. A. Impaired excitability

of somatostatin- and parvalbumin-expressing cortical interneurons in a mouse model of Dravet syndrome. *Proc. Natl. Acad. Sci. U. S. A.* **111**, E3139-48 (2014).
41. Hafezparast, M., Ahmad-Annuar, A., Wood, N. W., Tabrizi, S. J. & Fisher, E. M. C. Mouse models for neurological disease. *Lancet Neurol.* **1**, 215–224 (2002).
42. Akhtar, A. The flaws and human harms of animal experimentation. *Camb. Q. Healthc. Ethics* **24**, 407–419 (2015).
43. Du, X. & Parent, J. M. Using Patient-Derived Induced Pluripotent Stem Cells to Model and Treat Epilepsies. *Current neurology and neuroscience reports* **15**, 71 (2015).
44. Parent, J. M. & Anderson, S. A. Reprogramming patient-derived cells to study the epilepsies. *Nat. Neurosci.* **18**, 360–366 (2015).
45. Yang, N., Ng, Y. H., Pang, Z. P., Sudhof, T. C. & Wernig, M. Induced neuronal cells: how to make and define a neuron. *Cell Stem Cell* **9**, 517–525 (2011).
46. Johnson, M. A., Weick, J. P., Pearce, R. A. & Zhang, S.-C. Functional neural development from human embryonic stem cells: accelerated synaptic activity via astrocyte coculture. *J. Neurosci.* **27**, 3069–3077 (2007).
47. Muratore, C. R., Srikanth, P., Callahan, D. G. & Young-Pearse, T. L. Comparison and optimization of hiPSC forebrain cortical differentiation protocols. *PLoS One* **9**, e105807 (2014).
48. Tang, X. *et al.* Astroglial cells regulate the developmental timeline of human neurons differentiated from induced pluripotent stem cells. *Stem Cell Res.* **11**, 743–757 (2013).
49. Liu, Y. *et al.* Directed differentiation of forebrain GABA interneurons from human pluripotent stem cells. *Nat. Protoc.* **8**, 1670–1679 (2013).
50. Stover, A. E. *et al.* Process-based expansion and neural differentiation of human pluripotent stem cells for transplantation and disease modeling. *J. Neurosci. Res.* **91**, 1247–1262 (2013).
51. Prè, D. *et al.* A time course analysis of the electrophysiological properties of neurons differentiated from human induced pluripotent stem cells (iPSCs). *PLoS One* **9**, e103418 (2014).
52. Brafman, D. A. Generation, Expansion, and Differentiation of Human Pluripotent Stem Cell (hPSC) Derived Neural Progenitor Cells (NPCs). *Methods Mol. Biol.* **1212**, 87–102 (2015).
53. Yan, Y. *et al.* Efficient and rapid derivation of primitive neural stem cells and generation of brain subtype neurons from human pluripotent stem cells. *Stem Cells Transl. Med.* **2**, 862–870 (2013).
54. Devlin, A.-C. *et al.* Human iPSC-derived motoneurons harbouring TARDBP or C9ORF72 ALS mutations are dysfunctional despite maintaining viability. *Nat. Commun.* **6**, 5999 (2015).
55. Hartfield, E. M. *et al.* Physiological Characterisation of Human iPS-Derived Dopaminergic Neurons. *PLoS One* **9**, e87388 (2014).
56. Maroof, A. M. *et al.* Directed differentiation and functional maturation of cortical interneurons from human embryonic stem cells. *Cell Stem Cell* **12**, 559–572 (2013).
57. Mertens, J. *et al.* Differential responses to lithium in hyperexcitable neurons from patients with bipolar disorder. *Nature* **527**, 95–99 (2015).
58. Nicholas, C. R. *et al.* Functional maturation of hPSC-derived forebrain interneurons requires an extended timeline and mimics human neural development. *Cell Stem Cell*

12, 573–586 (2013).
59. Song, M., Mohamad, O., Chen, D. & Yu, S. P. Coordinated development of voltage-gated Na+ and K+ currents regulates functional maturation of forebrain neurons derived from human induced pluripotent stem cells. *Stem Cells Dev.* **22**, 1551–1563 (2013).
60. Sun, Y. *et al.* Properties of neurons derived from induced pluripotent stem cells of Gaucher disease type 2 patient fibroblasts: potential role in neuropathology. *PLoS One* **10**, e0118771 (2015).
61. Stover, A. E. *et al.* Process-based expansion and neural differentiation of human pluripotent stem cells for transplantation and disease modeling. *J. Neurosci. Res.* **91**, 1247–1262 (2013).
62. Burrows, C. K. *et al.* Genetic Variation, Not Cell Type of Origin, Underlies the Majority of Identifiable Regulatory Differences in iPSCs. *PLOS Genet.* **12**, e1005793 (2016).
63. Rouhani, F. *et al.* Genetic Background Drives Transcriptional Variation in Human Induced Pluripotent Stem Cells. *PLOS Genet.* **10**, e1004432 (2014).
64. Hu, B.-Y. *et al.* Neural differentiation of human induced pluripotent stem cells follows developmental principles but with variable potency. *Proc. Natl. Acad. Sci. U. S. A.* **107**, 4335–4340 (2010).
65. Vitale, A. M. *et al.* Variability in the Generation of Induced Pluripotent Stem Cells: Importance for Disease Modeling. *Stem Cells Translational Medicine* **1**, 641–650 (2012).
66. Mistry, A. M. *et al.* Strain- and age-dependent hippocampal neuron sodium currents correlate with epilepsy severity in Dravet syndrome mice. *Neurobiol. Dis.* **65**, 1–11 (2014).
67. Bassett, A. R. Editing the genome of hiPSC with CRISPR/Cas9: disease models. *Mamm. Genome* **28**, 348–364 (2017).
68. Chen, W. *et al.* Generation of the SCN1A epilepsy mutation in hiPS cells using the TALEN technique. *Sci. Rep.* **4**, 5404 (2014).
69. Liu, J. *et al.* CRISPR/Cas9 facilitates investigation of neural circuit disease using human iPSCs: mechanism of epilepsy caused by an SCN1A loss-of-function mutation. *Transl Psychiatry* **6**, e703 (2016).
70. Sandoe, J. & Eggan, K. Opportunities and challenges of pluripotent stem cell neurodegenerative disease models. *Nat Neurosci* **16**, 780–789 (2013).
71. Smith, J. G. W. *et al.* Isogenic Pairs of hiPSC-CMs with Hypertrophic Cardiomyopathy/LVNC-Associated ACTC1 E99K Mutation Unveil Differential Functional Deficits. *Stem cell reports* **11**, 1226–1243 (2018).

Chapter II

Astrocyte-enriched feeder layers from cryopreserved cells support differentiation of spontaneously active networks of human iPSC-derived neurons

This work has been published in Schutte RJ*, Xie Y*, Ng NN*, Figueroa P, Pham AT, O'Dowd DK. Astrocyte-enriched feeder layers from cryopreserved cells support differentiation of spontaneously active networks of human iPSC-derived neurons. *J Neurosci Methods*. 2018; 294:91–101.

2.1. Introduction

Human induced pluripotent stem cells (hiPSCs) can be differentiated *in vitro* into a wide variety of cell types including central nervous system neurons[1]. Patient-specific iPSC-derived neuronal cultures have proven to be an important tool for exploring the molecular mechanisms of a number of neurological disorders, including Parkinson's, amyotrophic lateral sclerosis, Huntington's, autism, schizophrenia, and epilepsy [2–8]. A critical requirement for understanding disease associated changes in neuronal function is that the derived cells not only have a neuronal morphology but that they are also capable of firing action potentials and forming functional synaptic connections.

Recent evidence demonstrates that the plating substrate can have significant influence on the development of functional properties of iPSC-derived neurons. Common substrates on which iPSC-derived neural progenitor cells are seeded include Matrigel, poly-D-lysine (PDL) or poly-L-ornithine (PLO) with laminin, and rodent astroglia[2,9–12]. Several studies have shown that compared to plating on cell-free extracellular matrices, co-culturing iPSC-derived neural progenitors onto rodent astroglial feeder layers promotes a greater degree of morphological development and functional maturation of neuronal excitability and synaptic transmission[13–15].

In most published protocols astroglial feeder cultures are prepared from the early postnatal rodent brain[10,12,15,16]. As this tissue source contains both neurons and glia, protocols have been developed to enrich the cultures for glia and eliminate neurons. Enrichment protocols often rely on differences in neuronal and glial response to culture media supplements and adherence to the substrate[17,18]. Harsh trituration of cortical tissue in the absence of glutamate receptor blockers can also be used to inhibit neuronal

survival[19,20]. While glial cells survive these enrichment protocols, an extended and unpredictable period of time is typically required for recovery and glial proliferation. The variability in the growth rate of primary astroglia to form feeder layers makes it difficult to coordinate their availability concurrent with the hiPSCs-derived neuronal progenitors at the appropriate stage of patterning for terminal differentiation. In addition, the possibility that some rodent neurons, even a small population, are present in the primary astroglial feeder layers complicates distinguishing between hiPSC-derived and rodent neurons in live cultures.

Cryopreservation of cells harvested from rodent primary astroglial cultures has been shown to be an effective way to eliminate neurons, while the astroglia retain the ability to proliferate when replated[21,22]. Therefore, we asked whether astroglial feeder layers generated from cryopreserved cells would support differentiation of functionally active hiPSC-derived neurons. Here we describe an efficient method using cryopreserved primary mouse astroglia to generate neuron-free, astrocyte-enriched feeder layers in 4-6 days. Immunostaining demonstrated that the feeder cultures were composed primarily of GFAP positive astrocytes with no evidence of β-III tubulin positive, GFAP negative neurons. iPSC-derived neural progenitors plated onto the astrocyte-enriched feeder layers formed spontaneously active networks of hiPSC-derived neurons within 21 days. In contrast, neural progenitors plated on biochemical substrates alone or when supplemented with glial conditioned medium were less effective in supporting functional neuronal differentiation in the same time frame. There was also a positive correlation between support layer confluence at the time of progenitor plating and the degree of synaptic connectivity. This efficient

method for preparation of astrocyte-enriched cultures will be of great value for neurological disease modeling and drug screening using hiPSC-derived neuronal cultures.

2.2. Methods

2.2.1 Preparation of frozen astroglia stocks from mouse brain primary cultures

Dissection of neonatal mouse brains was performed in adherence with approved animal use protocols and was consistent with a previously published protocol[19]. Postnatal cortical rinds were digested and triturated into a single cell suspension and seeded onto PDL-coated (Sigma-Aldrich, P7886) plastic 60 mm tissue culture dishes at 1 dish per brain. Cultures were maintained in minimal essential medium (MEM; Life Technologies, 11090-081) supplemented with 10% heat-inactivated fetal bovine serum (vol/vol) (Sigma-Aldrich, G8270), 2% 1 M D-(+)-glucose (vol/vol) (Sigma-Aldrich G8270), 1% penicillin/streptomycin (vol/vol) (Life Technologies, 15070-063) until 100% confluent (approximately 8-10 days). Confluent dishes were washed once with sterile Dulbecco's calcium- and magnesium-free phosphate-buffered saline (D-PBS; Gibco, 14190-144), then incubated for 8-10 minutes in 3 ml of 37°C TrypLE Express Enzyme (Life Technologies, 12604-021). TrypLE was then diluted with an additional 50% supplemented MEM (vol/vol) per dish before detaching the cells with gentle, repetitive pipetting. Cells were then centrifuged at 156 *g* for 5 min and gently resuspended at a concentration of 10^6 cells/ml in 4°C filtered freezing media containing 45% supplemented MEM (vol/vol), 45% conditioned stock MEM (vol/vol), and 10% dimethyl sulfoxide (vol/vol) (DMSO; Sigma-Aldrich, D2650). Aliquots of cell suspension (1.5 ml) were stored in 1.8 ml polypropylene cryovials (Sigma-Aldrich, V7634) and immediately transferred into a 2-propanol jacketed freezing container (Nalgene, 5100-0001) to slowly

cool at a rate of -1°C/min to a final temperature of -80°C. The entire process of expansion and cryopreservation was defined as a single passage. Frozen cell suspension was stored for a minimum of 24 hours and a maximum of 2 months prior to use. All media were equilibrated in a 37°C incubator with 5% CO_2 before use on the same day.

2.2.2 Preparation of astroglial feeder cultures from frozen stocks and astroglial conditioned media (GCM)

Cryovials of the frozen astroglial cell suspension were defrosted in a 37°C water bath with gentle swirling until only a small ice crystal remained. 37°C supplemented MEM (vol/vol) (sMEM) was added to the cryovial in a dropwise manner to a volume of approximately 2 ml before being transferred to a 15 ml conical with 3 ml warmed sMEM. Cells were then centrifuged at 156 *g* for 5 minutes and re-suspended in 37°C sMEM. Cell suspension concentration was determined using Trypan Blue exclusion staining (Trypan Blue 0.4%; Life Technologies, 15250-061). 5×10^4 cells were then seeded onto individual PDL-coated 12 mm round glass coverslips (Bellco Glass, 1943-10012A) contained in the wells of a 24-well plate. Cultures were maintained in sMEM in a 5% CO_2 incubator at 37°C, with half the media exchanged every 2 days. All media were equilibrated in a 37°C incubator with 5% CO_2 before use on the same day. A flow chart of the full procedure and the corresponding timeline are illustrated in **Figure II.1**.

To generate astroglial-conditioned media, frozen astroglia were seeded onto PDL-coated, tissue-treated 75 cm^2 cell culture flasks (Corning, 430641U). Flasks were grown to 100% confluence over a period of 5-7 days in 30 ml total sMEM. After reaching full confluence, the MEM was exchanged for neural differentiation media (NDM), prepared in a

separate protocol[9], for 24 hours, before exchanging back to sMEM for 48 hours. Flasks underwent a maximum of 2 NDM exchanges.

To study the effect of feeder layer percent confluence on iPSC-derived neurons, neural progenitors were plated in six conditions: PDL, PDL supplemented with GCM, PDL/laminin, and astroglial cultures of 20%, 50% and 100% confluence.

Figure II.1. **Culture process work flow from collection of tissue to plating of astrocyte-enriched cultures for iPSC-derived neuron differentiation.** (A) Cortical rinds are isolated from P0-P2 mouse coronal slices, triturated into a single cell suspension, and grown to confluence on PDL-coated dishes. Cells harvested from confluent cultures are resuspended in media and frozen for later use. (B) 4-6 days prior to need for astrocyte-enriched feeder layers the cells are thawed, plated onto PDL-coated coverslips, and grown to desired level of confluence. (C) iPSCs are patterned into neural progenitors, which are plated onto astrocyte-enriched feeder layers for the final stage of neuronal differentiation. (D) Timeline of astroglial cultures and neural differentiation from iPSCs.

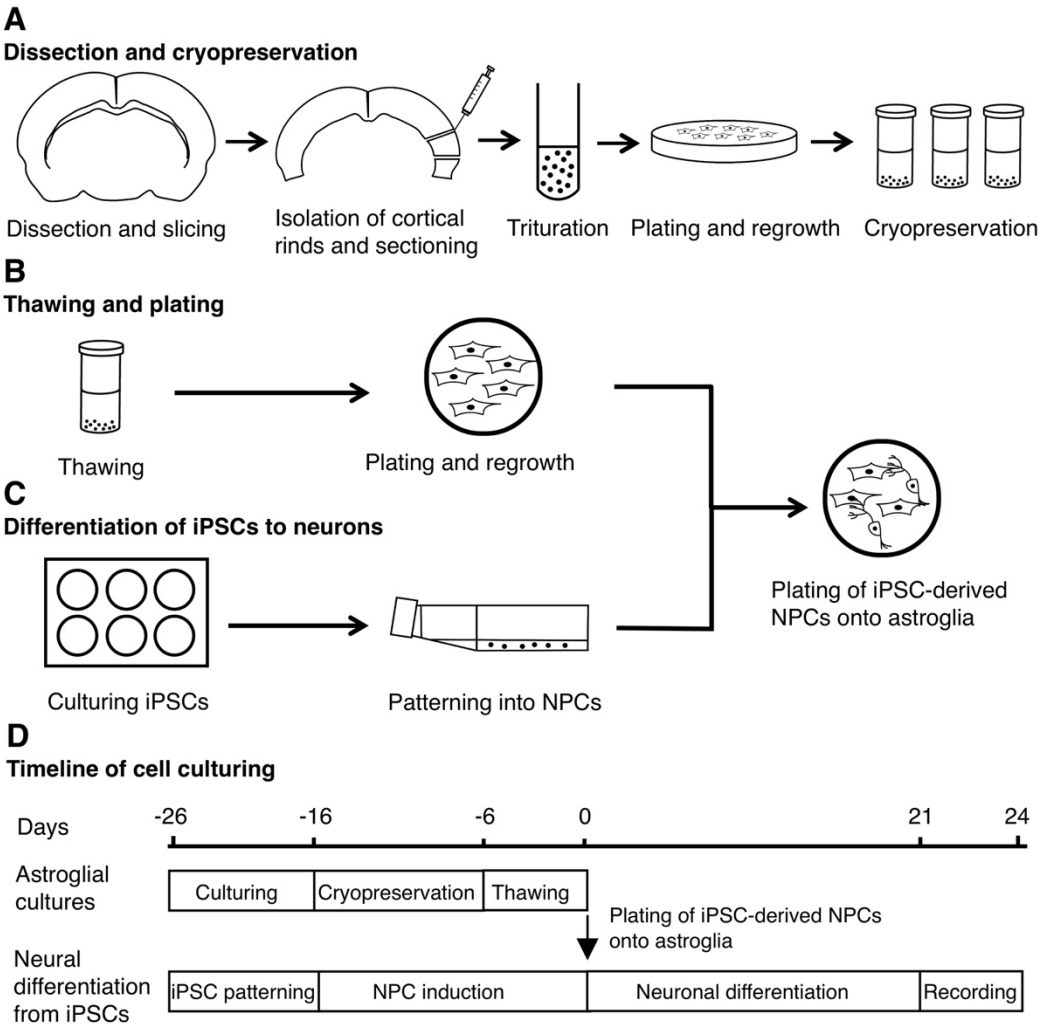

2.2.3 Immunostaining

Astroglial feeder cultures were fixed in 4% paraformaldehyde (wt/vol) (Sigma-Aldrich, P6148) for 15 minutes at room temperature and washed three times with PBS. Cells were permeabilized and blocked using PBS with 4% bovine serum albumin (wt/vol) (BSA; Sigma-Aldrich, A4919), 0.25% Triton X-100 (vol/vol) (Sigma-Aldrich, X100), and 0.02% sodium azide (wt/vol) (Sigma-Aldrich, S2002) in 1× PBS (Sigma-Aldrich, P3813) for 1 h at room temperature. Cultures were exposed to primary antibody and incubated overnight at 4°C. Coverslips were then washed three times with PBS and incubated in 5% normal goat serum (vol/vol) (ThermoFisher Scientific, 16210-064), 0.25% Triton X-100, 0.02% sodium azide in 1× PBS containing a 1:1000 dilution of secondary antibody (Alexa-Fluor; Life Technologies) for 2 h at room temperature. Coverslips were washed twice with PBS before counter-staining with 4',6-diamidino-2-phenylindole (DAPI; Life Technologies, D9542). Fluoromount G (SouthernBiotech, 0100-01) was used to mount coverslips on glass slides. Images were taken using a Zeiss M2 Imager microscope and processed by Zen software. Primary antibodies used were β-III tubulin (Sigma-Aldrich, T8660; 1:1000 dilution) to identify neurons, glial fibrillary acidic protein (GFAP; DAKO Z0334; 1:1500 dilution) to identify astroglial cells, and DAPI (1:40000 dilution) to identify nuclei of all cells.

2.2.4 iPSC culture

The iPSC cell line used in this paper is Line 173 (SC173.1-SF6-2I2.M16, passages 9 through 21). Line naming followed National Stem Cell Resource Center nomenclature. Fibroblasts were isolated from a skin biopsy of a 56-year-old male donor with no known clinical diagnoses. Skin fibroblasts were reprogrammed by the National Stem Cell Resource

Center (Laboratory of Phillip H. Schwartz) using a previously published protocol[20]. iPSCs were maintained using feeder-free conditions based on published protocols[20,23].

2.2.5 Plating of hiPSC-derived neural progenitors onto astroglial feeder layers

The differentiation protocol was adapted from Liu et al., 2013 [24]with modifications as briefly outlined. On day 0, embryoid bodies were generated from confluent human iPSC cultures by manual scraping[25]. Detached culture fragments from 15 wells were collected in a conical tube and centrifuged at 156 *g* for 5 min. Pellets were gently resuspended in 15 ml human iPSC medium (hiPSCM;[9]) with DMH-1 (Tocris, 4126), SB-431542 (Stemgent, 04-0010) and rho-associated protein kinase inhibitor Y27632 (ROCK inhibitor; Stemgent, 04-0012) and then transferred to a T25 non-tissue treated flask (Thermofisher Scientific, 169900). Neural induction and patterning procedures were followed according to the original protocol [9]. On day 16, neural rosettes were isolated and collected following 1 h incubation with STEMDiff Neural Rosette Selection Reagent (STEMCELL Technologies, 05832). Cells were patterned into neural progenitor cells (NPCs) using the ventralizing small molecule purmorphamine (Stemgent, 04-0009) following the original protocol until day 25[9].

On day 26, neurospheres of NPCs were pre-treated with ROCK inhibitor, dissociated using Accutase (Life Technologies, A1110501), centrifuged at 156 *g* for 5 minutes, and resuspended in fresh neural induction medium (NIM) containing ROCK inhibitor. After counting cells with Trypan Blue exclusion, 2.5×10^4 cells were plated on PDL, PDL/laminin, and 20%, 50%, or 100% confluent mouse astroglial feeder layers grown on PDL. 24 h after plating, 50% of the NIM was replaced by neural differentiation medium (NDM) or GCM containing 0.4 μM γ-secretase inhibitor XXI (Compound E, Calbiochem, 565790), 10 ng/ml BDNF (Peprotech, 450-02), 10 ng/ml GDNF (Peprotech, 450-10), 10 ng/ml IGF-1 (Peprotech,

100-11), and 0.5 g/ml membrane permeable cyclic AMP (Sigma-Aldrich, D0260). 48 h after plating, all media were exchanged with NDM or GCM with 0.2 μM Compound E. 96 h after plating, all media were exchanged for NDM or GCM without Compound E. From this point, 50% culture media exchange with fresh NDM or GCM without Compound E was performed every other day. All media were equilibrated in a 37°C incubator with 5% CO_2 before use on the same day.

To prepare PDL- and laminin-coated (PDL/L) coverslips, 50 μl of natural mouse laminin (Invitrogen, 23017-015) was added onto each PDL-coated coverslip 2 hours prior to neural progenitor plating. PDL/L coverslips were then incubated at 37°C until use.

2.2.6 Electrophysiological recording

Whole-cell recordings were performed on human iPSC-derived neurons between days 21-24 post plating using unpolished borosilicate glass pipettes with an open tip resistance of 4-7 MΩ (VWR International, 53432-921). External solution contained (in mM): NaCl 120, KCl 5.4, $MgCl_2$ 0.8, $CaCl_2$ 1.8, glucose 15, HEPES 20, at pH 7.2-7.4 with osmolarity between 290 and 295 mOsm. Internal solution contains (in mM): potassium gluconate 120, NaCl 20, $CaCl_2$ 0.1, $MgCl_2$ 2, EGTA 1.1, HEPES 10, Na_2ATP 4.5 at pH 7.2 with osmolarity ~280 mOsm. Voltages were corrected for a -5 mV junction potential.

While holding the membrane potential at -75 mV with hyperpolarizing current, evoked action potentials (APs) were recorded from 600 ms depolarizing current injections under current-clamp, and spontaneous post-synaptic currents (sPSCs) were recorded for at least 1 minute under voltage-clamp at -75 mV. Data were acquired with an EPC7 amplifier

(List Medical), a Digidata 1320A D-A converter (Axon Instruments), and a Dell Optiplex GX110 computer running pClamp8 software (Axon Instruments).

2.2.7 Data Analysis and Statistics

Phase-contrast micrographs were imaged with EVOS™ XL Core Cell Imaging System (ThermoFisher Scientific, AMEX1000). Visual estimations of astroglial confluence were based on n = 5 independent experiments. Fluorescent micrographs, imaged with Zeiss Axio Imager M2 and processed using Zen software, were used to quantify astroglial confluence and marker expression. Immunofluorescence analyses were based on n = 3 independent experiments.

Electrophysiological data were analyzed using Clampfit 10.6 software (Axon Instruments). Only recorded cells with a stable resting membrane potential (no greater than ± 5 mV deviation) more hyperpolarized than -30 mV, input resistance > 400 MΩ, and stable sPSC voltage-clamp recording were accepted for analysis. Evoked APs were defined as regenerative events where the first AP in the train was at least 20 mV in amplitude and any subsequent events were scored as APs if they were at least 15 mV in amplitude. Spontaneously firing cells were classified as those in which at least one spontaneous action potential (sAP) above -10 mV was observed in the first 30 seconds of recording in the absence of holding current. Mini Analysis Program 6.0.7 (Synaptosoft) was used to identify sPSC events with an amplitude threshold of 10 pA (4× RMS noise level of 2.5 pA) and an area threshold of 15 pA·ms (1.5× amplitude threshold). sPSCs identified by the software were then verified individually, with double peaks manually included. Recordings with a baseline shifted by more than 50 pA or events with a 10-90% rise time larger than 3 ms were excluded.

Statistical analyses were performed in Prism 7 (GraphPad) and figures were generated using DeltaGraph 7.1 (Red Rock Software).

2.3. Results

2.3.1 Rapid reproducible growth of feeder layers from defrosted primary astroglia.

In previous studies we used astroglial feeder layers from primary cultures of neonatal mouse brains to support differentiation of hiPSC-derived neurons. Significant cell loss in the primary astroglial feeder cultures was observed during the first week. Proliferation of the remaining cells typically reached confluences of 50-100% in 14-21 days when they were used plating of neuronal progenitors. The extended and variable time period made coordinating progenitor production and astroglial support layer availability challenging.

In this study we instead used cryopreserved primary astroglial cells to prepare feeder layers. Astroglial feeder layers were prepared by seeding 5×10^4 defrosted primary astroglial cells onto PDL-coated glass coverslips. The percentage of surface area covered by astroglial cells (% confluence) was tracked and visually estimated from phase-contrast imaging of live cultures between 2 and 10 days after plating. At day 2 post plating, a small number of cells were observed and the majority of the surface area was cell-free (**Figure II.2A**). Astroglia proliferation was clearly apparent by day 4, with an increased number of cells and reduction in cell-free space observed. By day 8, the majority of the coverslip surface area was covered by cells. There was a steady and reproducible increase in % confluence from ~10% at 2 days after plating to ~100% by 8 days (**Figure II.2B**). These data demonstrate the reproducible recovery and growth of defrosted primary astroglial

cells, greatly facilitating coordination of hiPSC-derived neuronal progenitor plating and astroglial feeder layer availability.

Figure II.2. Rapid and reproducible growth of cells in cultures prepared from stocks of frozen primary astroglial cells. (A) Phase-contrast images of cells in live astroglial cultures at 2, 4, and 8 days after plating 5×10^4 cells onto PDL-coated coverslips. Scale bars represent 50 µm. (B) The percentage of surface area covered by astroglial cells was visually estimated from live cultures between 2 and 10 days after plating. Each point represents the mean ± SEM from 5 independent platings with 3 coverslips/plating.

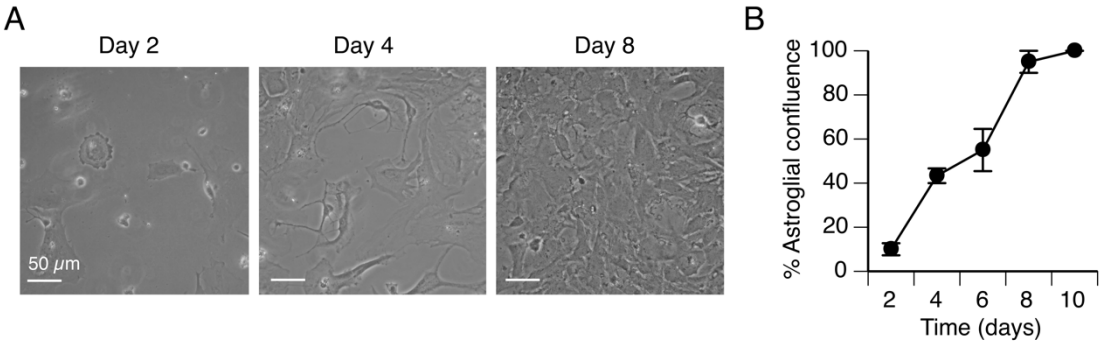

2.3.2 Feeder layers are composed of primarily GFAP positive astrocytes and are neuron-free.

To evaluate the contribution of astrocytes and neurons to the feeder layers prepared from the cryopreserved stocks, cultures were fixed 8 days after plating and co-stained with the nuclear marker DAPI, neuronal marker β-III tubulin, and astrocytic marker GFAP. The total number of cells in a single field was defined by the number of DAPI positive nuclei (**Figure II.3A**). A GFAP stained image of the same field of view revealed that almost all of the nuclei were surrounded by GFAP staining indicating the majority of the cells were astrocytes (**Figure II.3B**). While there was also one cell stained with the neuronal marker β-III tubulin (**Figure II.3C**), the merged image revealed that the cell was also GFAP positive so it was not classified as neuronal (**Figure II.3D**, white arrowhead). Quantitative analysis of stained cultures demonstrated that over 94% of the total cells in culture were GFAP positive astrocytes (**Figure II.3E**). The absence of β-III tubulin positive, GFAP negative cells indicate that no mouse neurons were present in these feeder layers. The remaining 6% of the total cells fall into two groups, 2% were positive for both GFAP, and β-III tubulin possibly representing early neuroglial progenitors (**Figure II.3D**, white arrowheads), and the remaining 4% were not stained with either GFAP or β-III tubulin (**Figure II.3D**, pink arrowheads).

Figure II.3. Feeder layers derived from cryopreserved astroglia are composed of GFAP positive astrocytes and are devoid of neurons. An immunofluorescent image of the astroglial feeder layer from a single field of view. (A) Nuclei of cells labeled by the nuclear marker DAPI. (B) The vast majority of the cells in the feeder layer were of astrocytic identity as indicated by their staining with anti- GFAP antibodies. (C, D) A cell labeled by the neuronal marker β-III tubulin indicated by the white arrowhead is also GFAP positive indicating it was unlikely to be a neuron. A small proportion of cells were not labeled with either marker (pink arrowheads). (E) The number of total cells in each field of view was determined by counting the DAPI positive nuclei. The cells stained for GFAP alone, β-III tubulin alone, both, or neither were determined for each field were expressed as a percentage of total cells. Analysis was performed on 9 randomly selected fields from three coverslips within each plating. Bars indicate mean + SEM, n = 3 independent platings.

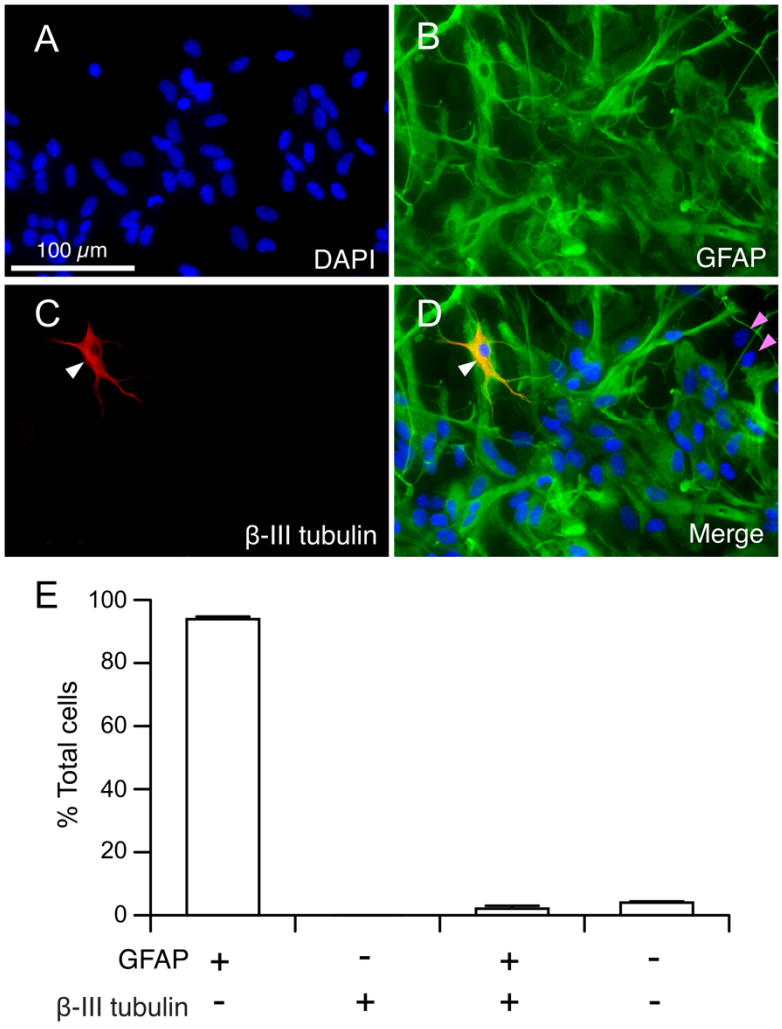

2.3.3 Astrocyte-enriched feeder layers from cryopreserved cells facilitate the morphological and functional differentiation of iPSC-derived neurons

Previous studies have shown that primary astroglial feeder layers promote development of neuritic processes and excitability of hiPSC-derived neurons[13,16]. One study used 50% confluent glia for their experiments to promote functional maturation[26].However, the effect of different degrees of glia confluence was not reported. To evaluate how the presence and confluence of astrocyte-enriched feeder layers prepared from cryopreserved cells affect differentiation of hiPSC-derived neurons, progenitors were plated onto a monolayer of 20%, 50%, or 100% confluent feeder layers. These were compared to those plated on PDL, PDL supplemented with astroglial-conditioned medium (GCM), or a combination of PDL/laminin (PDL/L).

When examined at 21 days post plating, qualitative differences between the culture conditions were apparent in fluorescence images. As revealed by immunostaining with βIII-tubulin antibody, typically progenitors in the PDL and GCM conditions resulted in fewer cells with neuronal morphology and relatively limited branching of the neurites (**Figure II.4A, B**). Those plated onto PDL/laminin resulted in more cells with neurites than PDL alone (**Figure II.4C**). The most consistent and robust differentiation of neurons with highly branched processes was observed when progenitors were plated on feeder layers enriched for GFAP-positive astroglia (**Figure II.4D**). Cultures plated on 20% confluent astrocyte-enriched feeder layers predominantly formed a lattice pattern on the glass coverslips. These hiPSC-derived neurons were isolated into islands of various sizes and connected to each other by neurite bundles (**Figure II.4E**). Cultures plated on 50% and 100% confluent astroglia had neurons and branching neurites more evenly distributed over the confluent astroglial layer

(**Figure II.4F, G**). Cell size was also evaluated by determining the cell capacitance through whole-cell recordings. There was no effect of feeder layer confluence on average whole cell capacitance but hiPSC-derived neurons grown without feeder layers had a significantly smaller mean capacitance than those grown on feeder layers (**Table II.1**). Furthermore, the input resistance of the cells grown without feeder layers was higher. Both of these electrical measurements are consistent with the visual observations that feeder layers facilitate growth of hiPSC-derived neurons.

Active membrane properties of neurons grown in the different conditions were also evaluated by whole-cell recordings. In all six growth conditions over 75% of the hiPSC-derived neurons fired at least one action potential in response to a depolarizing stimulus (**Figure II.5A, B**). However, the peak firing frequency was significantly higher in neurons grown on astroglial feeder layers compared to those grown in PDL, GCM, and PDL/laminin conditions, despite having similar resting membrane potentials (**Figure II.5C, Table II.1**). This is consistent with the astroglial feeder layers supporting more rapid maturation of excitability. While there was considerable variability in maximal evoked firing frequency, this was significantly higher in the neurons grown on the 20% confluent feeder layers compared to those on 50 and 100% confluent feeder layers.

Figure II.4. Astroglial feeder layers prepared from cryopreserved primary cultures facilitate the morphological differentiation of hiPSC-derived neurons. (A-C) Immunostaining of βIII-tubulin-positive and GFAP-negative derived neurons at 21-24 days after plating on PDL, PDL supplemented with GCM and PDL/laminin. (D) Immunostaining of βIII-tubulin-positive derived neurons grown on top of GFAP-positive astroglial feeder layers. Scale bars represent 20 µm. (E-G) Phase-contrast images of iPSC-derived neurons at 21-24 days after plating on astroglial feeder layers of 20%, 50% and 100% confluence, respectively. Scale bars represent 100 µm.

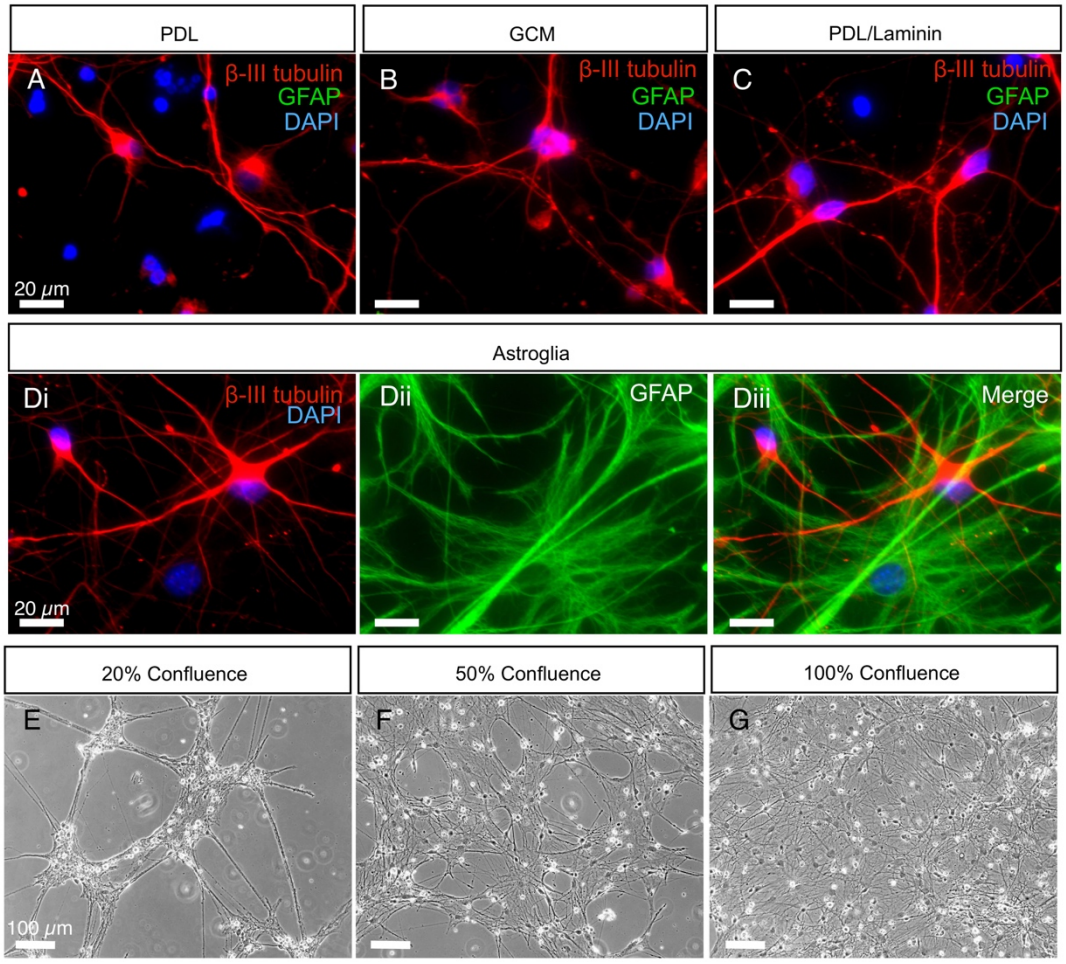

Table II. 1. Passive membrane properties of neurons plated on PDL, PDL supplemented with GCM, PDL/laminin, and astroglial cultures of 20%, 50%, and 100% confluence.

	Cell capacitance (pF)	Input resistance (GΩ)	RMP (mV)
PDL	24.1 ± 2.8 (14)	3.3 ± 0.5 (16)	-47.5 ± 2.6 (16)
GCM	23.1 ± 3.4 (14)	3.6 ± 0.5 (14)	-52.3 ± 2.6 (14)
PDL/laminin	17.6 ± 1.6 (9)	2.2 ± 0.3 (12)	-43.7 ± 2.8 (12)
20% confluence	33.6 ± 2.9 (16) ^{c1}	1.5 ± 0.1 (16) $^{a3, b4}$	-46.9 ± 1.8 (16)
50% confluence	31.6 ± 2.0 (16)	1.3 ± 0.2 (17) $^{a3, b4}$	-47.3 ± 2.3 (17)
100% confluence	37.5 ± 3.5 (18) $^{a1, b1, c3}$	1.1 ± 0.1 (18) $^{a4, b4}$	-45.0 ± 1.7 (17)

Data reported as mean ± SEM. Number of included cells indicated in parentheses. a, b and c superscripts represent significance to PDL, GCM and PDL/laminin groups, respectively. 1, 3, and 4 superscripts denote $p < 0.05$, 0.001, and 0.0001, respectively (one-way ANOVA with *post hoc* Bonferroni test).

Figure II.5. Astroglial feeder layers facilitate maturation of intrinsic firing properties of hiPSC-derived neurons. (A) Traces of AP firing (APs) evoked by depolarizing current injections in neurons plated on the indicated substrate at 21-24 days post plating. (B) Percentage of recorded neurons that fire ≥ 1 AP. No significant difference in % of firing APs between groups (p=0.12, Chi-square test). (C) Peak firing frequency is significantly higher in neurons grown on astroglial feeder layers compared to the other three groups (one-way ANOVA with *post hoc* Bonferroni test. *,**, **** denote p < 0.05, 0.01, and 0.0001 respectively. Data are represented as mean + SEM. Numbers in the parentheses represent the number of recorded neurons.

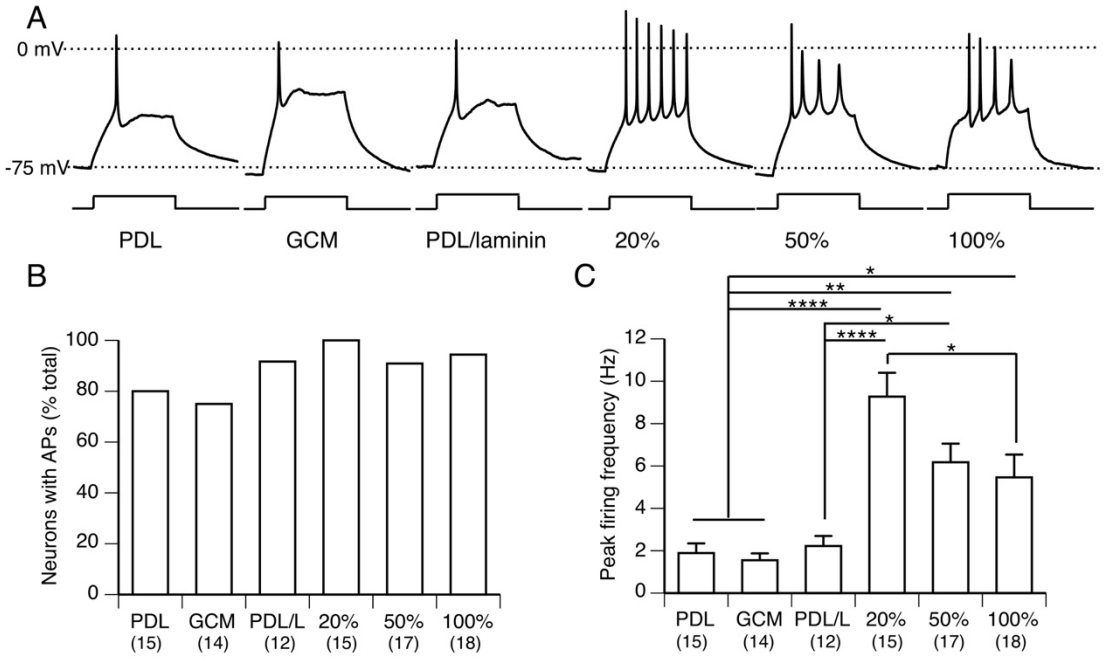

2.3.4 Astroglial feeder layers from cryopreserved cells support the development of spontaneous firing and synaptic activity in iPSC-derived neurons

Spontaneous firing was evaluated by gap-free current-clamp recordings for at least 1 minute in the absence of applied holding current (**Figure II.6A**). None of the neurons grown in PDL, GCM, and PDL/laminin conditions fired spontaneous action potentials (sAPs), whereas many of the neurons on feeder layers fired sAPs (**Figure II.6A**). The sAP firing frequency was quite variable and there was no significant association with the percent confluence of the feeder layers for the sample evaluated (**Figure II.6B**).

Assessment of spontaneous postsynaptic activity was based on gap-free voltage-clamp recordings from a holding potential of -75 mV for at least 1 minute. There was very little synaptic activity in the neurons without astroglial feeder layers, with the average frequency of spontaneous postsynaptic currents (sPSCs) being less than 0.1 Hz, while cells grown on feeder layers exhibited significantly higher sPSC frequencies with the average frequency increasing from 0.8 Hz in the 20% confluence condition to ~7 Hz in the 100% confluence condition (**Figure II.6C, D**). This suggests that astroglial feeder layers prepared from cryopreserved astroglia support functional development of synaptic activity in iPSC-derived neurons via physical contact, in addition to astrocyte-secreted factors[13]. One drawback to plating on 100% confluent feeder layers in our study was an increased incidence of detachment of the underlying astroglial layer from the glass coverslips during transfer to the recording chamber, which resulted loss of the overlying neurons as well. However, there was no obvious feeder layer detachment or difficulty obtaining recordings in cultures of 20% and 50% confluence.

Figure II.6. Astroglial feeder layers support spontaneous firing and spontaneous synaptic activity in hiPSC-derived neurons. (A) Representative traces of spontaneous action potentials (sAPs) at rest membrane potentials recorded from iPSC-derived neurons grown on indicated substrate at 21-24 days post plating. (B) sAP frequency at RMP, one-way ANOVA with *post hoc* Bonferroni test. (C) Overlay of two traces of spontaneous postsynaptic currents (sPSCs) recorded from neurons on indicated substrate held at -75 mV under voltage-clamp to illustrate the relative differences in sPSC frequencies. (D) sPSC frequency of neurons, one-way ANOVA test with *post hoc* Bonferroni test. Data are represented as mean + SEM. Numbers in the parentheses represent the number of recorded neurons. *** and **** denote p value < 0.001, and 0.0001 respectively.

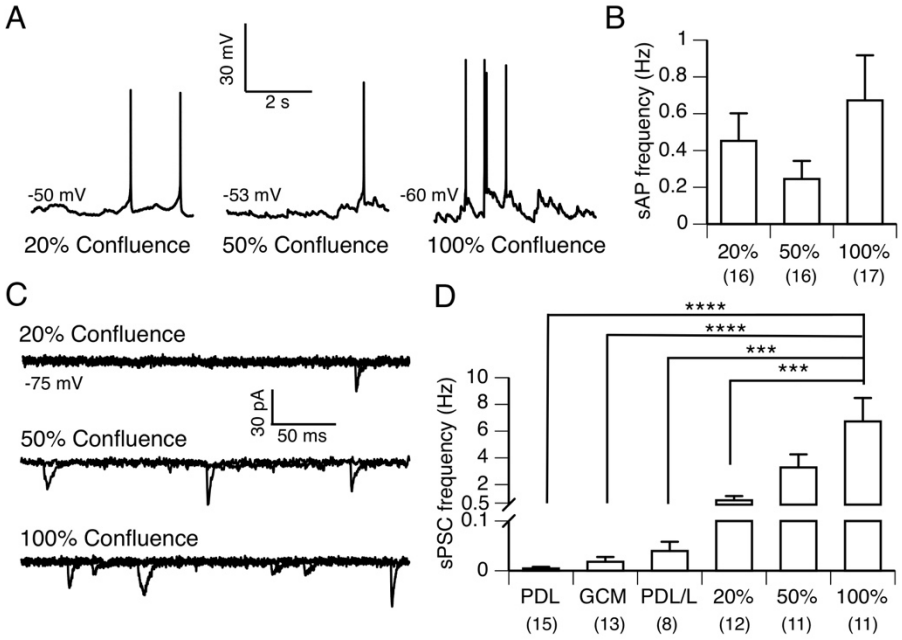

2.4. Discussion

Our results demonstrate more rapid morphological and functional differentiation of hiPSC-derived neurons on astroglial feeder layers prepared from cryopreserved cells compared with those plated in the absence of feeder layers. This protocol offers several advantages over using primary astroglia cultures: elimination of mouse neurons without a significant increase in time or effort, the ability to store cell suspension stocks for generation of feeder cultures at a later date, and significant reduction in the number of animals required.

While previous studies have shown that primary astroglial feeder layers prepared from mouse brain tissue can support rapid differentiation of functionally active neurons from human stem cell[20,26], one of the drawbacks is the potential for the presence of mouse neurons. These are not easily distinguished from human neurons in live cultures without introducing an exogenous marking system or requiring post-recording staining to confirm identity. Passaging glia cultures multiple times prior for use in neuronal derivation is a common practice to eliminate neurons[2,12,15]. While effective, this requires additional time and resources to grow glia and does not address the difficulty in synchronizing the timing of glia culture and neuronal progenitor availability. Protocols resulting in isolation of astrocytes based on differential adherence are also an option[17,18]; however, they involve vigorous shaking and careful timing of passaging. In contrast, cryopreservation of astroglial cells efficiently removes neurons as shown by the absence of β-III tubulin positive and GFAP negative cells in the cultures, meanwhile allowing for rapid and reproducible recovery. In addition, cryopreserved astroglial cells can be banked and used at a future date to generate astroglial support layers within a week, which enables thawing of the stocks at a relatively late stage of hiPSC patterning.

The protocol described in this paper can also significantly reduce the number of mice required to generate the astroglial feeder layers and the time required to prepare them. By expanding and passaging primary cultures on dishes for cryopreservation, the same number of newborn mice can be used to prepare 2-5 times as many astrocyte-enriched cultures as those from primary tissue. The efficacy of later passages has not been tested systematically but initial studies suggested that later passages were not as reliable in supporting functional maturation. Whether the astroglial passage number definitively affects the rate of functional development in derived neurons, however, will require additional investigation. Additionally, although the current protocol uses an initial glial seeding density of 5×10^4 cells, lower seeding densities can also be used, for example 2.5×10^4 cells. This typically requires an extra two days of culturing but effectively doubles the number of coverslips generated from a single vial of cryopreserved cells. When taken together, this protocol contributes to resource management and the ability to reproducibly generate neuron-free astroglial feeder layers.

It has been shown that a variety of biochemical substrates including PDL, PLO, fibronectin, integrins, and Matrigel can influence survival, proliferation and differentiation iPSC-derived neurons[16,27–31]. A combination of PDL/laminin has also been used to support functional differentiation of iPSC-derived neurons[32–36]. A study using high-resolution multielectrode arrays (MEAs) have shown increased spontaneous firing rate in iPSC-derived neurons without the use of astrocytes[37]. While this may indicate that astrocytes are not required for network maturation, future MEA studies may benefit by further evaluating synaptic maturation using functional analyses in neurons cultured with and without astrocytes[38,39]. In addition, astroglial feeder layers with confluences between 20-100% are

more effective at promoting maturation of functional properties than PDL supplemented with GCM. This indicates that astrocytes in our cultures may possibly regulate the functional development of derived neurons through a contact-dependent mechanism[13,16].

Plating neural progenitors onto astroglial cultures resulted in cultures where ~50% of the neurons fired spontaneous action potentials and 100% received postsynaptic input. This indicates the astroglial cells support formation of spontaneously active neural networks in culture. Future studies using MEAs and multisite calcium imaging will be useful in evaluating the spatiotemporal changes in neuronal network dynamics that occur in these cultures. Developmental changes in spontaneous burst firing rate have been detected using MEA to detect spikes in hiPSC-derived neurons co-cultured with rodent primary astrocytes[39,40].

The consequence of plating on fully confluent astroglia in our system is the loss of neurons when they are transferred to the recording chamber. In these cultures, the astroglia occupy the vast majority (over 95%) of the coverslip's surface area while the derived neurons on top are not themselves confluent. The underlying astrocytes behave as a sheet and when coverslips are removed from their culture well the astroglial sheet can lift off the coverslip removing the network of neurons with it. Additional studies will be necessary to determine the underlying cause of this detachment.

For studies focused on functional analysis of excitability and synaptic transmission in iPSC-derived neurons carrying different disease-causing mutations, our data indicate that 50% confluence provides an appropriate balance for functional studies, supporting spontaneously active neuronal networks while preserving the integrity of cell layer during transfer that is required for electrophysiological recording. Finally, the ability to reliably

generate astroglial cultures from the same stock allows enhanced control of the terminal differentiation environment, important for assaying differences between neurons derived from different iPSC clones or lines.

2.5. Bibliography

1. Srikanth, P. & Young-Pearse, T. L. Stem cells on the brain: modeling neurodevelopmental and neurodegenerative diseases using human induced pluripotent stem cells. *J. Neurogenet.* **28**, 5–29 (2014).
2. Brennand, K. J. *et al.* Modelling schizophrenia using human induced pluripotent stem cells. *Nature* **473**, 221–225 (2011).
3. Byers, B., Lee, H. & Reijo Pera, R. Modeling Parkinson's disease using induced pluripotent stem cells. *Curr. Neurol. Neurosci. Rep.* **12**, 237–242 (2012).
4. Kaye, J. A. & Finkbeiner, S. Modeling Huntington's disease with induced pluripotent stem cells. *Mol. Cell. Neurosci.* **56**, 50–64 (2013).
5. Lim, C.-S. *et al.* Understanding the molecular basis of autism in a dish using hiPSCs-derived neurons from ASD patients. *Mol. Brain* **8**, 57 (2015).
6. Marchetto, M. C., Brennand, K. J., Boyer, L. F. & Gage, F. H. Induced pluripotent stem cells (iPSCs) and neurological disease modeling: progress and promises. *Hum. Mol. Genet.* **20**, R109-15 (2011).
7. Parent, J. M. & Anderson, S. A. Reprogramming patient-derived cells to study the epilepsies. *Nat. Neurosci.* **18**, 360–366 (2015).
8. Sances, S. *et al.* Modeling ALS with motor neurons derived from human induced pluripotent stem cells. *Nat Neurosci* **16**, 542–553 (2016).
9. Liu, Y. *et al.* Directed differentiation of forebrain GABA interneurons from human pluripotent stem cells. *Nat. Protoc.* **8**, 1670–1679 (2013).
10. Sun, Y. *et al.* A deleterious Nav1.1 mutation selectively impairs telencephalic inhibitory neurons derived from Dravet Syndrome patients. *Elife* **5**, e13073 (2016).
11. Topol, A., Tran, N. N. & Brennand, K. J. A Guide to Generating and Using hiPSC Derived NPCs for the Study of Neurological Diseases. e52495 (2015). doi:doi:10.3791/52495
12. Zhang, Y. *et al.* Rapid single-step induction of functional neurons from human pluripotent stem cells. *Neuron* **78**, 785–798 (2013).
13. Johnson, M. A., Weick, J. P., Pearce, R. A. & Zhang, S.-C. Functional neural development from human embryonic stem cells: accelerated synaptic activity via astrocyte coculture. *J. Neurosci.* **27**, 3069–3077 (2007).
14. Muratore, C. R., Srikanth, P., Callahan, D. G. & Young-Pearse, T. L. Comparison and optimization of hiPSC forebrain cortical differentiation protocols. *PLoS One* **9**, e105807 (2014).
15. Prè, D. *et al.* A time course analysis of the electrophysiological properties of neurons differentiated from human induced pluripotent stem cells (iPSCs). *PLoS One* **9**, e103418 (2014).

16. Tang, X. *et al.* Astroglial cells regulate the developmental timeline of human neurons differentiated from induced pluripotent stem cells. *Stem Cell Res.* **11**, 743–757 (2013).
17. McCarthy, K. D. & de Vellis, J. Preparation of separate astroglial and oligodendroglial cell cultures from rat cerebral tissue. *J. Cell Biol.* **85**, 890–902 (1980).
18. Schildge, S., Bohrer, C., Beck, K. & Schachtrup, C. Isolation and culture of mouse cortical astrocytes. *J. Vis. Exp.* (2013). doi:10.3791/50079
19. Hilgenberg, L. G. W. & Smith, M. A. Preparation of Dissociated Mouse Cortical Neuron Cultures. *Journal of Visualized Experiments : JoVE* (2007). doi:10.3791/562
20. Stover, A. E. *et al.* Process-based expansion and neural differentiation of human pluripotent stem cells for transplantation and disease modeling. *J. Neurosci. Res.* **91**, 1247–1262 (2013).
21. Gómez-Lechón, M. J., Iborra, F. J., Azorín, I., Guerri, C. & Renau-Piqueras, J. Cryopreservation of rat astrocytes from primary cultures. *J. tissue Cult. methods* **14**, 73–77 (1992).
22. Yoshida, T. & Takeuchi, M. Primary culture and cryopreservation of mouse astrocytes under serum-free conditions. *Cytotechnology* **5**, 99–106 (1991).
23. Stover, A. E. & Schwartz, P. H. Adaptation of Human Pluripotent Stem Cells to Feeder-Free Conditions in Chemically Defined Medium with Enzymatic Single-Cell Passaging. *Methods Mol. Biol.* **767**, 137–146 (2011).
24. Maroof, A. M. *et al.* Directed differentiation and functional maturation of cortical interneurons from human embryonic stem cells. *Cell Stem Cell* **12**, 559–572 (2013).
25. Son, M.-Y., Kim, H.-J., Kim, M.-J. & Cho, Y. S. Physical passaging of embryoid bodies generated from human pluripotent stem cells. *PLoS One* **6**, e19134 (2011).
26. Kim, J.-E. *et al.* Investigating synapse formation and function using human pluripotent stem cell-derived neurons. *Proc. Natl. Acad. Sci. U. S. A.* **108**, 3005–3010 (2011).
27. Li, Y., Liu, M., Yan, Y. & Yang, S.-T. Neural differentiation from pluripotent stem cells: The role of natural and synthetic extracellular matrix. *World J. Stem Cells* **6**, 11–23 (2014).
28. Wang, H., Luo, X. & Leighton, J. Extracellular Matrix and Integrins in Embryonic Stem Cell Differentiation. *Biochemistry Insights* **8**, 15–21 (2015).
29. Flanagan, L. A., Rebaza, L. M., Derzic, S., Schwartz, P. H. & Monuki, E. S. Regulation of Human Neural Precursor Cells by Laminin and Integrins. *J. Neurosci. Res.* **83**, 845–856 (2006).
30. Ma, W. *et al.* Cell-extracellular matrix interactions regulate neural differentiation of human embryonic stem cells. *BMC Dev. Biol.* **8**, 90 (2008).
31. Harper, M. M., Ye, E.-A., Blong, C. C., Jacobson, M. L. & Sakaguchi, D. S. Integrins contribute to initial morphological development and process outgrowth in rat adult hippocampal progenitor cells. *J. Mol. Neurosci.* **40**, 269–283 (2010).
32. Berry, B. J. *et al.* Morphological and functional characterization of human induced pluripotent stem cell-derived neurons (iCell Neurons) in defined culture systems. *Biotechnol. Prog.* **31**, 1613–1622 (2015).
33. Wainger, B. J. *et al.* Intrinsic membrane hyperexcitability of amyotrophic lateral sclerosis patient-derived motor neurons. *Cell Rep.* **7**, 1–11 (2014).
34. Bardy, C. *et al.* Predicting the functional states of human iPSC-derived neurons with

single-cell RNA-seq and electrophysiology. *Mol Psychiatry* **21**, 1573–1588 (2016).
35. Hartfield, E. M. *et al.* Physiological Characterisation of Human iPS-Derived Dopaminergic Neurons. *PLoS One* **9**, e87388 (2014).
36. Mahairaki, V. *et al.* Induced pluripotent stem cells from familial Alzheimer's disease patients differentiate into mature neurons with amyloidogenic properties. *Stem Cells Dev.* **23**, 2996–3010 (2014).
37. Amin, H. *et al.* Electrical Responses and Spontaneous Activity of Human iPS-Derived Neuronal Networks Characterized for 3-month Culture with 4096-Electrode Arrays. *Front. Neurosci.* **10**, 121 (2016).
38. Boehler, M. D., Wheeler, B. C. & Brewer, G. J. Added astroglia promote greater synapse density and higher activity in neuronal networks. *Neuron Glia Biol.* **3**, 127–140 (2007).
39. Odawara, A., Saitoh, Y., Alhebshi, A. H., Gotoh, M. & Suzuki, I. Long-term electrophysiological activity and pharmacological response of a human induced pluripotent stem cell-derived neuron and astrocyte co-culture. *Biochem. Biophys. Res. Commun.* **443**, 1176–1181 (2014).
40. Odawara, A., Katoh, H., Matsuda, N. & Suzuki, I. Physiological maturation and drug responses of human induced pluripotent stem cell-derived cortical neuronal networks in long-term culture. *Sci. Rep.* **6**, 26181 (2016).

Chapter III

Reproducible and efficient generation of functionally active neurons from human hiPSCs for preclinical disease modeling

This work has been published in Xie Y*, Schutte RJ*, Ng NN*, Ess KC, Schwartz PH, O'Dowd DK. Reproducible and efficient generation of functionally active neurons from human hiPSCs for preclinical disease modeling. *Stem Cell Res*. 2018;26: 84–94.

3.1. Introduction

Neuronal cultures derived from human hiPSCs are a useful model system for exploring cellular mechanisms underlying the pathogenesis of neurological disorders and for developing novel therapies. Analyses of hiPSC-derived neurons from patients with defined neurological diseases have identified a variety of abnormalities. These include alterations in neuronal morphology, excessive excitability, dysfunctional synaptic connections, and altered mitochondrial function, many that are likely to contribute to different disease phenotypes[1–9]. hiPSC-derived neuronal cultures can also serve as a valuable platform for evaluating the effect of a drug or drug combinations on gene-specific deficits in neuronal differentiation and/or function[2,10]. However, disease modeling *in vitro* with hiPSC-derived neurons is still at an early stage and there are a number of outstanding questions about the properties of neurons generated by a variety of differentiation protocols.

It is important that consistent criteria are used to define hiPSC-derived neurons in culture. Similar to criteria for characterizing induced neuronal (iN) cells reviewed by Yang et al., cells designated as neurons differentiated from hiPSCs should not only have neuronal morphology and express neuron specific markers, but should also be electrically excitable[11]. In addition, the formation of functionally active synapses between neurons facilitates the use of cultures to explore how gene mutations potentially affect network activity. Second, there are a number of differentiation protocols used by different groups but little is known about the comparative efficiency with which these produce excitable cells[12–15]. In addition, it is not clear how the differentiation potentials of stem cells at different stages affect the

formation of functionally active neurons. Some protocols incorporate the use of neural stem/progenitor cells, a self-renewing multipotent population derived from hiPSCs, as starting source for neuronal differentiation[15–17]. Other protocols start from the hiPSC stage, and directly differentiate cells into neurons without using an expandable population of multipotent cells[4,8,13,18–24]. Finally, when considering a single protocol there has been limited discussion of reproducibility in terms of the rate and degree of maturation of firing properties and synaptic connectivity between platings and between independently generated hiPSC lines. Low efficiency and/or high variability can hamper the identification of altered functional properties of neurons between control and mutant groups.

The goal of this study was to identify a protocol that could reliably produce cultures from hiPSCs in which the majority of cells with neuronal morphology also fire action potentials and form synaptic connections. The efficiency of generating functionally active neurons from one hiPSC line obtained from a control patient was evaluated using two different protocols. The first protocol included generating an expandable neuronal stem cell population that was plated onto astroglial feeder layers for differentiation. In our previous experience this resulted in cultures containing functionally active neurons but the efficiency was low[15,25]. This was compared to a direct differentiation strategy that first patterns hiPSCs into neural progenitors (NPCs) that are differentiated without expansion[20]. The protocol was modified to include the use of astroglial feeder layers for differentiation. Direct differentiation resulted in production of functionally active neurons at a faster rate and with higher efficiency than the protocol including an expandable intermediate

population. In addition, the direct differentiation strategy resulted in cultures in which the rate and degree of neuronal maturation was similar between multiple platings from one control hiPSC line, and between two hiPSC lines from unrelated individuals with no known neurological disorders. hiPSC-derived neuronal cultures prepared using this direct differentiation will greatly facilitate identification of cellular defects in excitability and synaptic transmission associated with specific disease-causing mutations and drug discovery.

3.2. Methods

3.2.1 Preparation and maintenance of hiPSCs

Two human iPSC cell lines: Line 210 (SC210.12-SF6-2I3.M11S8 through S31) and Line 173 (SC173.1-SF6-2I2.M16S9 through S21). Both lines were generated by the Schwartz laboratory using a previously published protocol[15] from skin fibroblasts provided by the labs of Alfred George, Jr. and Kevin Ess (210 line) and Philip Schwartz (173 line). Both fibroblast donors were males with no known clinical diagnoses. Age at time of biopsy was 23 years (210 line) and 56 years (173 line).

hiPSCs were maintained in feeder-free conditions using published protocols[15,26]. Briefly, hiPSCs were grown on Matrigel (BD Sciences) and fed every day with basal hiPSC medium supplemented with 2% (vol/vol) StemPro (StemPro SFM Kit, including 50× supplement, D-MEM/F12+GlutaMax and 25% BSA solution, Life Technologies) and 20 ng/ml (basic fibroblast growth factor, Stemgent). For basal medium, the final concentration of BSA and beta-mercaptoethanol (Life Technologies) in D-MEM/F12+GlutaMax were 1.8% and 100 μM. Complete medium was equilibrated at 37 °C and 5% CO_2 before use.

hiPSCs were passaged upon reaching 100% confluence. Falcon 6-well plates were coated with a 1:30 dilution of Matrigel in D-MEM/F12+Glutamax and incubated for at least 20 minutes. hiPSCs were incubated with 10μm ROCK inhibitor (RI; rho-associated protein kinase inhibitor Y27632, Stemgent) one hour prior to dissociation with Accutase (Millipore) for 1 minute at room temperature. Cells were dislodged and collected in Dulbecco's calcium- and magnesium-free phosphate-buffered saline (D-PBS; Gibco, 14190-144). The cell suspension was gently triturated, collected in conical tubes and centrifuged at 156× *g* for 5 minutes. Cell pellets were gently re-suspended in complete hiPSC medium plus RI. Excess Matrigel solution was removed from pre-incubated wells. The cell suspension was added to each well and then flooded with complete hiPSC media with RI to a final volume of 2 ml per well. Typical splits were 1 well to 3 or 6 wells.

3.2.2 NSC culturing and neuronal differentiation

The 210 hiPSC line was also used to generate an expandable neural stem cell (exNSC 210) line. Line naming follows National Human Neural Stem Cell Resource nomenclature[15]. NSCs were maintained and passaged according to a previously published protocol with no alterations[15]. To prepare for neuronal differentiation, confluent NSC cultures were lifted using Enzyme Free Dissociation Buffer, dislodged, and collected using D-PBS. The cell suspension was then gently triturated, collected in conical tubes and centrifuged at 156× *g* for 5 min. After re-suspension in fresh NSC media (see published protocol) cell suspension was passed through a 37 μm reversible strainer (STEMCELL Technologies, 27215). This revised step to the protocol removes the large non-dissociated clusters of NSCs and allows plating of single cells on 50% confluent mouse glia at a density 2.2×10^4 cells/cm^2 per

coverslip. Neuronal differentiation was also performed as per the original protocol, but with the addition of 0.2 μM Compound E during the first 3 days of differentiation. Neuronal differentiation media contained 20 ng/ml BDNF and GDNF, 1 mM dibutyryl cAMP, and 200 nM freshly made ascorbic acid (Sigma-Aldrich). Feeding cultures involved a 50% exchange every 48 h for the duration of the culture's life. All media was prepared immediately prior to use and equilibrated at 37°C and 5% CO_2.

3.2.3 Direct differentiation of hiPSCs into neurons

The strategy used to pattern hiPSCs into neurons was adapted from a previously published protocol[20]. On day 0, embryoid bodies were generated from 100% confluent hiPSC cultures grown in a 6-well falcon plate by manual scraping in a parallel direction using a 1 ml pipette tip. Tissue fragments from 15 wells were collected in a conical tube. After centrifugation at 156× *g* for 5 min the pellet was re-suspended in 15 ml hiPSCM (human iPSC medium) and then transferred to a T25 non-tissue culture treated flask (Thermofisher Scientific). Neural induction and culturing protocols were followed as per the original protocol. On day 16, neural rosettes were collected using STEMDiff Neural Rosette Selection reagent (STEMCELL Technologies) based on vendor's protocol. MGE patterning was done using the ventralizing factors purmorphamine (Stemgen) and/or recombinant human sonic hedgehog (SHH; Peprotech) following the original protocol until day 25. Experiments using purmorphamine with SHH and purmorphamine alone were included in this study.

Neuronal differentiation was initiated on day 26, when progenitor neurospheres were dissociated using Accutase (Life Technologies), centrifuged at 156× *g* for 5 min, and

re-suspended in neural induction medium (NIM) containing Rho kinase (ROCK) inhibitor. These were plated at 2.2×10^4 cells/cm^2 per coverslip on 50% confluent mouse astroglial cultures. 24 h after plating, 50% of the NIM was replaced with complete NDM (Neural differentiation medium) containing 0.4 μM γ-secretase inhibitor XXI (Compound E; Calbiochem), 10 ng/ml BDNF (Peprotech), 10 ng/ml GDNF (Peprotech), 10 ng/ml IGF-1 (Peprotech), and 0.5 g/ml membrane permeable cyclic AMP (Sigma-Aldrich). 48 h after plating, all of the culture medium was replaced by complete NDM supplemented with 0.2 μM Compound E. 96 h after plating, culture medium was replaced with complete NDM and a 50% exchange with fresh complete NDM performed every 48 h for the duration of the culture's life. All media was prepared immediately prior to use and equilibrated at 37°C and 5% CO_2.

3.2.4 Astroglia Cultures

Astroglial cultures were generated using a previously published protocol[27,28]. Briefly, cortical rinds were dissected from the brains of P0-P2 ICR (CD-1) mouse pups (Envigo), enzymatically digested, and triturated into a single cell suspension. Suspension was plated on poly-d-lysine (PDL, Sigma) coated 60mm tissue culture dishes and allowed to grow to confluence. Once confluent, cultures were trypsinized (TrypLE, Life Tech), lifted, re-suspended in freezing media (Glia Culture Medium with 10% DMSO) and stored at -80°C. When needed, cells were defrosted and 4.4×10^4 cells/cm^2 per coverslip viable (identified by trypan blue staining) cells/cm^2 were plated onto PDL coated 12mm glass coverslips (Bellco). Astroglial feeder cultures were grown for 5-6 days to approximately 50% visually

determined confluence prior to seeding with neural progenitors for neuronal differentiation.

3.2.5 Immunostaining and imaging

Coverslips containing hiPSC- or exNSC-derived neurons were fixed in 4% paraformaldehyde (in PBS) for 15 min at room temperature and washed three times with PBS. Cells were permeabilized and blocked using PBS with 4% bovine serum albumin (wt/vol) (BSA; Sigma-Aldrich), 0.25% Triton X-100 (vol/vol) (Sigma-Aldrich), and 0.02% sodium azide (wt/vol) (Sigma-Aldrich) in 1× PBS (Sigma-Aldrich) for 1 h at room temperature. Cultures were exposed to primary antibody and incubated overnight at 4°C. After washing 3 times with PBS, coverslips incubated in 5% normal goat serum (vol/vol) (ThermoFisher Scientific), 0.25% Triton X-100, 0.02% sodium azide (wt/vol) in 1× PBS containing a 1:1000 dilution of secondary antibody (Alexa-Fluor; Life Technologies) for 2 h at room temperature. Coverslips were washed twice with PBS before staining nuclei with 4',6-diamidino-2-phenylindole (DAPI; Life Technologies). Fluoromount G (SouthernBiotech) was used to mount coverslips on glass slides. Images were taken using a Zeiss M2 Imager microscope and processed by Zen software. HuNu (1:250; Millipore), βIII-tubulin (1:2000; BioLegend) and GFAP (glial fibrillary acidic protein; 1:1500; DAKO) were used to characterize composition of cells generated from hiPSCs by the direct differentiation protocol. βIII-tubulin (Sigma-Aldrich) and GABA (Sigma-Aldrich) primary antibodies were used at 1:1000 and 1:4000 dilutions respectively for identification of GABAergic neurons. Neurons were identified by morphology, expression of βIII-tubulin in the soma and neurites, and nuclear localization of DAPI.

3.2.6 Whole-cell recording

Whole cell recordings were obtained from hiPSC-derived neurons at 5 different time points: 4-5, 10-11, 15-16, 21-23, and 35-38 days post plating. exNSC-derived neurons were examined at 21-23 days post plating. Electrophysiological recordings were performed with unpolished borosilicate glass pipettes with open tip resistance of 4-7 MΩ (VWR International). External solution contained (in mM): NaCl 120, KCl 5.4, $MgCl_2$ 0.8, $CaCl_2$ 1.8, glucose 15, HEPES 20, at pH 7.2-7.4. Osmolality was adjusted to 290 - 295 mOsm. Internal solution contained (in mM): potassium gluconate 120, NaCl 20, $CaCl_2$ 0.1, $MgCl_2$ 2, EGTA 1.1, HEPES 10, Na_2ATP 4.5 with pH at 7.2 and osmolality around 280 mOsm. Voltages were corrected for a -5 mV junction potential. Spontaneous action potential firing was recorded both at resting membrane potential and at -75 mV using a gap free protocol under current clamp. For evoked action potentials, membrane potential was held at -75 mV and cells were depolarized by a series of current injections. Spontaneous postsynaptic currents (sPSCs) were examined under voltage clamp at -75 mV.

Spontaneous excitatory and inhibitory postsynaptic currents (sEPSCs and sIPSCs) were separated at reversal potentials (-49 mV and -2 mV) with the same external solution mentioned above and CsGluconate internal solution containing (in mM): Cs^+ gluconate 130, EGTA 0.2, $MgCl_2$ 2, CsCl 6, HEPES 10, adenosine 5' triphosphate sodium salt 2.5, guanosine 5' triphosphate sodium 0.5 and phosphocreatine disodium 10. The identity of sEPSCs and sIPSCs were confirmed pharmacologically using 50 μM (2*R*)-amino-5-phosphonovaleric acid (APV; Tocris Bioscience), 10 μM 6-cyano-7-nitroquinoxaline-2,3-dione (CNQX; Sigma-Aldrich), 10 μM bicuculline methochloride (BMC; Tocris Bioscience), and/or 100 nM

strychnine (Sigma-Aldrich) bath applied in external solution. External solution was perfused through the chamber at a speed of 0.6 to 1 ml/min during recording.

3.2.7 Data Analysis and Statistics

Fluorescent micrographs processed using Zen software were used to quantify the percentage of GABAergic neurons**.** For each coverslip, at least 3 fields with equally distributed cells observed via DIC were chosen for counting. Counting was performed blind with respect to cell line. Represented data were based on n = 10 coverslips (Line 210) and n = 4 coverslips (Line 173).

Electrophysiological data were acquired with a List EPC7 amplifier, a Digidata 1320A D-A converter (Axon Instruments), and a Dell Optiplex GX110 computer running pClamp8 (Axon Instruments) software at room temperature. Clampfit 10.6 software (Axon Instruments) was used to analyze electrophysiological data.

Cells that were included in analyses had an input resistance ≥ 400 MΩ, whole-cell capacitance ≥ 5 pF, stable (no greater than a ± 5 mV deviation) resting membrane potentials more hyperpolarized than -30 mV, and stable sPSC voltage-clamp recordings. We characterized evoked action potentials as regenerative events with a peak depolarization of greater than or equal to -5 mV on the first AP and -15 mV in subsequent APs within the train. sPSCs recorded under voltage-clamp were analyzed using Mini Analysis 6.0.7 (Synaptosoft). sPSCs identified by the software had an amplitude ≥ 10 pA (2× RMS noise of 2.5 pA) and were then manually verified individually. sPSC recordings in which the baseline shifted by more than 50 pA were excluded. Electrophysiological data were represented based on n = number of independent experiments. All statistical analyses were

performed with Prism 7.0.2 (GraphPad Software) and all figures were generated using DeltaGraph 7.1 (Red Rock Software).

3.3. Results

3.3.1 hiPSCs-derived neurons mature more rapidly than those generated from an expandable NSC intermediate stage.

Our initial studies focused on the comparison of neurons derived using two different protocols from the same human control hiPSC line (Line 210) (**Figure III.1A**). The first protocol involved generating an expandable population of neural stem cells (exNSCs) from the hiPSCs[15] (**Figure III.1B**, top). The exNSCs were maintained as a renewable population and plated at a density of 2.2×10^4 cells/cm^2 onto 50% confluent astrocyte-enriched feeder layers to begin differentiation (D0) into exNSC-neurons. The second protocol was based on patterning hiPSCs into neural progenitor cells (NPCs) over a period of 26 days followed by immediate plating at a density of 2.2×10^4 cells/cm^2 onto the astrocyte-enriched feeder layers to begin differentiation (D0) into hiPSC-derived neurons (**Figure III.1B**, bottom). By the 3rd week of differentiation (D21-23 post plating), cultures prepared using both protocols contained cells with neurites that also expressed the neuron specific marker βIII-tubulin (**Figure III.1C**, top). The cultures generated via direct differentiation typically had a more extensive network of branched neurites compared to cultures generated through an exNSC intermediate stage (**Figure III.1C**, bottom).

Electrical excitability following 21 days of differentiation was compared in neurons derived using the two protocols. The typical exNSC-neuron displayed

passive changes in membrane potential or small failed spikes in response to depolarizing current injection (**Figure III.1D**, top). In contrast, the typical hiPSC-derived neuron fired multiple action potentials in response to stimulation (**Figure III.1D**, bottom). Evaluation of over 20 neurons using the two protocols demonstrated a significantly higher percentage of hiPSC-derived neurons firing at least one AP in response to a depolarizing current injection compared to exNSC-neurons ($p < 0.0001$; Chi-square test; **Figure III.1E**). These data demonstrate that the rate of maturation of excitability is faster in neurons generated by the direct differentiation protocol compared to those generated from an expandable NSC intermediate stage.

Consistent with more extensive neuritic arbors, the average whole-cell capacitance (C_m) of the hiPSC-derived neurons generated via direct differentiation was 2.5 times larger than exNSC-neurons (**Table III.1**). However, there was no significant difference in the input resistance (R_{in}) or resting membrane potential (RMP) between neurons generated from the two protocols at D21 post plating (**Table III.1**, $p > 0.2$, unpaired *t*-test with Welch's correction).

Figure III.1. Maturation of excitability is faster in hiPSC-derived neurons than in expandable NSC-derived neurons. (A) Flowchart of the two protocols utilized to generate neurons derived from the control hiPSC line 210. (B) The expandable NSC protocol includes generating an intermediate, regenerative population of neural stem cells (exNSCs) from the hiPSCs that are expanded before being differentiated into neurons. In the direct differentiation protocol, hiPSCs are patterned into neural progenitor cells (NPCs) that are directly differentiated, without expansion, into neurons. exNSCs and NPCs are both plated at the same density onto mouse cortical astroglia feeder layers to promote neuronal differentiation. (C) Immunostaining (D21 post plating) with a neuronal marker βIII-tubulin and a nuclei marker DAPI in exNSC- and hiPSC-derived cultures. (D) Representative recordings of typical evoked firing from exNSC- and hiPSC-derived neurons (D21 post plating). (E) The proportion of neurons that fired no AP, a single AP or multiple APs was significantly different in exNSC- and hiPSC-derived neurons ($p < 0.0001$,chi-square test, n = 22 exNSC-derived neurons and n = 26 hiPSC-derived neurons recorded at D21 post plating).

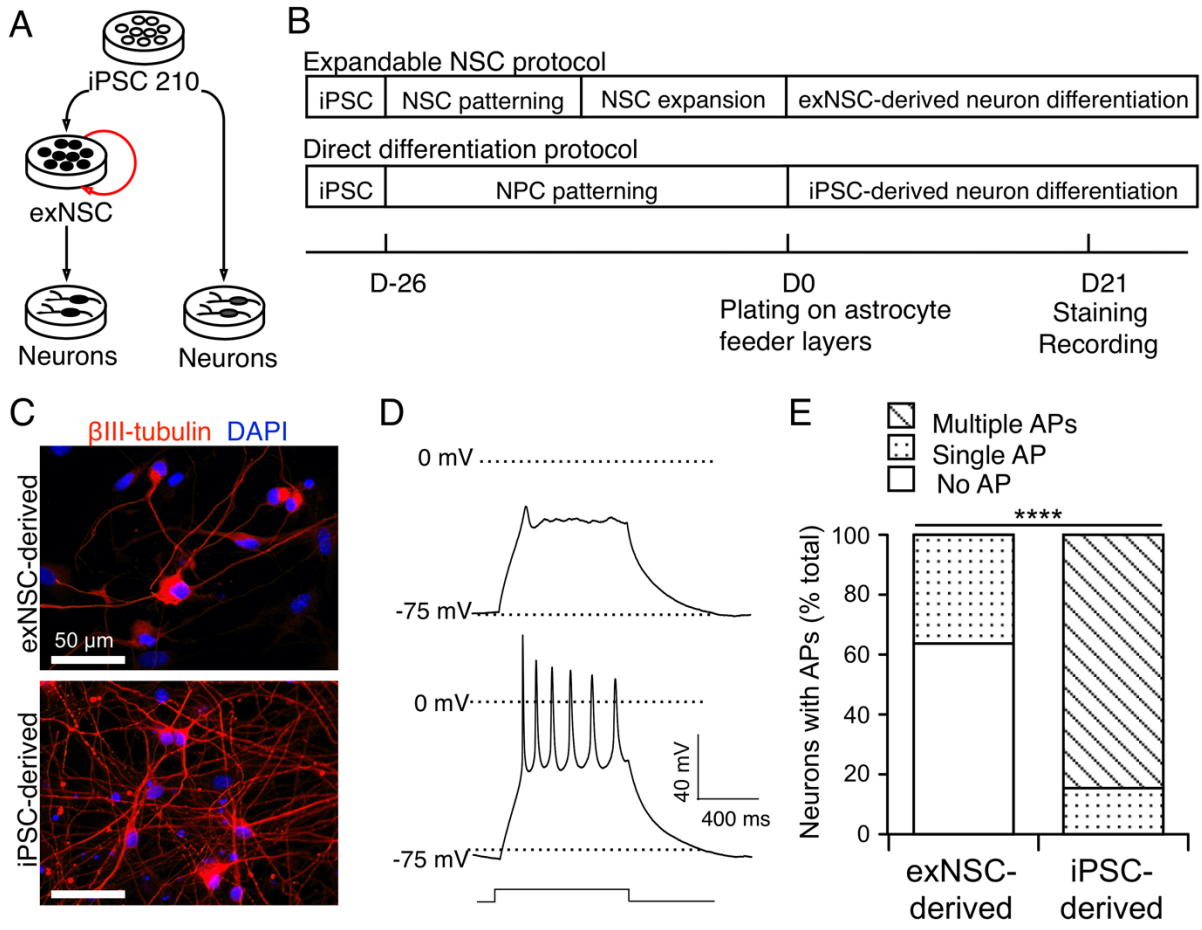

Table III.1. Passive membrane properties of neurons generated by an expandable NSC protocol and a direct differentiation protocol.

	exNSC-derived neurons	hiPSC-derived neurons
R_m (GΩ)	1.9 ± 2	1.8 ± 1.0
RMP (mV)	-59 ± 12	-57 ± 10
C_m (pF)	12 ± 4	32 ± 7***

Data reported as mean ± SD. *** represents $p < 0.0001$, unpaired *t*-test with Welch's correction. n = 22 for exNSC-derived neurons and 26 for hiPSC-derived neurons.

3.3.2 Direct differentiation protocol produces primarily neurons

Since the direct differentiation protocol results in a faster maturation of functionally active neurons than the exNSC protocol, the remainder of this work focuses on cultures prepared by direct differentiation. To determine if the hiPSCs give rise to astroglial cells as well as neurons we prepared cultures from the 210 line and from a second hiPSC control line (173) from an unrelated donor with no known neurological disorders. Cultures were fixed and immunostained at 3 weeks post plating. As hiPSC-derived NPCs are plated onto astrocyte feeder layers of mouse origin, human derived cells were identified by immunostaining with HuNu, a marker for human nuclei. HuNu positive cells that were also positive for the neuronal maker βIII-tubulin had classic neuronal morphology with branched neuritic processes and cell bodies that appeared to have volume in DIC optics (white arrows indicate the cell body of one neuron on both the overlay panel and the DIC panel for each cell line in **Figure III.2A**). There was also a small population of cells with irregularly shaped, flattened cell bodies that expressed HuNu but were not β-III tubulin positive (light blue arrowhead indicates one non-neuronal cell, on overlay panel and DIC panel for each cell line in **Figure III.2A**). When cultures were immunostained with antibodies of HuNu and GFAP, a small population of flattened, irregularly shaped cells were positive for both, identifying these as hiPSC derived astroglia (orange arrowhead indicates one astroglial cell for each cell line in **Figure III.2C**). The mouse astroglial cells in the feeder layer were identified as the DAPI positive, HuNu negative cells stained with GFAP. Quantitative analysis on 3 individual coverslips from 2 independent platings from both control lines revealed 98% of the human-derived cells were neurons and 2% were astroglia ($p > 0.75$, unpaired *t*-test with Welch's correction, **Figure III.2B and D**). These

data demonstrate that two independent control lines both give rise to predominantly neurons using the direct differentiation protocol.

Figure III.2. Direct differentiation of hiPSCs results in primarily neurons. (A) Immunostaining of control 210 and 173 hiPSC-derived cultures by DAPI, HuNu and βIII-tubulin antibodies at 3 weeks post plating. HuNu positive, βIII-tubulin positive cells are indicated by white arrows. HuNu positive, βIII-tubulin negative cells indicated by light blue arrowheads. (B) The proportion of hiPSC-derived neurons in cultures of control 210 and 173 at 3 weeks post plating. (C) Immunostaining of control 210 and 173 hiPSC-derived cultures by DAPI, HuNu and GFAP antibodies at 3 weeks post plating. HuNu positive, GFAP positive cells are indicated by orange arrowheads. $DAPI^{+}$ $HuNu^{-}$ identifies nuclei of mouse cells in the feeder layers that are enriched for astrocytes stained by GFAP. (D) The proportion of hiPSC-derived astrocytes in cultures of control 210 and 173 at 3 weeks post plating. Data represented as mean + s.e.m. Three coverslips from each of the two individual platings of each line were included. No significant difference in the percentage of hiPSC-derived neurons and astrocytes in the two lines, $p > 0.75$, unpaired *t*-test with Welch's correction.

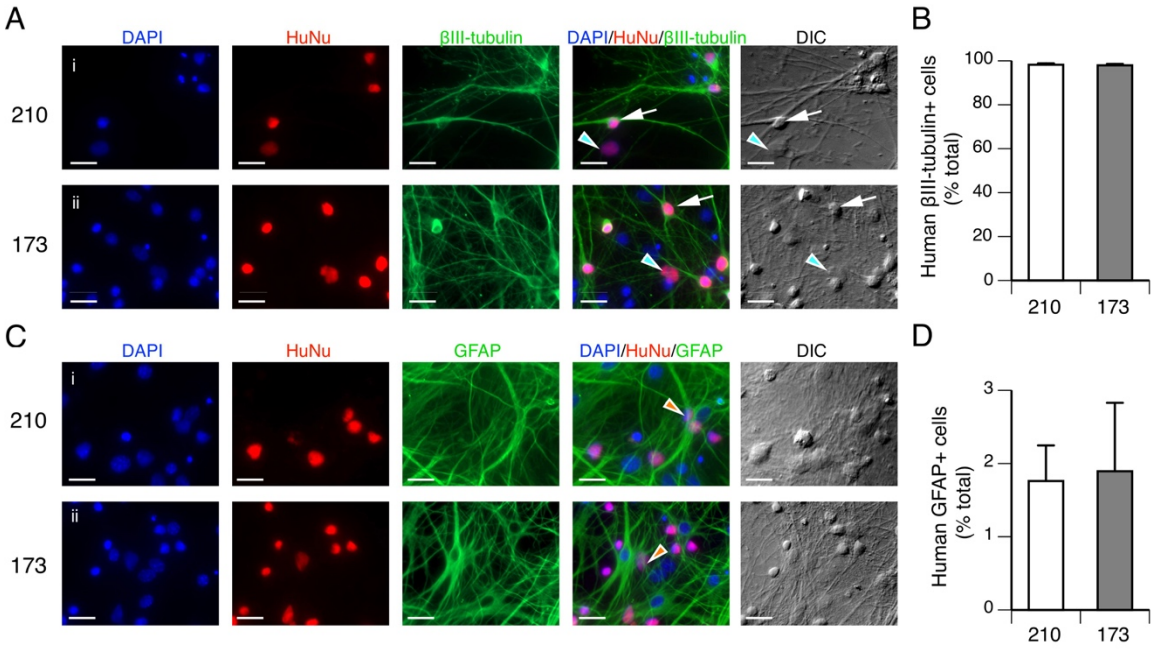

3.3.3 Intrinsic firing properties of hiPSC-derived neurons evaluated in multiple platings from two independent control hiPSC lines.

To evaluate the rate of neuronal maturation and determine if this is consistent across multiple platings from one hiPSC line and between different hiPSC lines, we generated neuronal cultures prepared from two control hiPSC lines (210 and 173) using the direct differentiation protocol. Multiple independent platings of each hiPSC line were evaluated over the course of 5 weeks post plating. All firing properties are presented as averages from 4 or more platings, with n representing number of platings. There were 5 or more individual neurons examined in each plating at each time point.

Cultures from both lines contained cells with βIII-tubulin positive neurites and the degree of neurite complexity increased with time in culture (**Figure III.3A**). The cultures also contained cells that fired action potentials in response to depolarizing current injections as early as D4-5 post plating and at each time point examined up through D35-38 post plating (**Figure III.3B**). Quantitative analysis of evoked firing focused on three properties: the percentage of cells capable of firing at least one AP (**Figure III.3C**), percentage of cells firing repetitively (2 or more APs) (**Figure III.3D**) and the average peak evoked firing frequency (**Figure III.3E**). There was a significant increase in all three properties as a function of time in culture in both cell lines (age effect: $p < 0.0001$; two-way ANOVA; **Figures III.3C-E**). The variance between plating was the lowest for the percentage of cells firing at least one AP as evidenced by the smaller error bar representing standard deviation (**Figure III.3C**). The highest variance between platings was seen in percentage of cells firing repetitively and firing frequencies, most prominently at the intermediate time periods between D10 and D23 post plating (**Figure III.3D and E**). However, there was no

difference in any of these properties between the control lines (cell line effect: $p > 0.98$, $p > 0.10$, $p > 0.17$, respectively; **Figures III.3C-E**; **Table III.3**).

Taken together, these data demonstrate that the direct differentiation protocol reliably produces cultures from hiPSCs in which a high percentage of cells with neuronal morphology are electrically excitable and the rate of maturation of firing properties is similar from plating to plating.

Figure III.3. Intrinsic firing properties of hiPSC-derived neurons mature at a similar rate from plating to plating in control lines, and between control hiPSC lines 210 and 173. (A) Immunostaining with βIII-tubulin antibody and DAPI on neurons derived from control hiPSC 210 and 173 at D4-5 and D21-23 post plating. (B) Representative traces of action potentials evoked in control hiPSC 210- and 173-derived neurons in response to a 600ms depolarizing current pulse at five recording windows between 4 and 38 days post plating. (C) The percentage of neurons capable of evoked firing, (D) repetitive firing (more than 2 APs) and (E) the peak firing frequency as a function of age. Data are reported as mean + SD. Number of individual platings at each time window from 2 lines is reported in the bottom of C-E with number of neurons in parentheses. All three properties were significantly different as a function of age (two-way ANOVA with *post hoc* Bonferroni test, results in Table 3). a, b, c and d denote significance from D10-11, D15-16, D21-23 and D35-38 post plating respectively within the same line. Numbers next to the letters represent degrees of significance with 1, 2, 3 and 4 denoting p value < 0.05, 0.01, 0.001 and 0.0001 respectively. There was no significant difference between cell lines (Table III.3).

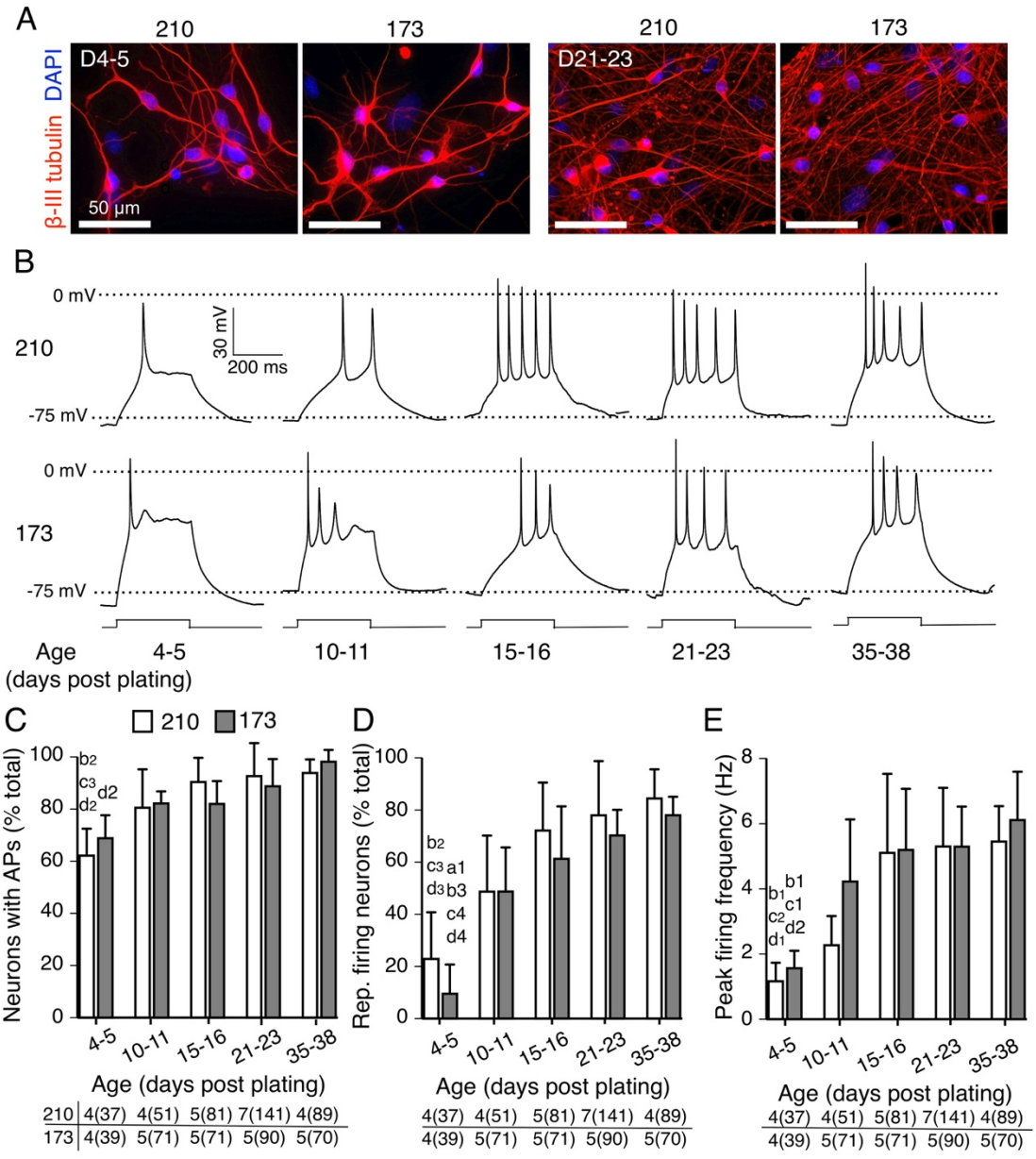
A
210
173
210
173
D4-5
D21-23
β-III tubulin DAPI
50 μm
B
0 mV
210
30 mV
200 ms
-75 mV
0 mV
173
-75 mV
Age
(days post plating)
4-5
10-11
15-16
21-23
35-38
C
210
173
Neurons with APs (% total)
Age (days post plating)
210 4(37) 4(51) 5(81) 7(141) 4(89)
173 4(39) 5(71) 5(71) 5(90) 5(70)
D
Rep. firing neurons (% total)
Age (days post plating)
4(37) 4(51) 5(81) 7(141) 4(89)
4(39) 5(71) 5(71) 5(90) 5(70)
E
Peak firing frequency (Hz)
Age (days post plating)
4(37) 4(51) 5(81) 7(141) 4(89)
4(39) 5(71) 5(71) 5(90) 5(70)

3.3.4 Formation of spontaneously active networks of excitatory and inhibitory cells

Neurons in both the control 210 and 173 cultures exhibited spontaneous firing patterns that were classified as irregular tonic firing with single spikes (**Figure III.4Ai and ii**) or burst firing (≥ 2 sAPs within a single depolarization) (**Figure III.4Aiii and iv**). In the absence of applied holding current a small percentage of hiPSC-derived neurons from both lines fired spontaneously in one of the two patterns as early as D4-5 post plating and this increased significantly as a function of age in culture ($p < 0.0001$; two-way ANOVA with *post hoc* Bonferroni test; **Figure III.4B**). In the control 210 cultures, the percentage of hiPSC-derived neurons firing spontaneously continued to increase steadily until D35-38. In contrast, in the control 173 derived neurons, there was no further increase in the percentage of cell firing spontaneously beyond D15-16 and this property was significantly different between the two control lines at the later time points (age effect: $p < 0.0001$; two-way ANOVA; **Figure III.4B**; **Table III.3**). About half of the spontaneously firing cells were spontaneously burst firing in both lines. The percentage of cells exhibiting burst firing significantly increased with age ($p < 0.001$; two-way ANOVA) and there was no significant difference between lines (cell line effect: $p > 0.63$; two-way ANOVA with *post hoc* Bonferroni test**; Figure III.4C**; **Table III.**3). When compared to evoked firing, spontaneous firing was marked by greater variability between platings within each line, indicated by larger standard deviations.

Figure III.4. hiPSC-derived neurons in both 210 and 173 lines are spontaneously active. (A) Spontaneous firing patterns classified as irregular tonic firing (i and ii) or burst firing (iii and iv) in hiPSC 210- and 173-derived neurons. RMP is indicated at the baseline of each trace. (B) The percentage of neurons exhibiting spontaneous firing (C) or the subset with burst firing (D) at 5 time windows over 5 weeks. Data are represented as mean + SD. Number of individual platings at each time window from 2 lines is reported in the bottom of B and C with number of neurons in parentheses. Two-way ANOVA (results in **Table III.3**) with *post hoc* Bonferroni test. c and d denote significance from D21-23 and D35-38 post plating respectively within the same line. Numbers next to the letters represent degree of significance with 1 and 2 denoting p value < 0.05 and 0.01 respectively.

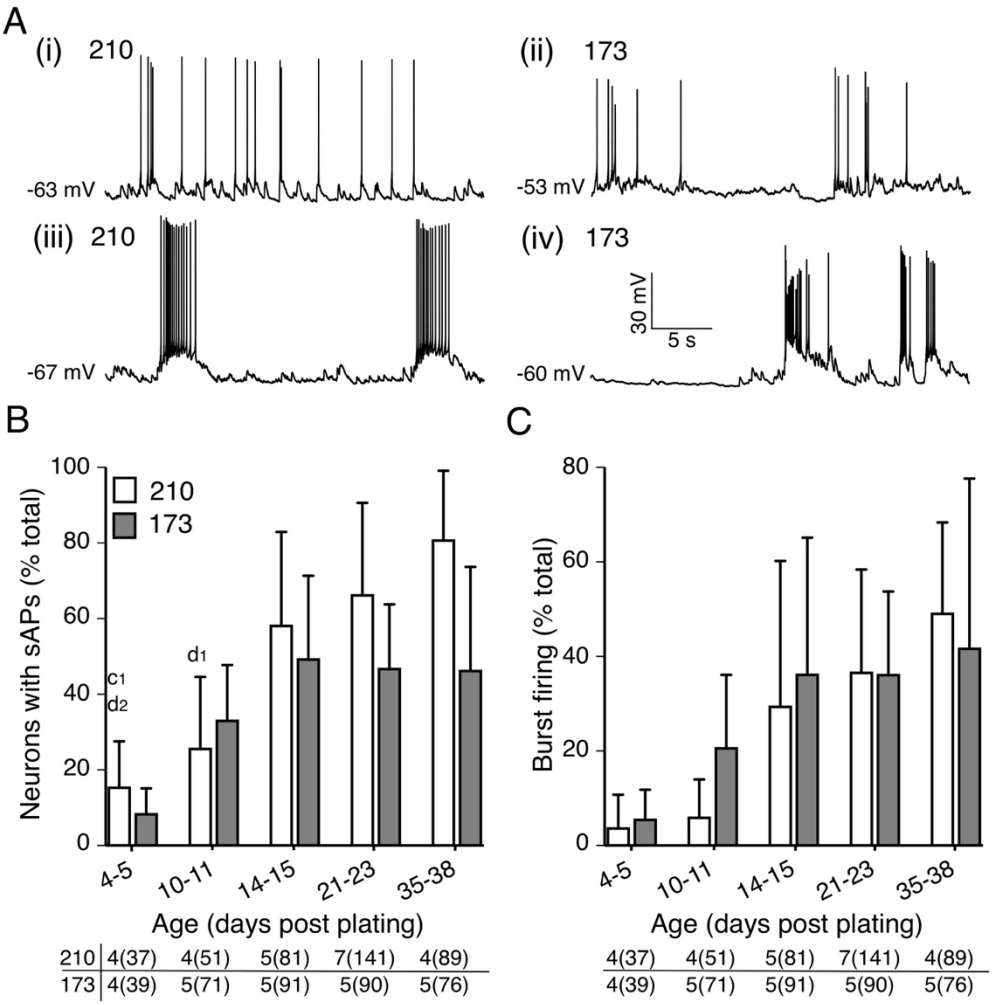

210	4(37)	4(51)	5(81)	7(141)	4(89)
173	4(39)	5(71)	5(91)	5(90)	5(76)

4(37)	4(51)	5(81)	7(141)	4(89)	
4(39)	5(71)	5(91)	5(90)	5(76)	

Spontaneous synaptic activity was also observed in neurons derived from both control hiPSC lines (**Figure III.5A**). To quantify the degree of synaptic connectivity, the percentage of neurons with spontaneous PSPs or PSCs was determined at a holding potential of -75 mV. Over 40% of cells from both control hiPSC lines had detectable sPSP and/or sPSCs at the earliest time point, D4post plating (**Figure III.5B**). Assessment of the sPSC frequency demonstrated a steady and significant increase from 0.02 Hz for D4-5 cells to a mean of 4-5 Hz by D35-38 post plating (age effect: $p < 0.001$; two-way ANOVA with *post hoc* Bonferroni test; **Figure III.5C**). The variance in this property between platings became larger over time, with the greatest variance at D35-38 post plating when the sPSC frequencies ranged from 1 to 13 Hz. There was no significant difference between the control lines in the percentage of cells with spontaneous synaptic input or the sPSC/P frequency (cell line effect: $p > 0.13$ and $p > 0.85$, respectively; two-way ANOVA with *post hoc* Bonferroni test; Figures **III.5B and C**).

A subpopulation of neurons derived from control hiPSC line 210 and 173 was examined to determine the identity of the receptors mediating synaptic transmission. At the reversal potential for chloride mediated currents (-49 mV), all of the fast decaying currents were completely blocked by 50 μM APV and 10 μM CNQX, indicating they were spontaneous excitatory postsynaptic currents (sEPSC) mediated by AMPA and NMDA receptors (**Figure III.5D**). At the reversal potential for glutamatergic currents (-2 mV), the large majority of slow decaying currents were blocked by a $GABA_A$ receptor antagonist BMC in 10 μM. A small percentage was insensitive to BMC, but could be blocked by an antagonist of glycine receptors

strychnine in 100 nM (**Figure III.5D**). This suggests the cultures from both lines contain a predominantly glutamatergic neurons and GABAergic neurons, and a small proportion of glycinergic neurons. Over 75% of neurons derived from hiPSC lines 210 and 173 received both excitatory and inhibitory synaptic input at day 21-23 post plating, demonstrating a functional neural network with both excitation and inhibition ($p=0.16$, chi-square test; **Figure III.5E**).

Figure III.5. Functionally active networks of synaptically connected excitatory and inhibitory cells in cultures from both control hiPSC lines. (A) Representative traces of sPSCs in neurons derived from control hiPSC lines 210 and 173. Holding potential -75 mV. (B) The percentage of neurons exhibiting sPSCs as a function of age in culture. (C) Developmental increase in sPSC frequency in neurons from control hiPSC 210 and 173. Data are reported as mean + SD. Number of individual platings at each time window from 2 lines is reported in the bottom of B and C with number of neurons in parenthesis. Two-way ANOVA with *post hoc* Bonferroni test (results in **Table III.3**). b, c, and d denote significance from D15-16, D21-23 and D35-38 post plating, respectively, within the same line. Numbers next to the letters represent degrees of significance with 1 and 2 denoting p value < 0.05 and 0.01 respectively. (D) Characterization of sEPSCs at the presence of glutamate receptor blockers APV and CNQX at -49 mV and sIPSCs at the presence of $GABA_A$ receptor blocker BMC and glycine receptor blocker strychnine at -2 mV in neurons from 210 (top) and 173 (bottom) lines at D21-23 post plating. (E) Proportion of neurons from 210 and 173 hiPSC lines with both sEPSCs and sIPSCs at D21-23 post plating. n= 25 and 27 neurons from 210 and 173 respectively.

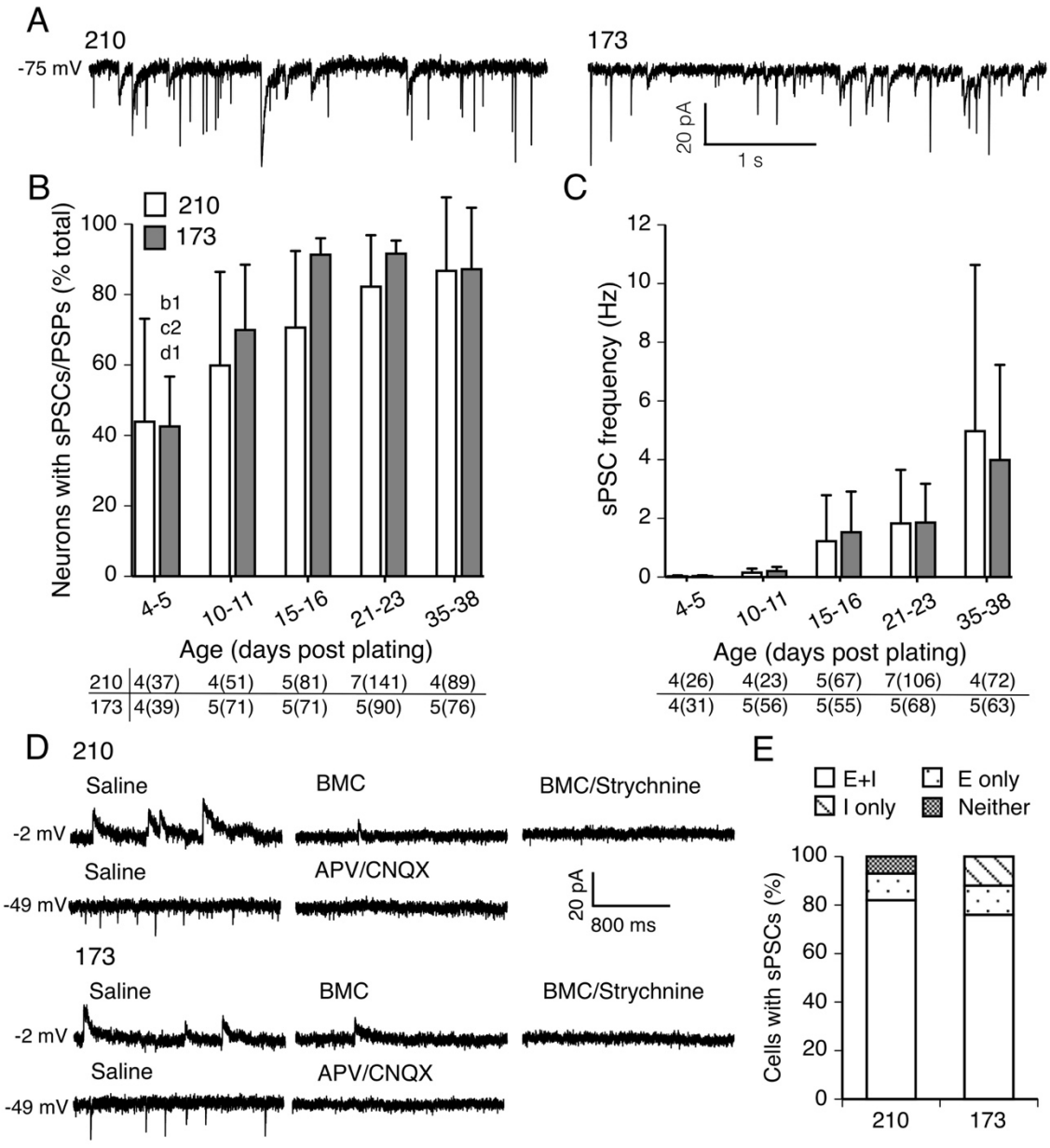
A
210
-75 mV
173
20 pA
1 s
B
210
173
Neurons with sPSCs/PSPs (% total)
b1
c2
d1
4-5
10-11
15-16
21-23
35-38
Age (days post plating)
210 4(37) 4(51) 5(81) 7(141) 4(89)
173 4(39) 5(71) 5(71) 5(90) 5(76)
C
sPSC frequency (Hz)
Age (days post plating)
4(26) 4(23) 5(67) 7(106) 4(72)
4(31) 5(56) 5(55) 5(68) 5(63)
D
210
Saline
BMC
BMC/Strychnine
-2 mV
Saline
APV/CNQX
-49 mV
20 pA
800 ms
173
Saline
BMC
BMC/Strychnine
-2 mV
Saline
APV/CNQX
-49 mV
E
E+I
E only
I only
Neither
Cells with sPSCs (%)
210
173

There was a steady decrease in input resistance over time between 2 and 5 weeks in culture and this property was similar between the two lines (**Table III.2**). In both the 210 and 173 hiPSC-derived neurons the mean whole cell capacitance increased steadily over time and there was no change in the resting membrane potential (C_m age effect: $p < 0.0001$; RMP age effect: $p > 0.18$; two-way ANOVA with *post hoc* Bonferroni test; Table 2; **Table III.3**). Although a two-way ANOVA identified that the resting membrane potential was slightly more hyperpolarized in 210 compared to 173 (cell line effect: $p < 0.05$; two-way ANOVA); subsequent *post hoc* analyses were unable to resolve any significant time points between lines (**Table III.2**; **Table III.3**). The whole cell capacitance was larger in 210 cells (cell line effect: $p < 0.0001$; two-way ANOVA with *post hoc* Bonferroni test), and this was significant at D15-16 and D21-24 post plating (**Table III.2**; **Table III.3**). Overall, these data demonstrate that the direct differentiation protocol results in a rate and degree of maturation in excitability and synaptic transmission that is consistent from plating to plating, and similar for most properties examined between two different control hiPSC lines.

Table III.2. Passive membrane properties of directly differentiated neurons from control hiPSC line 210 and 173.

	Line	Days post-plating 4-5	10-11	15-16	21-24	35-38
R_m (GΩ)	210	2.6 ± 0.4 4(36)	2.5 ± 0.2 5(51)	2.2 ± 0.4 5(81)	1.6 ± .0.5 7(131)	1.4 ± 0.4 4(101)
	173	2.7 ± 0.6 4(39)	2.3 ± 0.4 6(47)	1.9 ± 0.3 6(48)	1.7 ± 0.2 6(65)	1.2 ± 0.2 6(52)
RMP (mV)	210	-53.5 ± 8.4 4(36)	-50.8 ± 6.4 5(51)	-55.1 ± 4.5 5(81)	-54.1 ± 3.6 7(131)	-53.4 ± 4.1 4(101)
	173	-50.2 ± 2.3 4(39)	-50.0 ± 3.2 6(47)	-54.7 ± 5.0 6(48)	-50.1 ± 2.5 6(65)	-48.6 ± 2.7 6(52)
C_m (pF)	210	25.5 ± 3.0 4(36)	25.2 ± 3.2 5(51)	33.0 ± 5.2[a] 5(81)	37.0 ± 8.5[b] 7(131)	43.5 ± 15.9 4(101)
	173	15.1 ± 1.8 4(31)	19.0 ± 2.2 6(58)	19.1 ± 3.2[a] 6(50)	23.4 ± 1.8[b] 6(63)	34.4 ± 3.7 6(69)

Data reported as Mean ± SD with number of individual platings (total number of neurons).
[a]$p < 0.01$, [b]$p < 0.001$, denotes significance between cell lines at given time point post plating (two-way ANOVA with Bonferroni *post hoc* test).

Table III.3. Summary of two-way ANOVA statistical analyses on directly differentiated neurons from control hiPSC line 210 and 173.

	Age	Line	Interaction
Evoked firing (% total)	**** ($p < 0.0001$)	ns ($p = 0.98$)	ns ($p = 0.40$)
Multiple firing (% total)	**** ($p < 0.0001$)	ns ($p = 0.10$)	ns ($p = 0.92$)
Firing frequency	**** ($p < 0.0001$)	ns ($p = 0.17$)	ns ($p = 0.59$)
sAP (% total)	**** ($p < 0.0001$)	* ($p = 0.03$)	ns ($p = 0.22$)
Burst sAP (% total)	** ($p = 0.0014$)	ns ($p = 0.63$)	ns ($p = 0.84$)
sPSC/PSPs (% total)	**** ($p < 0.0001$)	ns ($p = 0.13$)	ns ($p = 0.67$)
sPSC frequency	*** ($p = 0.0004$)	ns ($p = 0.85$)	ns ($p = 0.97$)
R_m	**** ($p < 0.0001$)	ns ($p = 0.33$)	ns ($p = 0.55$)
RMP	ns ($p = 0.18$)	* ($p = 0.04$)	ns ($p = 0.72$)
C_m	**** ($p < 0.0001$)	**** ($p < 0.0001$)	ns ($p = 0.53$)

Two-way ANOVA utilized to examine effects of age (days post plating), cell line identity, and interaction between both. *, **, ***, and **** reflect $p < 0.05$, 0.01, 0.001 and 0.0001 respectively.

3.3.5 Identification of GABAergic neurons

The observation of both glutamatergic and GABAergic synaptic currents indicated that despite the use of ventralizing factors our protocol supports differentiation of excitatory and inhibitory neurons. To quantify the percentage of total hiPSC-derived neurons that are GABAergic, cultures were fixed at D21-23 and stained with anti-βIII-tubulin and anti-GABA antibodies (**Figure III.6A**). Approximately 30% of the neurons were GABA-positive and there was no significant difference in the percent of total neurons that were GABA-positive in the 210 and 173 hiPSC-derived neuronal cultures ($p > 0.14$, unpaired *t*-test with Welch's correction; **Figure III.6B**). These data in conjunction with the synaptic current recordings confirm that our direct differentiation protocol produced mixed cultures with both inhibitory GABAeric and excitatory glutamatergic neurons.

Figure III.6. Cultures from 210 and 173 contain a similar percentage of GABAergic neurons. (A) Cultures differentiated from the control 210 and 173 hiPSC-derived neurons were stained with nuclei marker DAPI, βIII-tubulin and GABA antibodies to identify GABAergic neurons at D21 post plating. (B) The proportion of GABAergic neurons in neuronal cultures of control 210 and 173 at D21 post plating. Data represented as mean + s.e.m. Number of coverslips from each line indicated on the graph. There was no significant difference in the percentage of GABAergic neurons in the two lines, $p > 0.14$, unpaired *t*-test with Welch's correction.

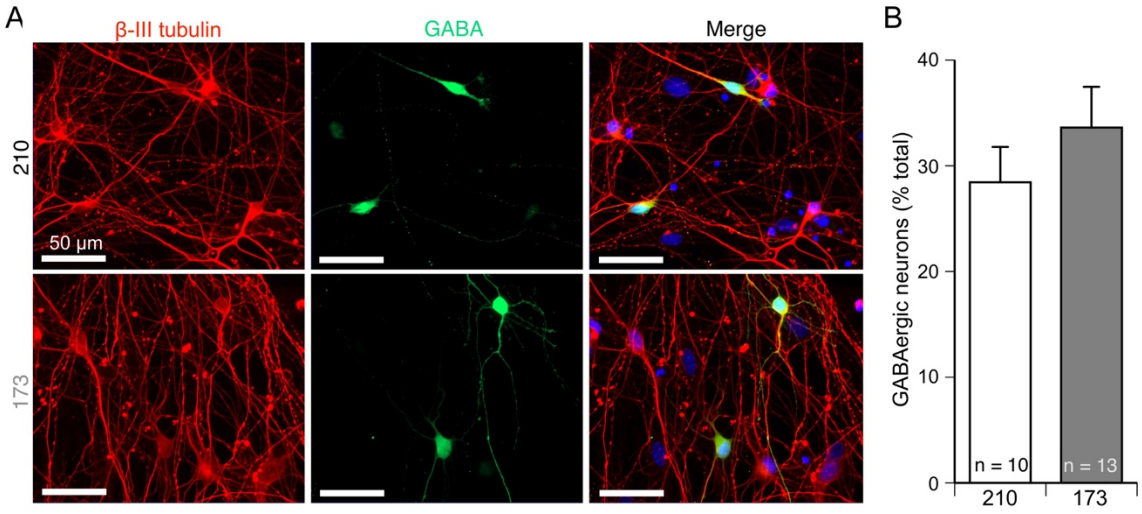

3.4. Discussion

3.4.1 Difference in maturation of excitability in expandable intermediate population vs direct differentiation

In our study, neurons generated by the direct differentiation protocol were more electrically excitable than the expandable NSC-derived neurons over the first 5 weeks of neuronal differentiation. From previous studies in our lab we know that neurons in cultures from expandable NSCs at later times are able to develop repetitive firing properties[15]. Another study using expandable NPC-derived neurons also reported an extended timeline of maturation, with the large majority of the cells capable of firing multiple action potentials in NPC cultures by 6 weeks post plating[29]. Therefore, it is likely that at least some of the difference between the expandable NSC or NPC strategy versus the direct differentiation protocol is the rate as opposed to capacity for maturation. A recent study predicting functional states of expandable NPC-derived neurons with RNA-seq and electrophysiology reports a decline in degree of maturation with increased passage number of the intermediate population[30]. However, by day 30 post plating, the differentiation of excitability and synaptic activity in the neurons was similar to neurons generated by the direct differentiation in the present paper. Enhanced neuronal function observed in the Bardy study may be due to the BrainPhys growth medium that has been shown to support action potential firing and synaptic transmission in hiPSC-derived neurons[31]. Future studies will be important to determine if the BrainPhys medium can further increase the rate and/or the degree of maturation in directly differentiated neurons.

*3.4.2 Reproducibility in rate/degree of functional maturation between platings and b*etween *hiPSC lines*

The direct differentiation protocol results in a high percentage of functionally active cells in each plating from two different hiPSC lines. However, there were differences in the degrees of variance and in the rate of maturation between properties. In general, hiPSC-derived neurons from both lines exhibited a lower degree of variability in evoked firing vs spontaneous activity at each time point. This suggests that, in order to identify functional changes associated with a specific mutation, the direct differentiation protocol is better suited to resolving differences in intrinsic excitability, and small differences in spontaneous firing or synaptic transmission will require a larger number of trials establish significance[4,6,32,33].

The control lines in the present study were from donors of different ages, 23 and 56. The similarly high percentage of neurons to glial cells derived from both hiPSCs lines in the direct differentiation protocol suggest donor age does not affect the efficiency of producing neuronal cells. This is consistent with a previous study using a different differentiation protocol demonstrating donor age did not influence the percentage of hiPSC-derived cells positive for ISL, a motor neuron marker[34]. In addition, while donor age does not appear to influence the rate/degree of the majority of functional properties examined we cannot rule out the possibility that donor age affects the two properties that were different between the line: maturation of the percentage of cells firing spontaneous action potentials and resting membrane potential. It would be interesting to systematically study the effect of age on functional development of neurons using multiple iPSCs lines.

Whole-cell capacitance increased steadily as a function of age in neurons derived from both cell lines. However, while the 173 vs the 210 derived neurons had a smaller capacitance at each time point, indicative of lower total membrane surface area, the differentiation of functional properties was comparable. This indicates that cell size in this case is not highly correlated with functional differentiation. In addition the difference in whole cell capacitance does not appear to be a property of the specific hiPSC cell line because a set of neurons derived from the 173 line in our previous study had capacitance values similar to those of the 210 line in the current study[28]. One possibility is that a variance in the size of embryoid bodies and neurospheres during the initial phase of patterning, could affect exposure to morphogens and result in variance in the starting cell size. This could be further examined using Aggrewell™ plating methods to control the size of embryoid bodies by plating a similar amount of dissociated cells into pocket-like microwells[35].

3.4.3 Neuronal subtypes in culture

The ability to generate well-defined, populations of excitatory or inhibitory neurons is an important prerequisite for use of pluripotent stem cells in human transplantation studies. A recent study demonstrated that exposure to different levels of purmorphamine can produce nearly pure yields of glutamatergic, GABAergic, or medium spiny neurons[36]. Having precise control over the terminal phenotype of grafted cells bypasses concerns of unintended integration of other subtypes and can balance excitatory and inhibitory neuronal network activity in the recipient[37–39]. Therefore it was surprising that only 30-40% of the neurons generated in the direct differentiation protocol were GABAergic, using a concentration of SMAD inhibitors and purmorphamine that in other similar protocols

yielded cultures in which 80-90% of the neurons were GABAergic[13,20,36]. This difference could have arisen from variations in the size of embryoid bodies and neuroepithethelial tissue generated during the patterning process, in which the generation of distinct morphogen gradients may contribute to regional specification of neurons[40]. Another difference could have arisen from the use of astroglial feeder layers for the differentiation phase in the present study. Previous studies have shown that astrocytes are important for regulating the microenvironment of differentiating neurons through cell-cell contact and secreted factors[41,42].

There are important advantages in having mixed cultures of excitatory and inhibitory neurons for disease modeling. First, the mix of functional glutamatergic and GABAergic neurons more accurately reflects a native neural network, with the number of excitatory cells outnumbering GABAergic. Second, both excitatory and inhibitory inputs are essential for maintaining a stable E/I ratio in neurons, which play an important role in cortical functions in mammalian cerebral cortex[43]. Imbalance of E/I is associated with epilepsy, autism and fragile X syndrome[44,45]. Therefore, generating neuronal cultures with both excitatory and inhibitory neurons, instead of pure population of certain cell types, facilitates understanding in the altered relationship of E/I in the disease models *in vitro*.

In conclusion, direct differentiation of neurons from hiPSC lines resulted in the reproducible and efficient generation of electrophysiologically active neuronal cultures from independent donors. The establishment of baseline parameters concerning the development and maturation of derived neurons is critical for interpretation of data obtained using this rapidly evolving platform. In particular, for investigations utilizing non-isogenic iPSC lines from affected individuals and related (or unrelated) controls, a quantitative characterization

of electrophysical properties and their variation resulting from the selected differentiation protocol is required. The functional outcomes of the differentiation protocol utilized in this study establishes a platform for the identification of mutational or drug-induced functional alternations, which is at the core of pre-clinical disease modeling.

3.5 Bibliography

1. Brennand, K. J. & Gage, F. H. Concise review: the promise of human induced pluripotent stem cell-based studies of schizophrenia. *Stem Cells* **29**, 1915–1922 (2011).
2. Brennand, K. J. *et al.* Modelling schizophrenia using human induced pluripotent stem cells. *Nature* **473**, 221–225 (2011).
3. Chiang, C.-H. *et al.* Integration-free induced pluripotent stem cells derived from schizophrenia patients with a DISC1 mutation. *Molecular psychiatry* **16**, 358–360 (2011).
4. Devlin, A.-C. *et al.* Human iPSC-derived motoneurons harbouring TARDBP or C9ORF72 ALS mutations are dysfunctional despite maintaining viability. *Nat. Commun.* **6**, 5999 (2015).
5. Kim, K.-Y., Hysolli, E. & Park, I.-H. Neuronal maturation defect in induced pluripotent stem cells from patients with Rett syndrome. *Proc. Natl. Acad. Sci. U. S. A.* **108**, 14169–14174 (2011).
6. Liu, J. *et al.* CRISPR/Cas9 facilitates investigation of neural circuit disease using human iPSCs: mechanism of epilepsy caused by an SCN1A loss-of-function mutation. *Transl Psychiatry* **6**, e703 (2016).
7. Sun, Y. *et al.* A deleterious Nav1.1 mutation selectively impairs telencephalic inhibitory neurons derived from Dravet Syndrome patients. *Elife* **5**, e13073 (2016).
8. Sun, Y. *et al.* Properties of neurons derived from induced pluripotent stem cells of Gaucher disease type 2 patient fibroblasts: potential role in neuropathology. *PLoS One* **10**, e0118771 (2015).
9. Robicsek, O. *et al.* Abnormal neuronal differentiation and mitochondrial dysfunction in hair follicle-derived induced pluripotent stem cells of schizophrenia patients. *Mol. Psychiatry* **18**, 1067–1076 (2013).
10. Marchetto, M. C. N. *et al.* A model for neural development and treatment of Rett syndrome using human induced pluripotent stem cells. *Cell* **143**, 527–539 (2010).
11. Yang, N., Ng, Y. H., Pang, Z. P., Südhof, T. C. & Wernig, M. Induced Neuronal Cells: How to Make and Define a Neuron. *Cell Stem Cell* **9**, 517–525 (2017).
12. Maroof, A. M. *et al.* Directed differentiation and functional maturation of cortical interneurons from human embryonic stem cells. *Cell Stem Cell* **12**, 559–572 (2013).
13. Nicholas, C. R. *et al.* Functional maturation of hPSC-derived forebrain interneurons requires an extended timeline and mimics human neural development. *Cell Stem Cell* **12**, 573–586 (2013).

14. Srikanth, P. & Young-Pearse, T. L. Stem cells on the brain: modeling neurodevelopmental and neurodegenerative diseases using human induced pluripotent stem cells. *J. Neurogenet.* **28**, 5–29 (2014).
15. Stover, A. E. *et al.* Process-based expansion and neural differentiation of human pluripotent stem cells for transplantation and disease modeling. *J. Neurosci. Res.* **91**, 1247–1262 (2013).
16. Brafman, D. A. Generation, Expansion, and Differentiation of Human Pluripotent Stem Cell (hPSC) Derived Neural Progenitor Cells (NPCs). *Methods Mol. Biol.* **1212**, 87–102 (2015).
17. Yan, Y. *et al.* Efficient and rapid derivation of primitive neural stem cells and generation of brain subtype neurons from human pluripotent stem cells. *Stem Cells Transl. Med.* **2**, 862–870 (2013).
18. Hartfield, E. M. *et al.* Physiological Characterisation of Human iPS-Derived Dopaminergic Neurons. *PLoS One* **9**, e87388 (2014).
19. Liu, Y. *et al.* Dravet syndrome patient-derived neurons suggest a novel epilepsy mechanism. *Ann. Neurol.* **74**, 128–139 (2013).
20. Liu, Y. *et al.* Directed differentiation of forebrain GABA interneurons from human pluripotent stem cells. *Nat. Protoc.* **8**, 1670–1679 (2013).
21. Mertens, J. *et al.* Differential responses to lithium in hyperexcitable neurons from patients with bipolar disorder. *Nature* **527**, 95–99 (2015).
22. Prè, D. *et al.* A time course analysis of the electrophysiological properties of neurons differentiated from human induced pluripotent stem cells (iPSCs). *PLoS One* **9**, e103418 (2014).
23. Song, M., Mohamad, O., Chen, D. & Yu, S. P. Coordinated development of voltage-gated Na+ and K+ currents regulates functional maturation of forebrain neurons derived from human induced pluripotent stem cells. *Stem Cells Dev.* **22**, 1551–1563 (2013).
24. Zhang, Y. *et al.* Rapid single-step induction of functional neurons from human pluripotent stem cells. *Neuron* **78**, 785–798 (2013).
25. Brick, D. J. *et al.* The Autism Spectrum Disorders Stem Cell Resource at Children's Hospital of Orange County: Implications for Disease Modeling and Drug Discovery. *Stem Cells Transl. Med.* **3**, 1275–1286 (2014).
26. Stover, A. E. & Schwartz, P. H. Adaptation of Human Pluripotent Stem Cells to Feeder-Free Conditions in Chemically Defined Medium with Enzymatic Single-Cell Passaging. *Methods Mol. Biol.* **767**, 137–146 (2011).
27. Hilgenberg, L. G. W. & Smith, M. A. Preparation of Dissociated Mouse Cortical Neuron Cultures. *Journal of Visualized Experiments : JoVE* (2007). doi:10.3791/562
28. Schutte, R. J. *et al.* Astrocyte-enriched feeder layers from cryopreserved cells support differentiation of spontaneously active networks of human iPSC-derived neurons. *J. Neurosci. Methods* **294**, 91–101 (2018).
29. Tang, X. *et al.* Astroglial cells regulate the developmental timeline of human neurons differentiated from induced pluripotent stem cells. *Stem Cell Res.* **11**, 743–757 (2013).
30. Bardy, C. *et al.* Predicting the functional states of human iPSC-derived neurons with single-cell RNA-seq and electrophysiology. *Mol Psychiatry* **21**, 1573–1588 (2016).
31. Bardy, C. *et al.* Neuronal medium that supports basic synaptic functions and activity of human neurons in vitro. *Proc. Natl. Acad. Sci. U. S. A.* **112**, E2725-34 (2015).

32. Hu, B.-Y. *et al.* Neural differentiation of human induced pluripotent stem cells follows developmental principles but with variable potency. *Proc. Natl. Acad. Sci. U. S. A.* **107**, 4335–4340 (2010).
33. Kim, J.-E. *et al.* Investigating synapse formation and function using human pluripotent stem cell-derived neurons. *Proc. Natl. Acad. Sci. U. S. A.* **108**, 3005–3010 (2011).
34. Boulting, G. L. *et al.* A functionally characterized test set of human induced pluripotent stem cells. *Nat. Biotechnol.* **29**, 279–286 (2011).
35. Stover, A. E. & Schwartz, P. H. The generation of embryoid bodies from feeder-based or feeder-free human pluripotent stem cell cultures. *Methods Mol. Biol.* **767**, 391–398 (2011).
36. Yuan, F. *et al.* Efficient generation of region-specific forebrain neurons from human pluripotent stem cells under highly defined condition. *Sci. Rep.* **5**, 18550 (2015).
37. Cunningham, M. *et al.* Human PSC-derived maturing GABAergic interneurons ameliorate seizures and abnormal behavior in epileptic mice. *Cell stem cell* **15**, 559–573 (2014).
38. Fortin, J. M. *et al.* Transplantation of Defined Populations of Differentiated Human Neural Stem Cell Progeny. *Sci. Rep.* **6**, 23579 (2016).
39. Hunt, R. F., Girskis, K. M., Rubenstein, J. L., Alvarez-Buylla, A. & Baraban, S. C. GABA progenitors grafted into the adult epileptic brain control seizures and abnormal behavior. *Nat. Neurosci.* **16**, 692–697 (2013).
40. Suzuki, I. K. & Vanderhaeghen, P. Is this a brain which I see before me? Modeling human neural development with pluripotent stem cells. *Development* **142**, 3138–3150 (2015).
41. Berg, D. A., Belnoue, L., Song, H. & Simon, A. Neurotransmitter-mediated control of neurogenesis in the adult vertebrate brain. *Development* **140**, 2548–2561 (2013).
42. Chung, W.-S., Allen, N. J. & Eroglu, C. Astrocytes Control Synapse Formation, Function, and Elimination. *Cold Spring Harb. Perspect. Biol.* **7**, a020370 (2015).
43. Xue, M., Atallah, B. V & Scanziani, M. Equalizing excitation-inhibition ratios across visual cortical neurons. *Nature* **511**, 596–600 (2014).
44. Gibson, J. R., Bartley, A. F., Hays, S. A. & Huber, K. M. Imbalance of neocortical excitation and inhibition and altered UP states reflect network hyperexcitability in the mouse model of fragile X syndrome. *J. Neurophysiol.* **100**, 2615–2626 (2008).
45. Nelson, S. B. & Valakh, V. Excitatory/Inhibitory Balance and Circuit Homeostasis in Autism Spectrum Disorders. *Neuron* **87**, 684–698 (2017).

Chapter IV

Comparisons of dual isogenic human iPSC pairs identify functional alterations directly caused by an epilepsy associated *SCN1A* mutation

4.1. Introduction

Genetic epilepsy with febrile seizure plus (GEFS+) is a form of epilepsy with febrile seizures that persists beyond six years of age[1]. The clinical phenotype of GEFS+ is characterized by febrile seizures beginning in infancy that persist beyond 6 years of age and in some cases individuals also experience myoclonic, atonic and/or absence seizures[2]. Mutations in a variety of genes that encode ion channels and neurotransmitter receptors have been identified in individuals with GEFS+[3–12]. One hot spot for mutations causing GEFS+ is the *SCN1A* gene which encodes the alpha subunit of the Nav1.1 voltage-gated sodium channel. Approximately 50 missense mutations at locations throughout *SCN1A* are associated with different individuals diagnosed with GEFS+[13]. There are also multigenerational families in which individuals with the same *SCN1A* mutation exhibit a broad range of seizure phenotypes[14,15].

The heterogeneity of disease phenotypes arising from different mutations in the same gene, and from the same mutation between individuals complicates understanding of the underlying cellular mechanisms. Model systems that aid in mapping the links between individual *SCN1A* mutations and their cellular effects can facilitate development of more effective patient-specific drug therapies. Zebrafish, knock-in *Drosophila* and mouse models have all been important tools in this endeavor[16] but evolutionary distances leading to species-specific mechanisms may lead to failed therapies in patients[17,18].

In recent years, patient-derived induced pluripotent stem cells (iPSCs) that can be differentiated into neurons have emerged as a new model to explore how epilepsy-associated *SCN1A* mutations affect activity and sodium channel properties in human neurons. These studies have focused on mutations associated with Dravet syndrome (DS), a

form of epilepsy that is typically more severe than GEFS+. Previous studies in iPSC-derived neurons have shown that nonsense R1645X, and missense S1328P and Q1923R mutations in *SCN1A* associated with DS confer impaired excitability and reduced sodium current density in inhibitory neurons, giving rise to hyperactivity in neural networks[19–21]. However, examination of the DS-associated *SCN1A* missense mutations, Q1923R and F1415I, revealed increased excitability and increased sodium current amplitudes in excitatory neurons[22]. Further, the IVS14+3A>T mutation which causes truncation of DIIS2 and S3 of Nav1.1 affects both excitatory and inhibitory neurons[23].

In addition to alterations caused by discrete mutations, differences in genetic background represent a major source of variability that complicates interpretation of any experimental findings as they can influence phenotypic differences[24,25]. Evaluation of a large cohort of control and patient iPSC lines can help assess the contribution of mutations to disease phenotypes[26]. This is problematic when evaluating potential changes in electrophysiological properties that require examination at the single cell level in multiple cells from a large number of cell lines. However, a more direct way to examine the effect of a mutation independent of genetic background is to compare the cellular changes caused by a single mutation in isogenic pairs of control and mutant iPSC lines[20,26–29]. A recent study of the DS-associated *SCN1A* Q1923R mutation used transcription activator-like effector nucleases (TALENs) to generate an isogenic corrected line by removing the *SCN1A* mutation. Comparison of the isogenic corrected versus the patient line revealed a decrease in sodium current density in inhibitory neurons in the patient line. Comparison of the isogenic corrected line with a control line from a different genetic background revealed additional alterations in the voltage dependence of sodium current activation and action

potential (AP) threshold suggesting these might be associated with the genetic background of the patient. An isogenic mutant line in which the mutation had been introduced into the control would have been able to distinguish whether this was due to genetic background or interaction between the mutation and the genetic background.

The current study focuses on assessing the contribution of the autosomal dominant *SCN1A* K1270T mutation identified in a GEFS+ family to the etiology of the disease[14]. Two isogenic pairs of iPSC lines generated by CRISPR/Cas 9 gene editing were used: 1a) control (unaffected sibling), 1b) mutated control homozygous for the K1270T mutation, and 2a) patient heterozygous for the K1270T *SCN1A* mutation (GEFS+ sibling), 2b) corrected patient. All 4 iPSC lines in the two isogenic pairs can be differentiated into functional mixed neuronal cultures containing both GABAergic and glutamatergic neurons that expressed Nav1.1. Comparison of electrophysiological properties of neurons within and between pairs identified mutation-dependent alterations independent of genetic background. There were also differences found to be associated with the genetic background and others the result of interactions between the mutation and the background. Such CRISPR/Cas9-based disease modeling strategy with dual isogenic pairs of iPSC-derived neurons represents a promising platform for studying the causality of mutations related to genetic diseases and developing patient-specific therapies based on disease mechanisms.

4.2. Methods

4.2.1 Preparation and maintenance of hiPSCs

Skin fibroblasts were collected from two male siblings of the GEFS+ family by Kevin Ess (Vanderbilt University Medical Center) after obtaining informed consent using IRB

approved protocol #080369. The control fibroblast donor had no known clinical diagnoses; the patient sibling had four febrile seizures beginning at 6 months of age and four generalized atypical absence seizures since the age of two[14]. Age at time of biopsy the control sibling was 23 years and the patient sibling was 21 years old.

Skin fibroblasts were reprogrammed into iPSCs using nonintegrating Sendai virus by the Schwartz laboratory as published[30]. Two human iPSC lines were generated, SC210.12-SF6-2I3.M11S8 (control) and SC215.19-SF4-2I8.M10S6 (patient). iPSCs were maintained in feeder-free conditions following published protocols[30,31].

4.2.2 CRISPR/Cas9 editing on iPSCs derived from two siblings

To generate a mutated control line, the K1270T mutation was knocked into an iPSC line generated from the unaffected sibling (SC210.12-SF6-2I3-M11S8-S4-S6-S2). The 20-nt guide RNA (sgRNA) 5'-CTTCTAAAATGGGTGGCATA-3' was designed using the CRISPR design tool (http://crispr.mit.edu) from the Zhang laboratory and cloned into plasmid pSpCas9(BB)-2A-Puro (Px459) V2.0 (Addgene, 62988). Plasmid constructs were purified with the Endo-free Plasmid Maxiprep kit (Qiagen). The 140-nt repair template ssODN1 5'-GATTAAGACGATGTTGGAATATGCTGACAAGGTTTTCACTTACATTTTCATTCTGGAAATGC TTCTAACATGGGTGGCATATGGATATCAAACATATTTCACCAATGCCTGGTGTTGGCTGGACTTC TTAATTGTTGATG-3' (Integrated DNA Technologies) was designed with two homologous arms flanking the Cas9 cleavage site, the threonine codon (ACA) at the mutation site and an addition of a silent EcoRV mutation.

To generate a corrected patient line, the mutation was removed from a patient iPSC line (SC215.19-SF4-2I8.M10S6-S2-S2). sgRNA (5'-CTTCTAACATGGGTGGCATA-3')

complementary to the target sequence of mutated allele was cloned into the same plasmid. The 140-nt repair template ssODN2 5'- GATTAAGACGATGTTGGAATATGCTGACAAGGTTT TCACTTACATTTTCATTCTGGAAATGCTTCTAAAATGGGTGGCATATGGCTATCAAACATATTTC ACCAATGCCTGGTGTTGGCTGGACTTCTTAATTGTTGATG-3' (Integrated DNA Technologies) was similar to ssODN1 but with the lysine codon at the mutation site (AAA) and without EcoRV silent mutation. 8 x 10^5 cells were co-transfected with 3 μg plasmid-sgRNA construct and ssODN (0.6 μM final concentration) with Amaxa Human Stem Cell Nucleofector Kit 1 (Lonza) and program A-023 for the Amaxa Nucleofector Device II. To obtain low seeding density, the transfected cell suspension was diluted in a 1:6 - 1:8 ratio and plated into Matrigel (BD Biosciences)-coated wells of 6-well plates. 24 hours post-transfection, cells were treated with 2 μg/ml puromycin (Sigma-Aldrich) in StemPro complete media containing 0.58 μl/ml SMC4 (Corning). 48 hours post-transfection, cells were switched to normal StemPro complete media containing 0.58 μl/ml SMC4. Continued maintenance required media that included 50% conditioned media from 70-90%-confluent unedited iPSC cultures and 50% StemPro complete media with 55 μM β-mercaptoethanol (Invitrogen), 1×StemPro (Invitrogen), 20 ng/ml bFGF (Stemgent) and 0.58 μl/ml SMC4. 6-8 days post-nucleofection, isolated iPSC colonies with 20-30 cells were formed, picked manually using customized glass hooks, and transferred to single wells in 96- or 48-well plates with pre-wet 20 μl barrier micropipette tips. StemPro complete media supplemented with 0.58 μl/ml SMC4 was used for daily feeding. At 100% confluence, clones were split with pre-warmed 62 μl (96-well plate) or 125 μl (48-well plate) of Accutase (Millipore) in a 1:2 ratio. Cells were eventually expanded into two wells in a 48-well plate to be used for freezing as well as sequencing and/or restriction digestion,

respectively. All media for feeding and splitting were prepared immediately prior to use and equilibrated at 37°C and 5% CO_2.

A protocol for freezing iPSCs in low density was modified from Stover *et al* [31]. Cells at 100% confluence were cryopreserved with pre-chilled freezing medium containing 40% conditioned medium from 70-90% confluent culture, 40% StemPro complete medium, 10% DMSO (Sigma-Aldrich), 10% bovine serum albumin (25% BSA, Gibco) with addition of 0.58 µl/ml SMC4. To increase viability of cells during defrosting, clones from 48-well plates were frozen with 50-250 µl of freezing medium depending on the size of pellets after centrifugation and were stored in 1.2 ml cryo-vials at -80°C.

Genomic DNA was extracted with 10-13 µl of QuickExtract DNA Extraction Solution (Epicentre). Fragments around the intended mutation sites were amplified by PCR in 50 µl reactions with Taq DNA polymerase (Invitrogen), forward primer 5'-CTACCATAGATTCCAT CCCCCAA -3' and reverse primer 5'- TTCCACCAATAGTCTTTCCCCTG -3'. PCR products were confirmed by gel electrophoresis and purified with MinElute PCR Purification Kit (Qiagen) prior to sequencing (Retrogen). MacVector software was used to analyze sequencing data.

Additionally, a subset of mutated control clones was subject to restriction digestion by EcoRV prior to sequencing analysis. As we observed the absence of EcoRV mutation in some of the positive clones with K1270T mutation, direct sequencing was used to screen the remaining clones.

The top five potential off-target sites from CRISPR/Cas9 editing as identified by the CRISPR design tool (http://crispr.mit.edu) from the Zhang laboratory, were *SCN7A*, *FLII*, *SCN2A*, *SCN3A* and *SCN9A*. To determine if any of these were also affected by the editing in the mutated control or the patient corrected line, primers were used to interrogate the

relevant region of homology in each gene. PCR conditions were 94 °C, 45 s, 60 °C, 33 s and 72 °C, 55 s for 35 cycles.

To evaluate the expression level of off targets, mRNA was extracted from neuronal cultures of another control iPSC cell line 173 (SC173.1-SF6-2I2.M16S9 through S21) that shows similar rate and degree of functional maturation to our current control line at D21-24 post plating[32]. cDNA was synthesized following the instructions of TRIzol (Thermo Fisher) and SuperScript™ III First-Strand Synthesis SuperMix for qRT-PCR kit (Thermo Fisher), followed by nested PCR. Expression of the off-target gene was compared to *SCN1A* and normalized to *ACTB*. Nested PCR conditions were 94 °C, 45 s, 60 °C, 33 s and 72 °C, 60 s for 35 cycles for all primers. Primers for sequencing and nested PCR are in **Table IV.1**.

All 4 iPSC lines were karyotyped and cell lines at low passage were expanded for cryopreservation. When samples were thawed for expansion and use in differentiation studies, the *SCN1A* gene was sequenced every 20-30 passages. Research was approved by hSCRO (#2011-1023) and IBC protocols (#2011-1377).

Table IV.1. Primers for off-target gene sequencing and expression

Gene	Reference	Direction	Sequence
Off-target gene sequencing			
SCN7A	NG_031928.1	Fwd	5' ACAAGCATAGTGAACCAGCCCT 3'
		Rev	5' GATCAGCCCTGCACTTGTGAAC 3'
FLII	NG_023243.1	Fwd	5' GGCTGCAGACAAGAGCAAGAAA 3'
		Rev	5' CACAGCTGTTCTTTCTGCCCAG 3'
SCN9A	NG_012798.1	Fwd	5' CAGCACTGGTGAGAAGGCTAGA 3'
		Rev	5' ACTTGATGTGCCCCTCATCCTC 3'
SCN2A	NG_008143.1	Fwd	5' CCCTTGGTTGACTGAAATGCCC 3'
		Rev	5' TGCGAAATGTGAGTGTGCAAAA 3'
SCN5A	NG_008934.1	Fwd	5' GGAGAATCACTTGAACCCGGGA 3'
		Rev	5' GGCAGGACCCTGTCTCCTATTT 3'
SCN3A	NG_042289.1	Fwd	5' TTCCCTGCCAGCATTTTCACAC 3'
		Rev	5' ACAATTCTCCCTGTGTTTGCTCT 3'
Off-target gene expression			
SCN1A	NM_001165963.2	Fwd (ext)	5' TCCTTCGGGATCCATGGAACTG 3'
		Rev (ext)	5' CGTTTTCCCAGCAGCACGTAAT 3'
		Fwd (int)	5' TGTCTCGGCATTGAGAACATTC 3'
		Rev (int)	5' ATTGGTGGGAGGCCATTGTAT 3'
SCN7A	NM_002976.3	Fwd (ext)	5' AGCTGAGGGAAAACTAGTGCCC 3'
		Rev (ext)	5' GTGGATCAGGACCCCTACAAGG 3'
		Fwd (int)	5' AGAACCTAAGGGCCTTGTTCCC 3'
		Rev (int)	5' ACACAAGATGGAAGCCGCATTG 3'
ACTB	NM_001101.5	Fwd	5' CCACCATGTACCCTGGCATT 3'
		Rev	5' ACTCCTGCTTGCTGATCCAC 3'

a. Off-target gene expression was examined by nested PCR that uses two sets of primers.
b. Fwd, rev, ext and int are abbreviated for forward, reverse, external set and internal set of primers.

4.2.3 Differentiation of two pairs of isogenic iPSCs into neurons

Two pairs of isogenic iPSCs (4 lines total) within 40 passages of the original generation were patterned into neurons as described[32]. Neural progenitor cells derived from iPSCs were plated on top of 50-70% confluent mouse astroglial feeder layers that were prepared following a published protocol[33].

At D17 post-plating, excitatory and inhibitory neurons were labeled by transfection with CaMKII-eGFP (Addgene, 50469) and GAD1-mCherry (Genecopoeia, HPRM15652-PM02) plasmids in Opti-MEM (Gibco) and DNA-in (MTI-GlobalStem) or ViaFect (Promega) reagents.

4.2.4 Immunostaining and imaging

To evaluate the expression of pluripotency markers, iPSCs were plated onto glass coverslips coated with Matrigel diluted 1:30 in DMEM/F-12 + Glutamax (Gibco). iPSCs were maintained using StemPro medium (section 2.2). When grown to ~70% confluence, coverslips were fixed and stained as described [32]. Primary antibodies OCT-3/4 (1:100; Santa Cruz Biotechnology, sc-5279), SOX2 (1:100; Santa Cruz Biotechnology, sc-365823) and NANOG (1:50; Santa Cruz Biotechnology, sc-293121) were used to characterize the pluripotency of the iPSCs. 4',6-diamidino-2-phenylindole (DAPI; Life Technologies) staining was added to visualize nuclei.

iPSC-derived neurons were stained with antibodies of βIII-tubulin (1:1000; Sigma-Aldrich, T8660) and GABA (1:4000; Sigma-Aldrich, A2052) to assess the proportion of GABAergic neurons. Neurons were identified by morphology, expression of βIII-tubulin in the cell bodies and neuronal processes, and nuclear localization of DAPI. Identities of neurons labeled by GAD1-mCherry and CaMKII-eGFP plasmids were verified by staining

with antibodies of GABA and CaMKII (1:800; Cell Signaling Technology, 3362) respectively. Expression of Nav1.1 was examined in $GABA^+$ (1:100; Aldrich-Sigma, A0310) and CaMKII-$eGFP^+$ cells by staining with anti-Nav1.1 antibody (1:800; Alomone Labs, ASC-001).

Images were taken by a Zeiss M2 Imager fluorescence microscope and processed using the supplied Zen software.

4.2.5 Whole-cell recording

Whole-cell recordings were obtained from iPSC-derived inhibitory and excitatory neurons at D21-23 post-plating at room temperature. This time period was selected based on studies in two control cell lines demonstrating that a high percentage of neurons were functionally active by this age[32]. Patch pipettes were pulled from unpolished borosilicate glass (VWR International) by PC-10 pipette puller (Narishige). Open tip resistance was 6-8 MΩ. External solution contained (in mM): 120 NaCl, 5.4 KCl, 0.8 $MgCl_2$, 1.8 $CaCl_2$, 15 glucose, 20 HEPES, with pH at 7.2-7.4. Osmolality was adjusted to 290 - 295 mOsm. Internal solution contained (in mM): 120 potassium gluconate, 20 NaCl, 0.1 $CaCl_2$, 2 $MgCl_2$, 1.1 EGTA, 10 HEPES, 4.5 Na_2ATP with pH at 7.2. Osmolality was around 280 - 283 mOsm. Voltages were corrected for a 5 mV junction potential. To record evoked action potentials, membrane potential was held at -75 mV by injecting sub-threshold currents and cells were depolarized by a series of current injections.

Excitatory and inhibitory postsynaptic currents (EPSCs and IPSCs) were separated at reversal potentials (-49 mV and -2 mV) with a gap-free protocol under voltage clamp. Recordings of spontaneous PSCs (sPSCs) were performed with the standard external solution and a cesium gluconate internal solution containing (in mM): 130 Cs^+ gluconate,

0.2 EGTA, 2 $MgCl_2$, 6 CsCl, 10 HEPES, 2.5 adenosine 5' triphosphate sodium salt, 0.5 guanosine 5' triphosphate sodium and 10 disodium phosphocreatine. Voltages were corrected for a 7 mV junction potential. Miniature postsynaptic currents (mPSCs) were recorded in external solution containing 1 μM TTX (tetrodotoxin; Alomones Labs).

Isolated sodium currents were recorded with external solution containing (in mM): 120 NaCl, 5.4 KCl, 0.8 $CoCl_2$, 15 glucose, 20 HEPES, 2.5 tetraethylammonium and 1.0 4-aminopyridine. The same cesium gluconate internal solution for PSC recording was used for sodium current recording. Voltages were corrected for a 10 mV junction potential. P/N leak subtraction was turned on. The voltage dependence of activation was determined with a step protocol. Cell membrane potential was increased from a holding potential of -100 mV to a range of potentials between -100 mV and 30 mV for 45 s with a step interval of 5 or 10 mV. Currents recorded at the shared voltage steps were included for current density analysis and G-V graph plotting. Peak transient currents were plotted against holding potentials and fit with the following equation:

$$I = \frac{(V-Vrev)\times Gmax}{1+\exp\left(-\frac{V-Vhalf}{k}\right)} \quad (1)$$

where I is the peak current amplitude, V is the holding potential of each pulse, V_{rev} is the reversal potential, G_{max} is the maximal conductance, V_{half} is the voltage with 50% channels activated, and k is the slope. Current data in 5 mV and 10 mV step intervals were used for fitting. Conductance was calculated with the following equation:

$$G = \frac{I}{V-Vrev} \quad (2)$$

where G is conductance, and I, V, V_{rev} were as described in equation (1).

The voltage dependence of steady-state inactivation was analyzed with a two-step protocol. It began with a holding potential of -100 mV. Next the conditioning pulse was increased through a series of voltage steps from -100 mV to 30 mV for 90 ms with a step interval of 5 or 10 mV. Currents recorded at the shared voltage steps were included for G-V graph plotting. A test pulse at -10 mV for 90 ms was immediately applied and followed by a holding potential of -100 mV. The peak current amplitude during test pulses were normalized to that during the first test pulse and then plotted against the holding potential of the conditioning pulse. The I-V curves were fitted to the following equation:

$$\mathrm{I} = \frac{1}{1+exp\frac{V-Vhalf}{k}} \quad (3)$$

where I is the normalized peak current amplitude during the test pulses, V_{half} is the voltage with 50% channels inactivated, and k is the slope. Current data in 5 mV and 10 mV step intervals were used for fitting.

The recovery from steady-state inactivation was determined using a second two-pulse protocol. Following a holding potential of -100 mV for 27 ms, two test pulses at -10 mV for 90 ms were separated by a time interval with a range of 1-10 ms with an increment of 1 ms in the first protocol, and 10-50 ms with an increment of 5 ms in the subsequent protocol. Peak current amplitude from the second pulse was normalized to the average current amplitude from the first pulse to calculate the fractional recovery. The data of recovery were fitted using the following equation:

$$\mathrm{I} = \mathrm{A} \times \exp\left(-\frac{t}{\tau}\right) + B \quad (4)$$

where I is the normalized current amplitude, A is the relative percentage of recovered currents, t is the time interval, and τ is the time constant of recovery.

Electrophysiological data were collected with a List EPC7 amplifier and a Digidata 1320A D-A converter (Axon Instruments), or a MultiClamp 700B amplifier and a Digidata 1440A D-A converter (Axon Instruments). Recordings were obtained by pClamp8 or pClamp10 (Axon Instruments) software with a Bessel filter at 2 kHz and a low-pass filter at 10 kHz.

4.2.6 Data Analysis and Statistics

Counting from fluorescent micrographs was conducted in a blinded fashion with respect to cell line. For each coverslip, at least 3 fields with evenly distributed cells observed via DIC were chosen for counting. 3 coverslips each from individual plating of an iPSC cell line were included for counting the number of cells expressing pluripotency markers.

Electrophysiological data were analyzed using Clampfit 10.6 (Molecular Devices). Cells that were included in electrophysiological analyses had an amplitude of leak current smaller than 50 pA at a holding potential of -75 mV. Evoked action potentials (APs) recorded under current clamp were included if they had a stable baseline at -65 ~ -85 mV with sub-threshold current injection, a peak amplitude ≥ -5 mV on the first AP and ≥ -15 mV in subsequent APs within the train. AP events were excluded if the maximum firing frequency deviated from mean by more than ± 2SD. Rheobase data were excluded if the resting membrane potentials (RMP) were more depolarized than -35 mV. AP properties were examined in the first AP at rheobase that first elicited AP firing. AP threshold was identified as the first derivative of the membrane potential (dV/dt) 5% or higher than the peak rate of change. AP amplitude was defined as the change of membrane potential from

the threshold to the peak. AP amplitude and half-width data were not included if the cell did not fire evoked AP. PSCs recorded under voltage-clamp were analyzed using Mini Analysis 6.0.7 (Synaptosoft). PSCs were identified as events with an amplitude ≥ 5 pA (2× RMS noise of 2.5 pA) and were then manually verified individually. Cells were excluded from sodium current analysis if their current density in the range of -10 - 40mV was 2SD beyond the mean.

Electrophysiological data are presented with n = number of recorded cells and the number of individual platings shown in parentheses. All data were analyzed with D'Agostino-Pearson normality test. Statistical tests were selected based on the normality test results and performed in Prism 7.0.2 (GraphPad Software). Figures were generated using DeltaGraph 7.1 (Red Rock Software).

4.3. Results

4.3.1 Two pairs of isogenic iPSCs generated by CRISPR/Cas9 editing

The autosomal dominant K1270T *SCN1A* mutation identified in a GEFS+ family results in a lysine-to-threonine conversion in the second transmembrane segment of the third homologous domain in the α subunit of the human Nav1.1 protein[14] (**Figure IV.1A**). Skin fibroblasts were collected from two male siblings (an unaffected control and a GEFS+ patient) and both were reprogrammed into iPSC lines using the nonintegrating Sendai virus (**Figure IV.1B**). To examine the contribution of the K1270T mutation to disease phenotypes, two pairs of isogenic lines were included in this study. In the first pair, the GEFS+ K1270T mutation (c.4227A>C) was knocked into the unaffected sibling derived control line using CRISPR/Cas9. For the second isogenic pair, the K1270T mutation in the

patient line was corrected (c.4227C>A; **Figure IV.1C**). The mutated control clone with desired sequence was homozygous, likely the result of the short distance (9 bp) between the Cas9 cut site and the K1270T mutation locus[34].

Sequencing of DNAs from the iPSC lines in the 2 isogenic pairs confirmed that the control line did not have the mutation at site 1270 (*SCN1A*$^{+/+}$). The mutated control was homozygous for the mutation (*SCN1A*$^{KT/KT}$) based on sequencing and this was further confirmed by the presence of the silent EcoRV mutation from the repair template in only one allele, demonstrating that the editing process did not also result in loss of one allele and therefore, a hemizygous clone. The patient line was confirmed to be heterozygous for the mutation (*SCN1A*$^{KT/+}$) and the mutation was absent in the corrected patient lines (*SCN1A*$^{+/+}$; **Figure IV.1D**). Comparison of the heterozygous patient lines with the engineered homozygous isogenic mutant provides a unique opportunity to evaluate gene dosage-dependent effects since two copies of *SCN1A* mutations are usually lethal to organisms *in vivo*[35,36].

Karyotypes of four iPSC lines were verified normal with 46, XY chromosomes (Figure IV.1E). Pluripotency of each of the 4 cell lines was confirmed by staining for expression of OCT-3/4, SOX2 and NANOG[37] (**Figure IV.1F**). The top five potential off-target sites for mutations were evaluated, including *SCN7A*, *FLII*, *SCN2A*, *SCN3A* and *SCN9A* (**Figure IV.2A**). There were no off-target mutations in candidate genes in the corrected patient line. In the homozygous mutated control line, there was a mutation in *SCN7A*, in addition to the K1270T knock-in mutation. Since *SCN7A* encodes a non-voltage-gated, TTX-insensitive Na_x sodium channel, it is unlikely to affect evaluation of sodium currents and firing properties that are both completely eliminated by addition of TTX to the recording solution (**Figure**

IV.2B). In addition, this gene is expressed in astrocytes, and neurons in circumventricular organs[38,39] and there is no evidence that this gene is expressed in our iPSC-derived neurons based on nested PCR reactions that resulted in clear amplification of *SCN1A* transcripts with undetectable levels of *SCN7A* (**Figure IV.2C**).

Figure IV.1. Isogenic pairs of iPSCs generated by CRISPR/Cas9 editing. (A) The K1270T mutation is located in the second transmembrane segment of the third homologous domain of Nav1.1 alpha subunit. (B) CRISPR/Cas9 editing was used to generate two isogenic pairs from iPSCs derived from two siblings in the GEFS+ family (control and patient) followed by differentiation into functional neurons. (C) Scheme of CRISPR/Cas9 editing design. Additional silent mutation introduced by ssODN1 resulted in an EcoRV restriction site for clone screening when knocking in the K1270T mutation. (D) Sequencing of two isogenic iPSC pairs confirmed the absence and the presence of the mutation. (E) All four lines had normal karyotypes (46, XY). (F) iPSCs of two isogenic pairs were stained with nuclei marker DAPI and pluripotency markers OCT-3/4, SOX2 and NANOG individually. The percentage of cells positive for each of the pluripotency markers. Scale bar represents 50 μm. Data represented as mean + s.e.m. Data represent counts from three fields in three coverslips from three platings for each genotype.

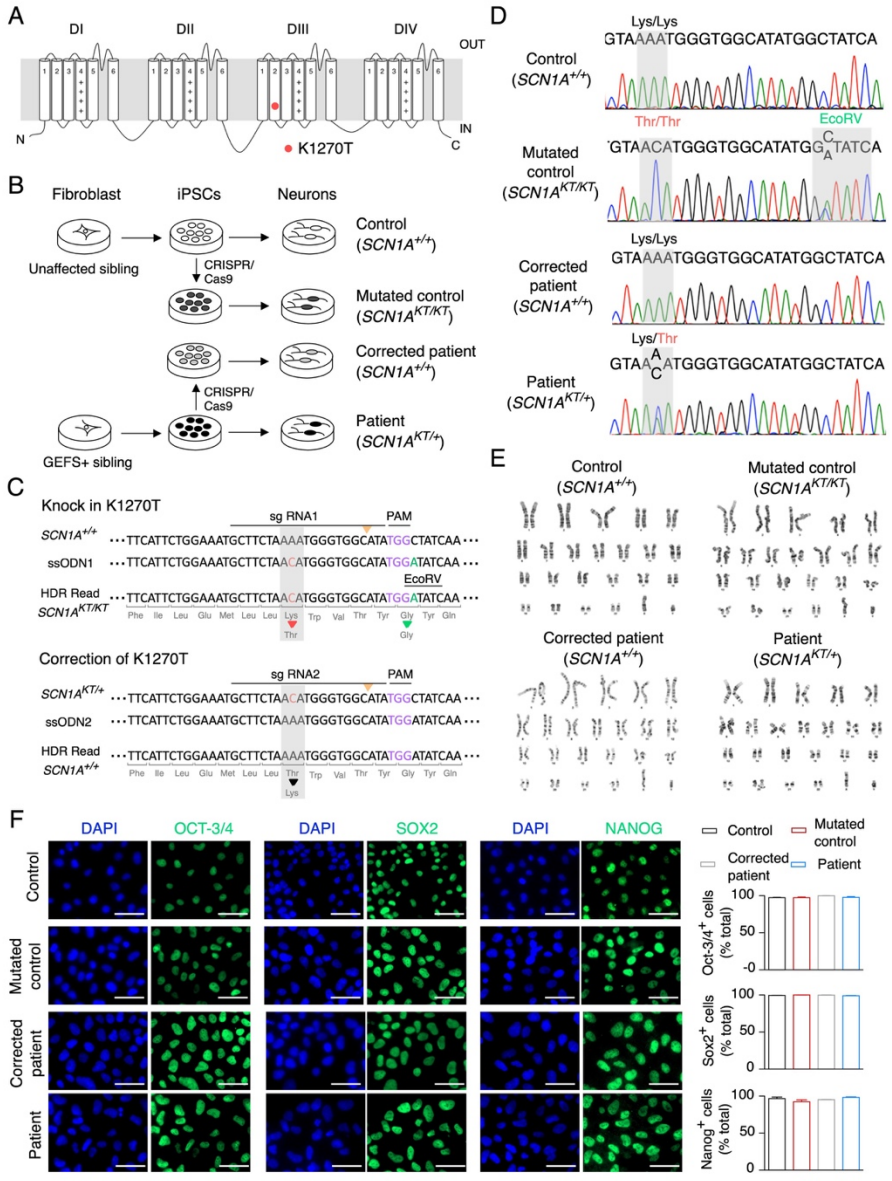
A
DI
DII
DIII
DIV
OUT
IN
N
C
K1270T
B
Fibroblast
iPSCs
Neurons
Unaffected sibling
CRISPR/ Cas9
Control (SCN1A+/+)
Mutated control (SCN1AKT/KT)
Corrected patient (SCN1A+/+)
Patient (SCN1AKT/+)
GEFS+ sibling
C
Knock in K1270T
sg RNA1
PAM
SCN1A+/+
ssODN1
HDR Read
SCN1AKT/KT
EcoRV
Correction of K1270T
sg RNA2
SCN1AKT/+
ssODN2
D
Lys/Lys
Control (SCN1A+/+)
Thr/Thr
EcoRV
Mutated control (SCN1AKT/KT)
Corrected patient (SCN1A+/+)
Lys/Thr
Patient (SCN1AKT/+)
E
Control (SCN1A+/+)
Mutated control (SCN1AKT/KT)
Corrected patient (SCN1A+/+)
Patient (SCN1AKT/+)
F
DAPI
OCT-3/4
SOX2
NANOG
Control
Mutated control
Corrected patient
Patient
Oct-3/4+ cells (% total)
Sox2+ cells (% total)
Nanog+ cells (% total)

Figure IV.2. Off-target analysis in the lines generated by CRISPR/Cas9 editing. (A) Sequences of the top five predicted off-target sites in *SCN7A*, *FLII, SCN2A*, *SCN3A* and *SCN9A*. Off-target mutation was identified in the *SCN7A* gene of the mutated control line. Regions highlighted in blue are the sites predicted to be modified by non-specific CRISPR/Cas9 editing. (B) Isolated sodium current recording in the derived neurons of the control line at D54 post plating. Sodium currents were completely eliminated in the presence of 1 µM TTX. (C) Expression of *SCN1A*, *SCN7A* and the housekeeping gene *ACTB* in the derived neurons of a control line at D21 post plating. Expected band sizes of *SCN1A*, *SCN7A* and *ACTB* are 220, 283 and 177 bp.

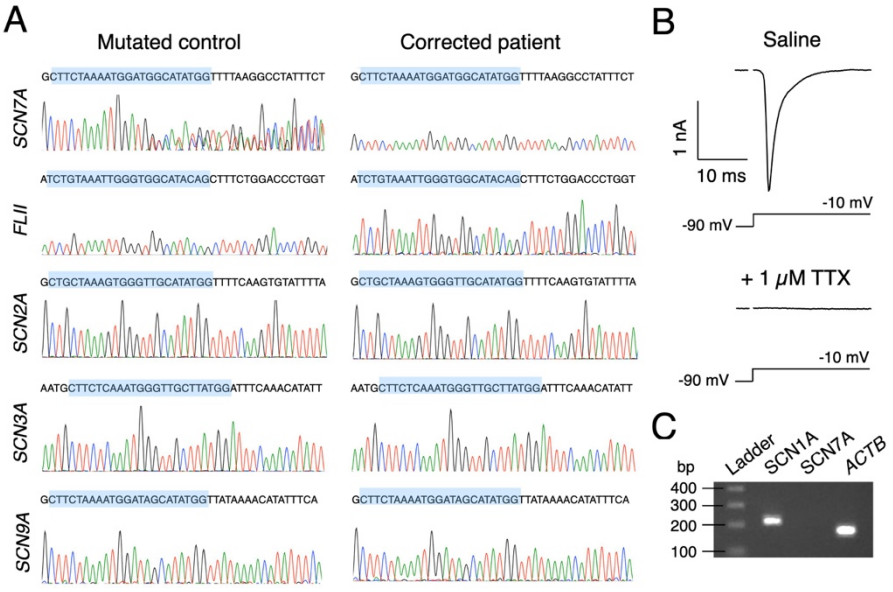

4.3.2 iPSC-derived neuronal cultures contain both inhibitory and excitatory neurons

We previously optimized a direct differentiation protocol that gives rise to neuronal cultures containing excitatory and inhibitory neurons[32,33]. With this protocol, iPSCs from both isogenic pairs were differentiated into neural progenitors followed by plating onto astroglial feeder layers for neuronal differentiation. To evaluate the morphology of neurons and quantify the proportion of inhibitory GABAergic and excitatory glutamatergic neurons in the cultures derived from the four iPSC lines, cultures were fixed at D21-24 post plating and stained with anti-βIII-tubulin and anti-GABA or anti-CaMKII antibodies. Cultures from all lines stained βIII-tubulin positive cells with elongated branched neurites (**Figure IV.3A**). GABAergic and glutamatergic neurons comprised 30-40% and ~50% of the total neuronal population respectively, with no significance between genotypes (**Figure IV.3B**).

In order to identify inhibitory and excitatory neurons during live recording, cells were transiently transfected with GAD1-mCherry and CaMKII-eGFP plasmids at D17 post plating. Visualization of the cultures with fluorescent illumination at D21-24 post plating was used to identify and record from mCherry expressing GAD1-positive inhibitory neurons and eGFP expressing CaMKII-positive excitatory neurons (white arrows, **Figure IV.3C**). The plasmid labeling strategy accurately identified GABAergic and glutamatergic neurons based on the colocalization of anti-GABA staining in 90.05% ± 3.26% of GAD1-mCherry$^+$ and anti-CaMKII staining in 97.15% ± 2.47% of CaMKII-eGFP$^+$ neurons examined. Further, *SCN1A* was expressed in both inhibitory and excitatory neurons based on anti-Nav1.1 antibody staining in both GABAergic and glutamatergic neurons (**Figure IV.3D**).

Figure IV.3. Cultures from two isogenic pairs contain a similar proportion of GABAergic and glutamatergic neurons. (A) Representative micrographs from cultures of two isogenic pairs of iPSC-derived neurons stained with neuronal subtype markers GABA or CaMKII antibodies to identify GABAergic and glutamatergic neurons at D21-24 post plating. (B) The percentage of GABAergic and glutamatergic neurons (white arrows) in neuronal cultures at D21-24 post plating in each line. (C) Identification of inhibitory (top) and excitatory (bottom) neurons at D21-24 post plating labeled with plasmids via transient transfection during live recording (white arrows). At least 3 coverslips of 2-3 individual platings were evaluated for each line. (D) Localization of Nav1.1 in GABAergic and glutamatergic neurons (white arrows). Data represented as mean + s.e.m. Ctrl = control, mut ctrl = mutated control, corr pt = corrected patient, and pt = patient. Scale bar represents 50 μm.

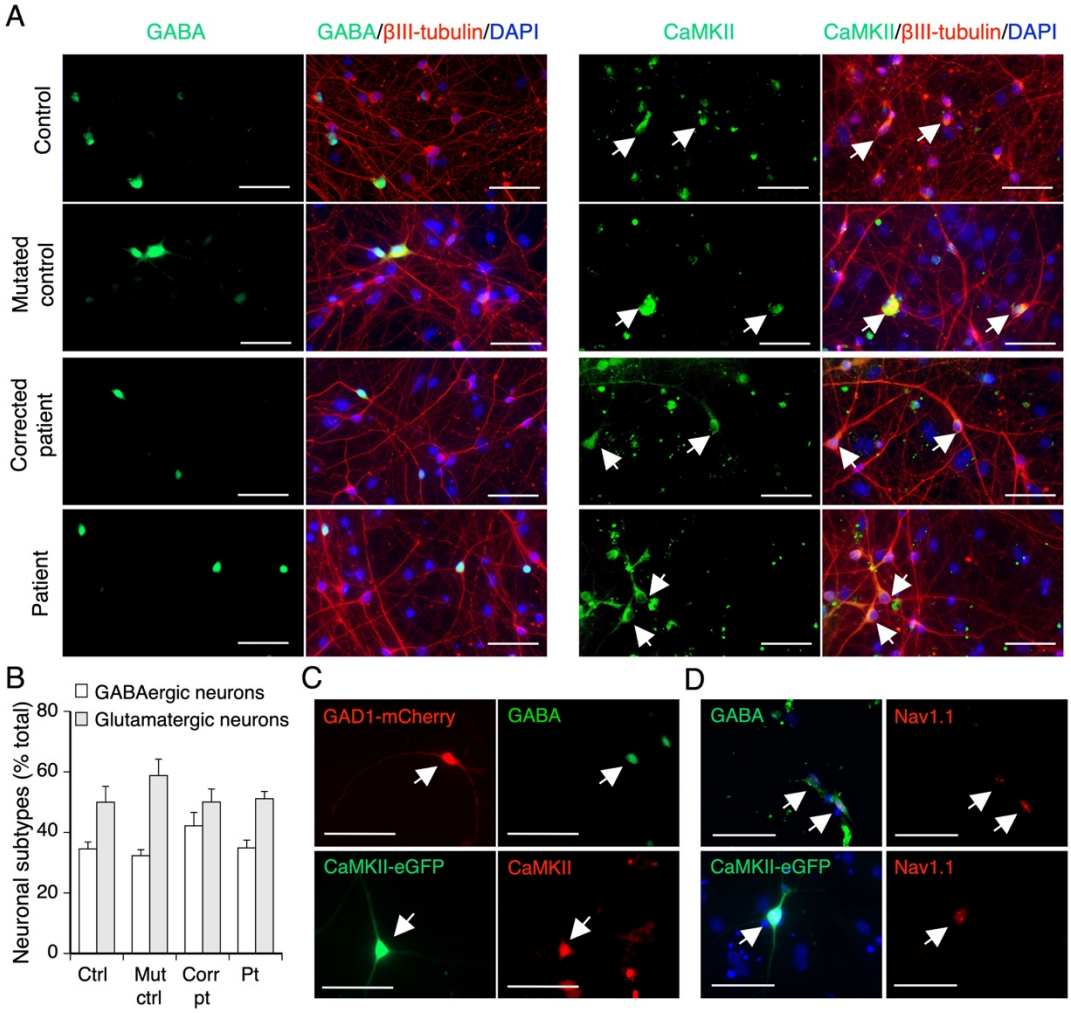

4.3.3. Inhibitory neurons: the K1270T mutation reduces evoked firing and sodium current in dose-dependent manner

To determine if the K1270T mutation causes cell type-specific alterations in excitability, evoked action potential recordings were obtained at D21-D24 post plating from iPSC-derived inhibitory neurons in cultures from two isogenic pairs: 1a) control (*SCN1A*$^{+/+}$), 1b) mutated control, homozygous (*SCN1A*$^{KT/KT}$); 2a) corrected patient (*SCN1A*$^{+/+}$), 2b) patient, heterozygous (*SCN1A*$^{KT/+}$). To account for variability between platings, and within plating, data for all electrophysiological properties represent recordings from multiple cells in at least three independent platings, and these values are presented in each figure or table.

Over 90% of inhibitory neurons in each genotype fired action potentials (**Figure IV.4A and 4D**). Assessment of firing frequency vs current step curves in each line demonstrated that the mean firing frequency was significantly lower in the homozygous mutated control line compared to the control line (interaction: $p < 0.0001$, genotype: $p = 0.0092$, two-way ANOVA with repeated measures; **Figure IV.4B**). The AP amplitude was significantly smaller in the homozygous mutated control line compared to the control ($p = 0.0073$, two-tailed unpaired *t* test; **Figure IV.4C**).

The heterozygous patient line compared to the corrected patient line had decreased firing frequency at small current steps. However, at current steps of 50 pA and above the firing frequency of the patient and the corrected patient line were largely overlapping and the two curves were not significantly different (**Figure IV.4E**). The AP amplitude in the heterozygous patient line was smaller than that in the corrected patient line, but the difference was not significant (**Figure IV.4F**). The reduction in firing frequency and AP

firing in the heterozygous patient line was approximately half that seen in the homozygous mutated line compared to the control line at the low current steps (**Figure IV.4B and IV.4E**). These data suggest that the impairment of action potential firing in inhibitory neurons is gene dose-dependent. There were no differences in AP rheobase, the injected current that first elicited AP firing, and half width within and between isogenic pairs (**Table IV.2**).

The control and the mutated control had similar input resistance (IR), whole cell capacitance (C_m) and rest membrane potential (RMP; **Table IV.3**). Interestingly while the patient line had comparable input resistance to the isogenic corrected line, it had a significantly smaller whole cell capacitance and a more depolarized RMP ($p = 0.024$, and < 0.0001 respectively, Mann-Whitney U test for C_m and unpaired *t* test for RMP; **Table IV.3**).

To examine whether reduced firing frequency and AP amplitude is associated with alterations in sodium current, isolated sodium currents were recorded in inhibitory neurons at D21-24 post plating. All inhibitory neurons in each genotype expressed sodium currents. Sodium currents were not well space clamped at this age in culture in any of the lines (**Figure IV.4G and IV.4I**), consistent with the localization of some sodium channels at sites electrically distant from the neuronal cell bodies as is typical of neurons that fire multiple APs. This is also consistent with many other studies in which iPSC-derived neurons that are capable of firing a train of APs do not have well clamped sodium currents[20–23,40]. However, comparative analysis of sodium current properties between control and patient lines in these studies, as in other published studies, provide insights into the disease mechanism. Therefore, our study focuses on comparing sodium current properties from a family of traces within and between isogenic pairs. While the absolute

values may not be reflective of the biophysical properties of sodium currents measured from single channels or in expression systems where there is good voltage control, they allow identification of properties that are or are not associated with the mutation in the native environment.

The mean sodium current density versus voltage curves, generated from analysis of inhibitory neurons in each line of an isogenic pair, were compared. In the mutated control line, homozygous for K1270T, the sodium current density was significantly reduced compared to the control line (interaction: $p = 0.016$, genotype: $p = 0.050$, two-way ANOVA with repeated measures; **Figure IV.4G and IV.4H**). In the patient line, heterozygous for the K1270T mutation, the mean sodium current density versus voltage curve was smaller at each voltage than the corrected line (**Figure IV.4I and IV.4J**). While the difference between the patient and the corrected patient line was not significant, it was about 50% less than that seen between the homozygous mutant and the control line (**Figure IV.4H and IV.4J**). This suggests that the K1270T mutation causes a gene dose-dependent reduction in sodium current density, consistent with the changes in firing frequency and AP amplitude.

Figure IV.4. In inhibitory neurons, the K1270T mutation causes impaired AP firing and reduced sodium current density. (A) Traces of action potential firing in inhibitory neurons of the first isogenic pair of the control (ctrl) and the homozygous mutated control (mut ctrl). (B) The input-output curves of action potentials in inhibitory neurons of the first isogenic pair. (C) AP amplitude of the first AP at rheobase in inhibitory neurons of the first isogenic pair. ** denotes $p < 0.001$, two-tailed unpaired *t*-test. (D-F) Same as A and B, but in inhibitory neurons of the second isogenic pair of the lines from the corrected patient (corr pt) and the heterozygous patient (pt). (G) Traces of voltage-gated sodium currents in inhibitory neurons of the first isogenic pair. The activation protocol started with a prepulse at -100 mV followed by a series of steps ranging from -100 to 30 mV in 10 mV intervals. (H) Current-voltage relationship in inhibitory neurons of the first isogenic pair. Whole cell currents were normalized to capacitance. (I-J) Same as G and H, but in inhibitory neurons of the second isogenic pair. Data presented as mean + s.e.m in C and F, and mean ± s.e.m with total number of neurons evaluated and the number of individual platings in parentheses for each line in B,E,H, and J. * and # represent significant differences in genotypes and interaction within an isogenic pair respectively, two-way ANOVA and *post hoc* Sidak's analysis. One to four symbols denote p values < 0.05, 0.01, 0.001, 0.0001 respectively.

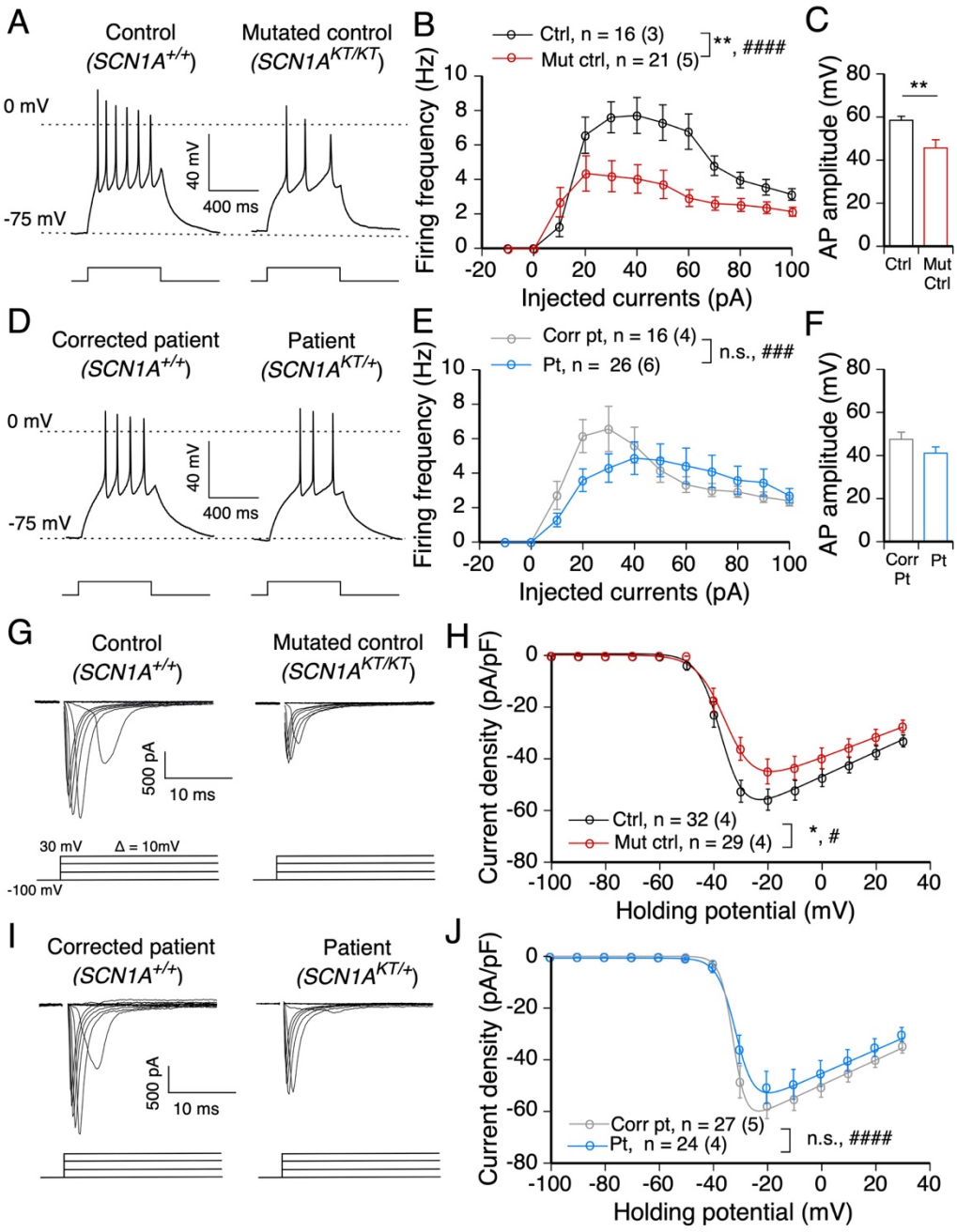
A
Control
(SCN1A+/+)
Mutated control
(SCN1AKT/KT)
0 mV
-75 mV
40 mV
400 ms
B
Ctrl, n = 16 (3)
Mut ctrl, n = 21 (5)
**, ####
Firing frequency (Hz)
Injected currents (pA)
C
AP amplitude (mV)
**
Ctrl
Mut Ctrl
D
Corrected patient
(SCN1A+/+)
Patient
(SCN1AKT/+)
0 mV
-75 mV
40 mV
400 ms
E
Corr pt, n = 16 (4)
Pt, n = 26 (6)
n.s., ###
Firing frequency (Hz)
Injected currents (pA)
F
AP amplitude (mV)
Corr Pt
Pt
G
Control
(SCN1A+/+)
Mutated control
(SCN1AKT/KT)
500 pA
10 ms
30 mV
Δ = 10mV
-100 mV
H
Current density (pA/pF)
Ctrl, n = 32 (4)
Mut ctrl, n = 29 (4)
*, #
Holding potential (mV)
I
Corrected patient
(SCN1A+/+)
Patient
(SCN1AKT/+)
500 pA
10 ms
J
Current density (pA/pF)
Corr pt, n = 27 (5)
Pt, n = 24 (4)
n.s., ####
Holding potential (mV)

Table IV.2. Measurements of excitability in two isogenic pairs

Cell type	Genotype	Rheobase (pA)	AP half-width (ms)
Inhibitory	Ctrl	18.8 ± 1.7 n = 13 (3)	3.6 ± 0.2 n = 16 (3)
	Mut ctrl	22.5 ± 3.8 n = 16 (5)	4.8 ± 0.6 n = 19 (5)
	Corr pt	15.3 ± 1.7 n = 15 (4)	4.6 ± 0.7 n = 16 (4)
	Pt	23.9 ± 3.3 n = 26 (6)	6.1 ± 0.8 n = 25 (6)
Excitatory	Ctrl	23.3 ± 2.4 n = 9 (3)	3.9 ± 0.4 n = 15 (3)
	Mut ctrl	21.3 ± 1.9 n = 15 (5)	3.9 ± 0.2 n = 29 (5)
	Corr pt	17.5 ± 1.9 n = 16 (5)	4.0 ± 0.5 n = 16 (5)
	Pt	18.7 ± 2.4 n = 32 (8)	4.2 ± 0.2 n = 33 (8)

a. Data reported as mean ± s.e.m with total number of neurons (number of individual platings) underneath.
b. Ctrl = control, mut ctrl = mutated control, corr pt = corrected patient, and pt = patient.

Table IV.3. Comparison of passive membrane properties in two isogenic pairs

Cell type	Genotype	IR (GΩ)	C_m (pF)	RMP (mV)
Inhibitory	Ctrl	1.6 ± 0.1 n = 16 (3)	27.3 ± 2.8 n = 15 (3)	-43.0 ± 2.7 n = 13 (3)
	Mut ctrl	1.6 ± 0.1 n = 21 (5)	27.8 ± 2.8 n = 22 (5)	-44.3 ± 2.7 n = 18 (5)
	Corr pt	1.6 ± 0.2 n = 22 (4)	32.1 ± 2.4* n = 22 (4)	-57.8 ± 1.3**** n = 17 (2)
	Pt	1.6 ± 0.1 n = 26 (6)	24.9 ± 2.3 n = 26 (6)	-45.8 ± 2.3 n = 13 (2)
Excitatory	Ctrl	1.0 ± 0.1 n = 16 (3)	30.5 ± 2.5 n = 15 (3)	-47.0 ± 0.3 n = 9 (3)
	Mut ctrl	1.3 ± 0.09* n = 30 (5)	32.6 ± 2.9 n = 28 (5)	-44.9 ± 2.3 n = 17 (5)
	Corr pt	1.3 ± 0.09 n = 24 (5)	31.3 ± 1.4 n = 24 (5)	-51.1 ± 2.0 n = 14 (2)
	Pt	1.5 ± 0.09 n = 48 (8)	36.7 ± 1.8 n = 48 (8)	-49.1 ± 2.4 n = 12 (2)

a. Data reported as mean ± s.e.m with total number of neurons and number of individual platings in parentheses.
b. Ctrl = control, mut ctrl = mutated control, corr pt = corrected patient, and pt = patient.
c. Statistically significant differences within isogenic pair: * $p < 0.05$ and **** $p < 0.0001$, two-tailed Mann-Whitney U test for IR and C_m and unpaired *t*-test for RMP.

No differences were observed in the voltage-dependence of activation, steady-state inactivation, or recovery from inactivation within the isogenic pairs (the mutated control line compared to the control; the patient compared to the corrected patient line; Figure S2). However, comparison between the isogenic pairs revealed a ~4 mV depolarized shift in voltage dependence of activation in the pair derived from the control compared to the pair derived from the patient (interaction: $p < 0.0001$, genotype: $p = 0.0065$, two-way ANOVA with repeated measures; **Table IV.4 and Figure IV.5A and 5B**). There was also a 3 mV depolarized shift in the voltage dependence of steady-state inactivation in the control vs the patient derived lines (interaction: $p < 0.0001$, genotype: $p = 0.2847$, two-way ANOVA with repeated measures; **Table IV.4 and Figure IV.5C and 5D**). Shifts between pairs are likely associated with the genetic background of the GEFS+ patient which would not be found if using unrelated control and patient cell lines. Time constant of recovery from inactivation was similar within isogenic pairs (**Table IV.4 and Figure IV.5E and 5F**).

Overall the differences within the isogenic pairs demonstrate that the K1270T mutation causes evoked firing, action potential amplitude and sodium current density recorded at the cell body in a gene dose-dependent manner in inhibitory neurons. The alterations observed in voltage dependence of activation and steady-state inactivation of sodium currents between isogenic pairs suggest these changes are associated with the genetic background, independent of the mutation.

Table IV.4. Comparison of voltage dependence of Nav in isogenic pairs

Cell type	Line	Activation		Inactivation		Recovery
		$V_{1/2}$ (mV)	k (mV)	$V_{1/2}$ (mV)	k (mV)	τ (ms)
Inhibitory	Ctrl, n = 32 (4)	-38.2 ± 1.4	1.7 ± 0.3	-44.0 ± 1.0	5.5 ± 0.2	3.0 ± 0.2
	Mut ctrl, n = 29 (4)	-35.1 ± 1.4	2.1 ± 0.3	-43.3 ± 0.6	6.3 ± 0.3	3.2 ± 0.2
	Corr pt, n = 27 (5)	-32.0 ± 0.9	2.2 ± 0.3	-41.0 ± 0.4	6.3 ± 0.3	2.8 ± 0.1
	Pt, n =24 (4)	-31.3 ± 1.3	2.5 ± 0.4	-41.0 ± 0.8	6.1 ± 0.3	2.9 ± 0.2
Excitatory	Ctrl, n = 36 (4)	-35.4 ± 1.1	1.7 ± 0.2	-43.2 ± 0.5	5.7 ± 0.1	3.0 ± 0.1
	Mut ctrl, n = 27 (4)	-35.3 ± 1.3	2.2 ± 0.3	-44.0 ± 0.9	5.8 ± 0.2	3.4 ± 0.2
	Corr pt, n = 26 (5)	-31.5 ± 1.0*	2.3 ± 0.3	-42.5 ± 0.7*	7.2 ± 0.5**	2.9 ± 0.1
	Pt, n = 26 (4)	-34.7 ± 1.0	2.0 ± 0.3	-40.5 ± 0.4	5.4 ± 0.2	3.1 ± 0.1

a. Data reported as mean ± s.e.m with total number of neurons and number of individual platings in parentheses for each line.
b. Ctrl = control, mut ctrl = mutated control, corr pt = corrected patient, and pt = patient.
c. Statistically significant differences within isogenic pairs: * $p < 0.05$ and *** $p < 0.001$, two-tailed unpaired *t*-test for activation and inactivation $V_{1/2}$, and Mann-Whitney U test for inactivation k.

Figure IV.5. Properties of Nav in inhibitory neurons. (A-B) Conductance vs voltage curves of activation in inhibitory neurons of the control vs the mutated control lines, and the corrected patient vs the patient lines respectively. (C-D) Current vs voltage curves of steady-state inactivation in inhibitory neurons of isogenic pairs. (E-F) Recovery of inactivation in both isogenic pairs. Data presented as mean ± s.e.m with total number of neurons and number of individual platings in parentheses evaluated in each line. Two-way ANOVA and *post hoc* Sidak's analysis.

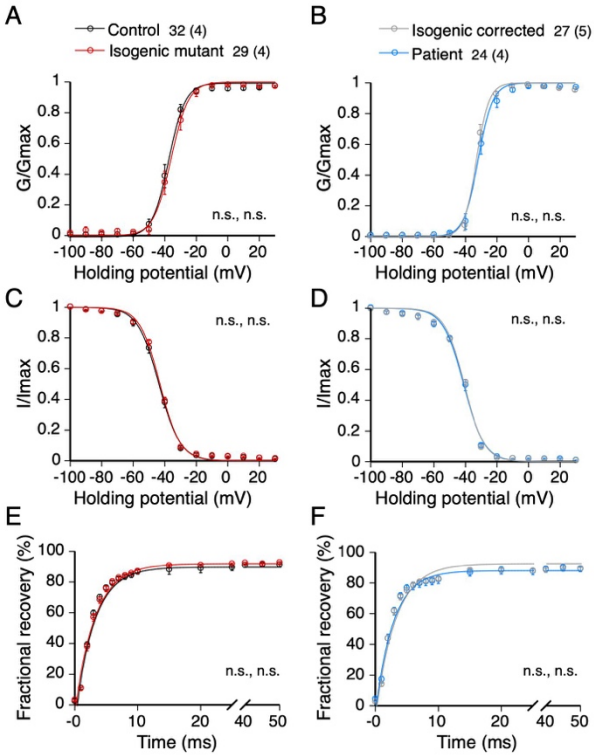

4.3.4 Excitatory neurons: the K1270T SCN1A mutation reduces sodium current density but does not reduce firing.

Previous studies in iPSC and mouse models have suggested that *SCN1A* mutations reduce evoked firing and sodium currents specifically in inhibitory neurons[21,35,36,41]. However, some studies in other *SCN1A* mutations showed excitability and sodium currents of both excitatory and inhibitory neurons are affected by *SCN1A* mutations[22,23,42]. Antibody staining demonstrated that both excitatory and inhibitory iPSC-derived neurons in our cultures express Nav1.1 channels. Therefore, it was important to evaluate evoked firing and sodium currents in iPSC-derived excitatory neurons in the same two isogenic pairs examined in the previous section at D21-24 post plating.

Over 93% of excitatory neurons in each genotype fired action potentials with injection of depolarizing currents (**Figure IV.6A and 6D**). The firing frequency versus injected current curves demonstrated the firing frequency in the homozygous mutated control was not different from the control (**Figure IV.6B**). Interestingly, the heterozygous patient line had a higher firing frequency at current injections over 30 pA (interaction: $p = 0.0042$, genotype: $p = 0.041$, two-way ANOVA with repeated measures; **Figure IV.6E**). Since increased firing frequency in excitatory neurons was only identified by comparing the two lines in the second isogenic pair and it was not observed in the first pair, it suggested that alteration in this property is associated with the interaction between the mutation and the patient genetic background which would not be found without using the dual isogenic pairs. There was no significant difference in the AP amplitude, rheobase and AP half-width within or between the isogenic pairs (**Figure IV.5C, IV.5F and Table IV.2**).

The input resistance in the mutated control was slightly higher than that of the control ($p = 0.025$, two-tailed Mann-Whitney U test; **Table IV.3**). However, there was no difference in the input resistance between the patient vs the corrected patient line (**Table IV.3**). The whole cell capacitance and RMP were similar within the isogenic pairs (**Table IV.3**).

Based on the lack of decrease in firing in excitatory neurons, and the increase in firing in the patient line, it seemed likely there would be no decrease in sodium current density in the mutated control and possibly an increase in the patient line. To evaluate this, isolated sodium currents were recorded at D21-24 post plating and like inhibitory neurons, all excitatory cells expressed sodium currents that were not well clamped (**Figure IV.5G and IV.5I**). Unexpectedly the current density vs voltage curve demonstrated a significant reduction in sodium current density recorded in the cell body in the homozygous mutated control line compared to the control line (interaction: $p < 0.0001$, genotype: $p = 0.0025$, two-way ANOVA with repeated measures; **Figure IV.5H**). The sodium current density in the heterozygous patient line was also smaller compared to the corrected patient line, but the differences was not significant (interaction: $p < 0.0001$, genotype: $p = 0.056$, two-way ANOVA with repeated measures; **Figure IV.5J**). The reduction of sodium current density in the heterozygous patient line was half the magnitude seen in the homozygous mutated control line (**Figure IV.5H and 5J**). This is similar to the dose-dependent reduction in sodium current seen in inhibitory neurons.

Since there was no concomitant reduction in firing frequency in the excitatory neurons in the homozygous mutant line, this suggests that the properties of other channels, for example potassium channels, in excitatory neurons are more influential in determining

the firing phenotype. However, this does not address how a decrease in sodium current in the patient line is consistent with a small but significant increase in excitatory neuron firing frequency. Comparison of other sodium current properties revealed two additional changes in the heterozygous patient line that were not seen in any of the other three lines. There was a hyperpolarized shift in the voltage-dependence of activation and a depolarized shift in steady-state inactivation in the heterozygous patient compared to the corrected patient line ($p = 0.028$ and 0.015 respectively, two-tailed unpaired *t* test; **Table IV.4 and Figure IV.7B and IV.7D**). These alterations are both likely to lead to increased channel opening probability over a larger voltage range that would result in an increased evoked firing rate only in this line (**Figure IV.6F**). The differences in activation and steady-state inactivation in only one of the four lines indicate this results from an interaction between the K1270T mutation and the patient genetic background.

Taken together, similar to the inhibitory neurons, the K1270T mutation causes reduced sodium current density in excitatory neurons in a dose-dependent manner. However, the decreased sodium current density caused by the mutation in excitatory neurons is not sufficient to reduce the evoked firing or AP waveforms in the mutated control line. Further, interactions between the mutation and the patient background appear to alter other properties of the sodium channel that increase firing in excitatory neurons of the patient line which may contribute to increased network activity.

Figure IV.6. In excitatory neurons, the K1270T mutation affects AP firing and decreases sodium current density. (A) Traces of action potential firing in excitatory neurons of the first isogenic pair of the control (ctrl) and the homozygous mutated control (mut ctrl). (B) The input-output curves of action potentials in excitatory neurons of the first isogenic pair. (C) AP amplitude of the first AP at rheobase in excitatory neurons of the first isogenic pair. (D-F) Same as A and B, but in excitatory neurons of the second isogenic pair of the lines of corrected patient (corr pt) and the heterozygous patient (pt). (G) Traces of voltage-gated sodium currents in excitatory neurons of the first isogenic pair. The activation protocol started with a prepulse at -100 mV followed by a series of steps ranging from -100 to 30 mV with a 10 mV interval. (H) Current-voltage relationship in excitatory neurons of the first isogenic pair. Whole cell currents were normalized to capacitance. (I-J) Same as G and H, but in excitatory neurons of the second isogenic pair. Data presented as mean + s.e.m in C and F, and mean ± s.e.m with total number of neurons evaluated and the number of individual platings in parentheses for each line in B,E,H, and J. * and # represent significant differences in genotypes and interaction within an isogenic pair respectively, two-way ANOVA and *post hoc* Sidak's analysis. One to four symbols denote p values < 0.05, 0.01, 0.001, 0.0001 respectively.

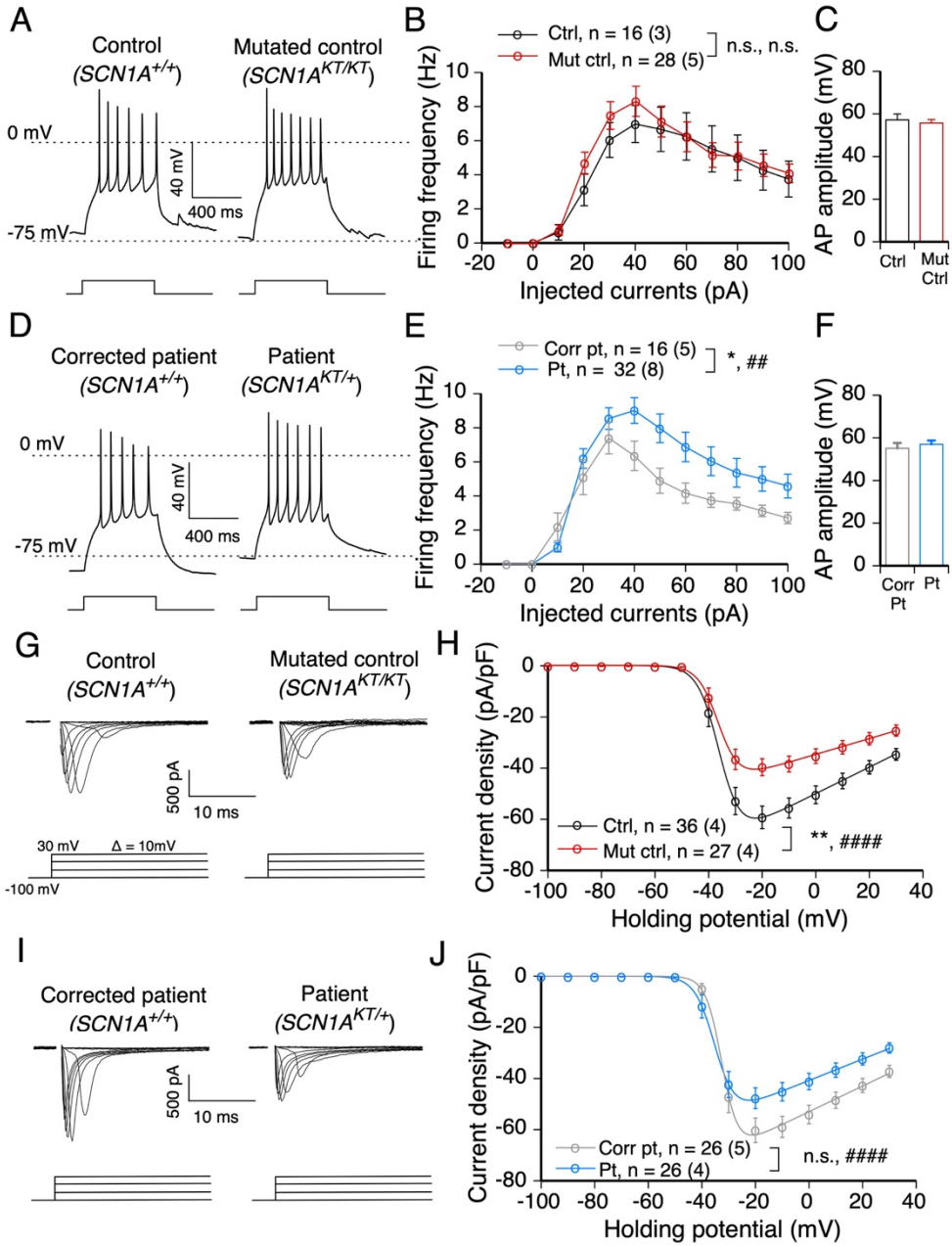
A
Control
(SCN1A+/+)
Mutated control
(SCN1AKT/KT)
0 mV
-75 mV
40 mV
400 ms
B
Ctrl, n = 16 (3)
Mut ctrl, n = 28 (5)
n.s., n.s.
Firing frequency (Hz)
Injected currents (pA)
C
AP amplitude (mV)
Ctrl
Mut Ctrl
D
Corrected patient
(SCN1A+/+)
Patient
(SCN1AKT/+)
0 mV
-75 mV
40 mV
400 ms
E
Corr pt, n = 16 (5)
Pt, n = 32 (8)
*, ##
Firing frequency (Hz)
Injected currents (pA)
F
AP amplitude (mV)
Corr Pt
Pt
G
Control
(SCN1A+/+)
Mutated control
(SCN1AKT/KT)
500 pA
10 ms
30 mV
Δ = 10mV
-100 mV
H
Current density (pA/pF)
Ctrl, n = 36 (4)
Mut ctrl, n = 27 (4)
**, ####
Holding potential (mV)
I
Corrected patient
(SCN1A+/+)
Patient
(SCN1AKT/+)
500 pA
10 ms
J
Current density (pA/pF)
Corr pt, n = 26 (5)
Pt, n = 26 (4)
n.s., ####
Holding potential (mV)

Figure IV.7. Properties of Nav in excitatory neurons. (A-B) Conductance vs voltage curves of activation in excitatory neurons of the control vs the mutated control lines, and the corrected patient vs the patient lines respectively. (C-D) Current vs voltage curves of steady-state inactivation in excitatory neurons of isogenic pairs. (E-F) Recovery of inactivation in both isogenic pairs. Data presented as mean ± s.e.m with total number of neurons and number of individual platings in parentheses. * and # represent significant differences in genotypes and interaction within an isogenic pair respectively, two-way ANOVA and *post hoc* Sidak's analysis. One and four symbols denote p values < 0.05, and 0.0001 respectively.

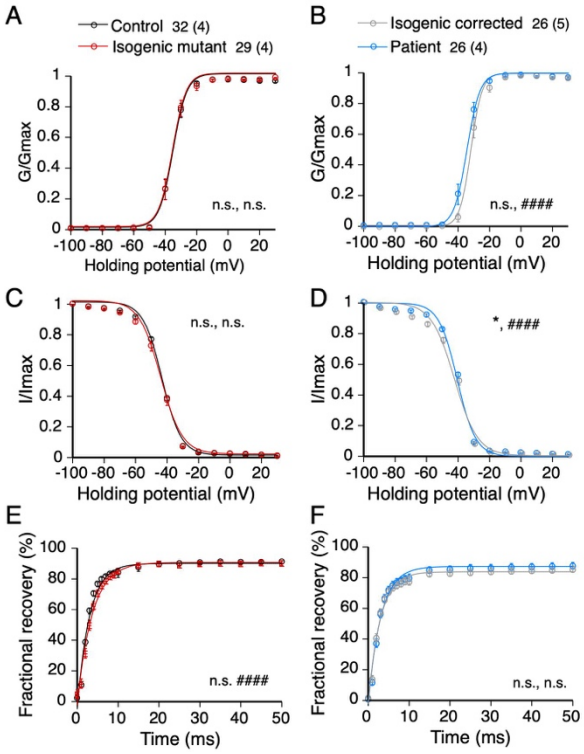

4.3.5. The K1270T mutation results in a hyperexcitable network.

A previous study from our laboratory found that the large majority of neurons in iPSC-derived cultures receive spontaneous glutamatergic and GABAergic synaptic input at D21-24 post plating[32]. To determine if the K1270T mutation, that specifically reduces firing of inhibitory neurons or increases firing of excitatory neurons in the patient line, causes an increase in excitability of the neuronal network, spontaneous excitatory and inhibitory post-synaptic currents (sEPSCs and sIPSCs) were recorded from excitatory neurons in each genotype.

All neurons that received both sEPSCs and sIPSCs were included for analysis. Recordings were obtained at two different holding potentials, -2 mV and -49 mV in each neuron corresponding to the reversal potential for EPSCs and IPSCs, respectively (**Figure IV.8A and 8D**). To determine whether there was any change in the balance of excitation vs inhibition, an index, (E-I)/(E+I) was used, where E and I represented amplitude or charge transfer of sEPSC and sIPSC respectively in excitatory neurons. This symmetric index ensures that E and I have the same scale, in contrast to an E/I ratio where the range is asymmetrical. An increase in the (E-I)/(E+I) index indicates an increase in excitatory drive or a decrease in inhibitory drive, and vice versa.

The (E-I)/(E+I) index based both on synaptic current amplitude and charge transfer, was significantly larger ($p = 0.0002$ and 0.0464 respectively, two-tailed Mann-Whitney U test) in the homozygous mutated control line compared to the control and these differences were significant ($p = 0.0002$ and 0.0464 respectively, two-tailed Mann-Whitney test; **Figure IV.8B and 8C**). There was a similar trend of larger (E-I)/(E+I) index in the heterozygous patient line compared to the corrected patient line but these differences were

not significant (**Figure IV.8E and 8F**). This indicates the mutation results in a dose-dependent increase of excitability in the neural networks formed in these cultures, consistent with the effects of mutation on sodium currents and evoked firing in inhibitory neurons. It also suggests that the increased firing frequency in the excitatory neurons in the patient line does not significantly affect network activity.

To test whether the increased excitatory drive in the network was also influenced by alterations in synaptic vesicle release, miniature excitatory and inhibitory PSCs (mEPSCs and mIPSCs) were recorded in excitatory neurons in the presence of 1 μM tetrodotoxin to block action potentials. The frequency, amplitude, and charge transfer of mEPSCs were similar between genotypes with the same genetic background (**Figure IV.9A-C**). There were also no changes in the mIPSCs (**Figure IV.9D-F**). This suggests that the K1270T mutation does not affect the synaptic vesicle release.

Together these data indicate that the K1270T mutation results in a dosage-dependent imbalance in excitation and inhibition that leads to hyperactivity in the neural network.

Figure IV.8. The K1270T mutation gives rise to a hyperactive neural network. (A) Spontaneous excitatory and inhibitory post-synaptic currents received by excitatory neurons in the first isogenic pair of the control (ctrl) and the mutated control (mut ctrl) line. (B) The ratio of spontaneous (E-I)/(E+I) amplitude in excitatory neurons of the first isogenic pair. (C) The ratio of spontaneous (E-I)/(E+I) of charge transfer in excitatory neurons of the first isogenic pair. (D-F) Same as A-C, but in excitatory neurons of the second isogenic pair of the corrected patient (corr pt) and the patient (pt) lines. Data reported as mean ± s.e.m. The total number of neurons and number of platings in parentheses for all four lines are 29 (7), 17 (4), 13 (3), and 18 (3) respectively. *p < 0.05 and ***p < 0.0001, two-tailed Mann-Whitney U test.

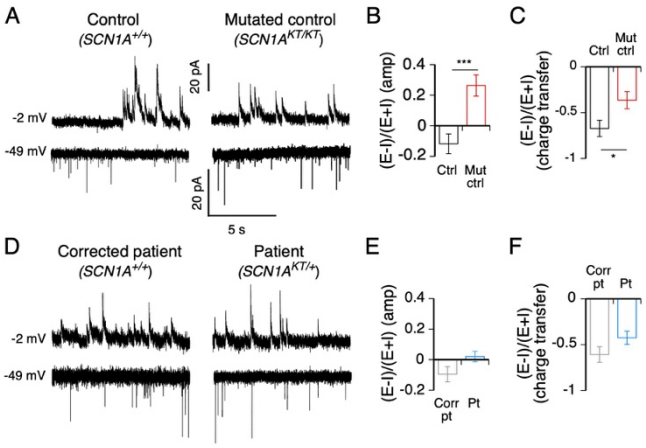

Figure IV.9. Miniature EPSCs and IPSCs received by excitatory neurons were unaltered by the K1270T mutation. (A-C) The frequency, amplitude and charge transfer of mEPSCs in the control (ctrl) vs the mutated control (mut ctrl), and the corrected patient (corr pt) vs the patient (pt) lines. (D-F) Same as A-C, but for mIPSCs. Data reported as mean + s.e.m. The total number of neurons and number of individual platings in parentheses for all four lines are ctrl: 9 (5), mut ctrl: 7 (3), corr pt:10 (4), and pt:10 (3).

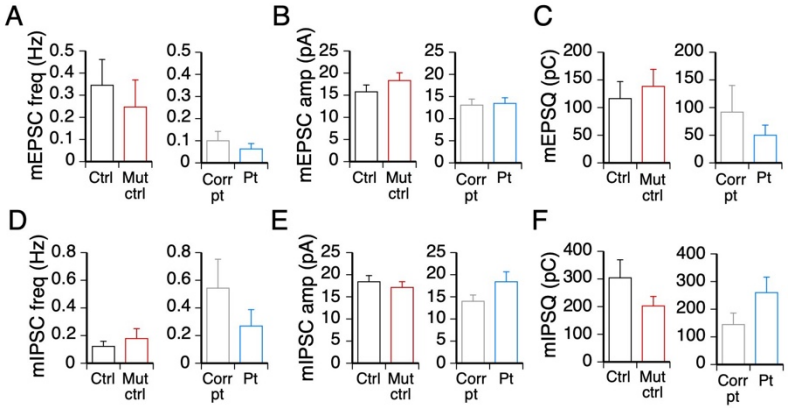

4.4. Discussion

4.4.1 Advantages of dual isogenic pair approach

Previous studies have used pairs of isogenic human iPSCs to explore relationship between gene mutations and phenotypes[29,43,44]. To our knowledge, ours is the first study to use two pairs of isogenic iPSCs (control sibling vs mutated control, and corrected patient vs patient sibling) to examine the direct relationship, independent of genetic background, between a single ion channel mutation and cellular mechanisms of genetic epilepsy. This approach is an efficient strategy to evaluate the causality of single gene mutations that require analysis at the single cell level to understand cellular mechanisms as is the case for the many different ion channel mutations linked to epilepsy.

Mutations that are not only necessary but sufficient to cause the functional change are identified as alterations that occur in both mutant lines, the patient line that carries the endogenous mutation and the mutated control line where K1270T was introduced by CRISPR, and not in the control or corrected patient lines that both lack the mutation but the corrected line has been subjected to CRISPR. In addition, since the patient line is heterozygous and the control mutated line is homozygous, this allows examination of the dose dependence on expression of specific properties. In the present study, decreases in firing frequency, AP amplitude, and sodium current density in inhibitory neurons, and reduction of sodium current density and increases in the (E-I)/(E+I) index of PSC amplitude and charge transfer in excitatory neurons in both mutant lines and not in either control lines, with the magnitude of effect all correlated with zygosity demonstrate they result from a dose-dependent effect of the K1270T mutation, independent of genetic background (**Table IV.5**). This comparative strategy also allows for identification of

alterations due to the genetic background based on changes that are found in both lines of one isogenic pair but not in the other isogenic pair[29], as is seen in the voltage dependence of Nav activation and inactivation in inhibitory neurons of the patient-derived pair only (**Table IV.5**). Further, a change in one mutant line that is not seen in the other mutant line or the controls, identifies alterations associated with an interaction between the mutation and the genetic background, as is observed in the voltage dependence of Nav activation and inactivation and increased firing frequency in excitatory neurons of the patient line (**Table IV.5**).

The GEFS+ patient from whom we collected skin fibroblast had prolonged febrile seizures and generalized afebrile absence seizures that are more severe than other members with the same *SCN1A* mutation in the pedigree[14]. It is likely that genetic background-dependent functional alterations that were observed in the patient line in the current study contribute to the differences in seizure phenotypes between patients in the GEFS+ family. It will be interesting to compare the genetic background of this individual to other GEFS+ family members to identify specific genetic modifiers that exacerbate or ameliorate the cellular defects. For instance, a missense mutation in *SCN9A* that encodes Nav1.7 has been identified in other *SCN1A*-associated epilepsy patients[45]. To identify genetic modifiers that are altered in the *SCN1A* GEFS+ mutants, single cell RNA sequencing or exome sequencing will be useful for screening candidates in a high-throughput manner[46,47].

Transcriptomic analysis in multiple iPSC lines generated from different individuals reveals genetic background variation accounts for differences between lines[48,49]. Therefore, it will be interesting to generate additional cell lines and multiple clones from each line via

genome editing to robustly interrogate the interaction between the mutation and genetic background in determining cellular phenotypes.

Table IV.5. Origins of effects

Origin	Mutation independent of background						Genetic background		Interaction between mutation and background		
Cell types	In			Ex			In		Ex		
Property	AP freq	AP amp	I_{Na^+}	I_{Na^+}	E/I (amp)	E/I (Q)	Nav act	Nav inact	AP freq	Nav act	Nav inact
Ctrl	-	-	-	-	-	-	-	-	-	-	-
Mut Ctrl (*SCN1A*$^{KT/KT}$)	↓↓	↓↓	↓↓	↓↓	↑↑	↑↑	-	-	-	-	-
Corr pt	-	-	-	-	-	-	↓	↓	-	-	-
Pt (*SCN1A*$^{KT/+}$)	↓	↓	↓	↓	↑	↑	↓	↓	↑	↓	↑

a. Ctrl = control, mut ctrl = mutated control, corr pt = corrected patient, and pt = patient.
b. In = inhibitory neurons, ex = excitatory neurons.
c. Amp = amplitude of synaptic currents, Q = charge transfer of synaptic currents.
d. Nav act = voltage dependence of activation of Nav, Nav inact = voltage dependence of steady-state inactivation of Nav
e. Number of arrows represent dosage dependent effects. In properties related to voltage, ↑ and ↓ represent more depolarized and hyperpolarized respectively.

4.4.2 Alterations in excitability and sodium current density in inhibitory neurons

Our results demonstrate that in inhibitory neurons, the K1270T *SCN1A* mutation causes dosage-dependent decrease in evoked firing frequency and AP amplitude. The reduced excitability and sodium currents in inhibitory neurons is consistent with a number of studies in mouse and iPSC model systems[21,35,36]. In particular, previous studies have shown impaired excitability in two subtypes of GABAergic neurons, parvalbumin (PV)- and somatostatin (SST)-expressing interneurons in mouse models of *SCN1A* epilepsy[50,51]. Selective deletion of *Scn1a* in PV and SST interneurons causes hyperactivity in neural networks and seizure behaviors, suggesting the importance of Nav1.1 in regulating inhibitory neuron activity and the E/I balance[52–54]. Our preliminary data reveal that GABAergic neurons in our cultures can be divided into at least two groups staining iPSC-derived neurons with anti-βIII-tubulin and PV or SST antibodies (data not shown). However, we did not observe fast spiking, bursting or adapting firing patterns characteristic of PV and SST interneurons in recorded GAD1-mCherry^{+} neurons. This suggests that functional maturation of interneuron subtypes require a longer time in culture. Future studies will be directed to determine the effect of *SCN1A* mutation in the electrophysiological properties of identified PV and SST interneurons.

iPSC-derived inhibitory neurons in the present study had large sodium currents, but they were not well space clamped. This is typical in neurons that are capable of firing multiple APs[20–23,40]. While evaluation of sodium currents that are not well space clamped does not resolve absolute biophysical properties, comparisons of sodium current properties within and between isogenic pairs are still informative in identifying alterations caused by the mutation. For example, pair wise comparisons demonstrate that the K1270T

mutation causes a decrease in sodium current density, independent of genetic background, in inhibitory neurons. Further studies will be necessary to determine if the reduction in sodium current density recorded at the cell bodies is due to a decrease in total number of sodium channels expressed or a change in localization of channels as channels distant from the cell soma might reduce their contribution to the recorded currents. This could be addressed by immune-electron microscopy to evaluate voltage-gated sodium channel localization in neurons from the different genotypes.

The dosage-dependent effect of the K1270T mutation is similar to the observations of sodium currents and evoked firing rate of bipolar cells that were selectively affected in the mouse model of Dravet Syndrome with partial deletion of *Scn1a*[36]. In another mouse model with GEFS+ *SCN1A* R1648H mutation, although dosage-dependent cellular effects were not observed, the homozygous mice had a higher susceptibility to seizures than the heterozygous mice in comparison to the wild types[35]. Therefore, our study is consistent with the findings *in vivo* and predicts a functional outcome of the K1270T mutation on the seizure generation in animal models.

4.4.3 Alterations in excitability and sodium current density in excitatory neurons

Previous studies have reported mutation of *SCN1A* has little effect on sodium currents in excitatory neurons[21,35,36]. In contrast we report that the K1270T mutation results in a similar dose-dependent decrease in sodium current density in excitatory and inhibitory neurons. This is consistent with Nav1.1 staining not only in GABAergic neurons but in our CaMKII-eGFP$^+$ neurons. While previous studies suggest that Nav1.1 is strongly

expressed in inhibitory neurons[55], other studies report that Nav1.1 is present in a subset of excitatory neurons[53,56].

Interestingly, the decrease in sodium current density does not result in reduced firing in the excitatory neurons as it does in inhibitory neurons. This indicates that the changes in the sodium current density were not sufficient to reduce excitability in this cell type. This could be due to compensation from potassium currents, as a voltage-gated potassium channel Kv8.2 has been shown to function as a genetic modifier increasing the susceptibility of an *Scn2a* mutant mouse to epilepsy[57,58]. Altered currents of Kv1 and Kv4 are associated with increased excitability in a subset of pyramidal neurons in a mouse model of fragile X syndrome[59]. *CACNB4* and *CACNA1A* that encode Cav have also been identified as genetic modifiers that result in a gain of function in families with *SCN1A* Dravet syndrome[60,61].

Further, the AP firing frequency is actually increased in the excitatory neurons in the patient line resulting from an interaction between the mutation and the patient genetic background. This is consistent with changes in the voltage-dependence of sodium current activation and inactivation only in the patient excitatory neurons. These changes predict that the channel is open over a wider voltage range and is thus consistent with the increase in AP firing seen in patient excitatory neurons. To explore the biophysical changes in finer detail it would be possible to lower the external sodium concentration to reduce the size of the sodium currents and increase potential for good voltage control[62]. One could also examine the biophysical properties of single sodium channels in excised or cell attached patches from the cell body[63,64]. Both of these would provide additional insight, but they also have the limitation of restricting analysis to a small population of channels in a restricted

location (on or near cell body) that may not represent the full population of channels that define the firing properties of the neurons.

4.4.4 Hyperactive neural network

Our previous study demonstrates that iPSC-derived neurons form functionally active neural networks that contain GABAergic and glutamatergic synaptic connections[32], allowing us to evaluate the effect the K1270T mutation on the network activity of the neuronal cultures. Our results reveal a gene dosage-dependent increase in excitatory drive relative to inhibitory drive in excitatory neurons, consist with decreased evoked firing in inhibitory neurons and/or increased evoked firing in excitatory neurons. These alterations in synaptic activity were identified only in the mutant lines, suggesting they are caused by the K1270T mutation, independent of the genetic background. It also indicates that the increased firing frequency in the excitatory neurons in the patient line due to the interaction between the mutation and the genetic background does not significantly affect network activity.

Hyperexcitable neural networks are implicated in epileptic disorders[65]. Therefore, our iPSC-derived neuronal cultures provide insights into the underlying mechanism of how an epilepsy-associated *SCN1A* mutation gives rise to increased probability of seizures in patients. To understand the effect of the mutation on the spontaneous network activity and network synchrony more broadly, our future studies will use multi-electrode arrays that allow for mechanistic study and anti-epileptic drug screening in a high-throughput manner[66].

4.4.5 Developmental maturation

Using our neuronal differentiation protocol that includes plating iPSC-derived neural progenitors onto astroglial feeder layers, the large majority of neurons fire multiple action potentials[32,33]. The derived neurons not only have sodium currents larger than 1 nA in average and fire multiple action potentials at 7-8 Hz comparable to other iPSC studies[21,23], but they also receive glutamatergic and GABAergic synaptic input within 3 weeks of plating. However, their electrophysiological properties are less mature than neurons expected in an adult brain, based on lower firing frequency, larger input resistance, and depolarized RMP. Single-cell transcriptome analysis reveals development of interneurons at D54 *in vitro* recapitulates those in human fetal cortex at 100 dpc[67]. While we cannot rule out the possibility that the K1270T mutation causes a developmental delay in neuronal development in culture, it seems unlikely to explain our results of reduced firing frequency and action potential AP in inhibitory neurons associated with the mutation because 1) there was no consistent change in RMP or input resistance and 2) the excitatory neurons of the mutated control and the patient lines were able to fire APs in similar or higher frequency compared to their controls. However future studies could evaluate effects of the mutation on further maturation in long-term cultures.

4.4.6 Off-target mutation

Sequences of the top five off-target sites from CRISPR/Cas9 editing, including *SCN7A*, *FLII*, *SCN2A*, *SCN3A* and *SCN9A* were examined. The corrected patient line did not have off-target mutations in the candidate genes (**Figure IV.2A**). While the mutated control line did not have off-target mutations in the other genes, it harbored one in *SCN7A*. It is very

unlikely that this mutation affected the results reported based on the following considerations. First, *SCN7A* encodes the Na_x sodium channel in heart, uterus, skeletal muscle, and peripheral nervous system and RT-PCR analysis demonstrated that it is not expressed in our iPSC-derived neurons. Secondly, the channel is insensitive to changes in membrane potential and TTX, a voltage-gated sodium channel blocker[68]. Isolated sodium currents in iPSC-derived neurons at D21-24 post plating were completely eliminated in the presence of 1 μM TTX (**Figure IV.4B**). Third, while it is possible that the off-target mutation in *SCN7A* could trigger homeostatic regulation by up- or down-regulating *SCN1A* expression, this is unlikely as the alterations in sodium currents/evoked firing in the homozygous mutated control line were in the same direction and twice as large as the heterozygous patient line that did not undergo editing process.

4.4.7 Comparison with the previous knock-in fly model

The reduced excitability observed specifically in iPSC-derived inhibitory neurons is consistent with the decreased excitability specifically in inhibitory neurons in the brains of K1270T GEFS+ knock-in *Drosophila*[69]. Since both flies and patients exhibit heat-induced seizures, this provides additional support to the hypothesis that reduced firing specifically in inhibitory neurons is critical to the disease phenotype in humans. However, the cellular defect associated with reduced excitability is distinct between the models demonstrating two independent mechanisms that result in a similar phenotype. In the iPSC-derived neurons there is a significant decrease in the amplitude of the transient currents that are the dominant form of sodium current in these neurons. In flies the reduced firing is associated with a hyperpolarized shift in the deactivation threshold of the large persistent

sodium currents characteristic of inhibitory neurons in the adult fly brain. It is possible that modifying the persistent currents in iPSCs by shifting their voltage dependence could moderate the deficits associated with a reduced transient sodium current.

In addition, an increase in excitability was observed in excitatory neurons of the patient line, consistent with the higher firing rate in excitatory neurons in the GEFS+ flies[16]. The alterations in fly are seen predominantly at high temperature, so it is possible that elevated temperatures will reveal additional or more severe alterations in sodium currents in iPSC-derived neurons, as the patient sibling from whom the skin fibroblast was collected showed more severe seizure phenotypes of febrile seizures compared to afebrile seizures[14].

4.4.8 Summary

Overall the CRISPR/Cas9-based disease modeling strategy with iPSC-derived neurons can validate clinically relevant phenotypes and reveal the sufficiency and necessity of *SCN1A* mutations for specific phenotypes in the human genetic background. Furthermore, a library of patient iPSCs with a variety of *SCN1A* mutations built using this approach, in combination with a high-throughput drug screening method such as multi-electrode array (MEA), will facilitate the development of personalized anti-epileptic medicine[70–72].

4.5. Bibliography

1. Scheffer, I. E. & Berkovic, S. F. Generalized epilepsy with febrile seizures plus. A genetic disorder with heterogeneous clinical phenotypes. *Brain* **120**, 479–490 (1997).
2. Miller, I. & Sotero de Menezes, M. *SCN1A-Related Seizure Disorders*. (University of Washington, Seattle, 2014).
3. Baulac, S. *et al.* First genetic evidence of GABA(A) receptor dysfunction in epilepsy: a

mutation in the gamma2-subunit gene. *Nat. Genet.* **28**, 46–48 (2001).
4. Dibbens, L. M. *et al.* GABRD encoding a protein for extra- or peri-synaptic GABAA receptors is a susceptibility locus for generalized epilepsies. *Hum. Mol. Genet.* **13**, 1315–1319 (2004).
5. Escayg, A. *et al.* Mutations of SCN1A, encoding a neuronal sodium channel, in two families with GEFS+2. *Nat. Genet.* **24**, 343–345 (2000).
6. Escayg, A. *et al.* A novel SCN1A mutation associated with generalized epilepsy with febrile seizures plus--and prevalence of variants in patients with epilepsy. *Am. J. Hum. Genet.* **68**, 866–873 (2001).
7. Harkin, L. A. *et al.* Truncation of the GABA(A)-receptor gamma2 subunit in a family with generalized epilepsy with febrile seizures plus. *Am. J. Hum. Genet.* **70**, 530–536 (2002).
8. Sugawara, T. *et al.* A missense mutation of the Na+ channel alpha II subunit gene Na(v)1.2 in a patient with febrile and afebrile seizures causes channel dysfunction. *Proc. Natl. Acad. Sci. U. S. A.* **98**, 6384–6389 (2001).
9. Wallace, R. H. *et al.* Generalized epilepsy with febrile seizures plus: mutation of the sodium channel subunit SCN1B. *Neurology* **58**, 1426–1429 (2002).
10. Wallace, R. H. *et al.* Febrile seizures and generalized epilepsy associated with a mutation in the Na+-channel beta1 subunit gene SCN1B. *Nat. Genet.* **19**, 366–370 (1998).
11. Wallace, R. H. *et al.* Mutant GABA(A) receptor gamma2-subunit in childhood absence epilepsy and febrile seizures. *Nat. Genet.* **28**, 49–52 (2001).
12. Wallace, R. H. *et al.* Neuronal sodium-channel alpha1-subunit mutations in generalized epilepsy with febrile seizures plus. *Am. J. Hum. Genet.* **68**, 859–865 (2001).
13. Meng, H. *et al.* The SCN1A mutation database: updating information and analysis of the relationships among genotype, functional alteration, and phenotype. *Hum. Mutat.* **36**, 573–580 (2015).
14. Abou-Khalil, B. *et al.* Partial and generalized epilepsy with febrile seizures plus and a novel SCN1A mutation. *Neurology* **57**, 2265–2272 (2001).
15. Goldberg-Stern, H. *et al.* Broad phenotypic heterogeneity due to a novel SCN1A mutation in a family with genetic epilepsy with febrile seizures plus. *J. Child Neurol.* **29**, 221–226 (2014).
16. Schutte, S. S., Schutte, R. J., Barragan, E. V & O'Dowd, D. K. Model systems for studying cellular mechanisms of SCN1A-related epilepsy. *J. Neurophysiol.* **115**, 1755–1766 (2016).
17. Marian, A. J. Modeling human disease phenotype in model organisms: 'It's only a model!' *Circ. Res.* **109**, 356–359 (2011).
18. Maxwell, E. K. *et al.* Evolutionary profiling reveals the heterogeneous origins of classes of human disease genes: implications for modeling disease genetics in animals. *BMC Evol. Biol.* **14**, 212 (2014).
19. Higurashi, N. *et al.* A human Dravet syndrome model from patient induced pluripotent stem cells. *Mol. Brain* **6**, 19 (2013).
20. Liu, J. *et al.* CRISPR/Cas9 facilitates investigation of neural circuit disease using human iPSCs: mechanism of epilepsy caused by an SCN1A loss-of-function mutation. *Transl Psychiatry* **6**, e703 (2016).

21. Sun, Y. *et al.* A deleterious Nav1.1 mutation selectively impairs telencephalic inhibitory neurons derived from Dravet Syndrome patients. *Elife* **5**, e13073 (2016).
22. Jiao, J. *et al.* Modeling Dravet syndrome using induced pluripotent stem cells (iPSCs) and directly converted neurons. *Hum. Mol. Genet.* **22**, 4241–4252 (2013).
23. Liu, Y. *et al.* Dravet syndrome patient-derived neurons suggest a novel epilepsy mechanism. *Ann. Neurol.* **74**, 128–139 (2013).
24. Liang, G. & Zhang, Y. Genetic and epigenetic variations in iPSCs: potential causes and implications for application. *Cell stem cell* **13**, 149–159 (2013).
25. Vitale, A. M. *et al.* Variability in the Generation of Induced Pluripotent Stem Cells: Importance for Disease Modeling. *Stem Cells Translational Medicine* **1**, 641–650 (2012).
26. Sandoe, J. & Eggan, K. Opportunities and challenges of pluripotent stem cell neurodegenerative disease models. *Nat Neurosci* **16**, 780–789 (2013).
27. Bassett, A. R. Editing the genome of hiPSC with CRISPR/Cas9: disease models. *Mamm. Genome* **28**, 348–364 (2017).
28. Chen, W. *et al.* Generation of the SCN1A epilepsy mutation in hiPS cells using the TALEN technique. *Sci. Rep.* **4**, 5404 (2014).
29. Smith, J. G. W. *et al.* Isogenic Pairs of hiPSC-CMs with Hypertrophic Cardiomyopathy/LVNC-Associated ACTC1 E99K Mutation Unveil Differential Functional Deficits. *Stem cell reports* **11**, 1226–1243 (2018).
30. Stover, A. E. *et al.* Process-based expansion and neural differentiation of human pluripotent stem cells for transplantation and disease modeling. *J. Neurosci. Res.* **91**, 1247–1262 (2013).
31. Stover, A. E. & Schwartz, P. H. Adaptation of Human Pluripotent Stem Cells to Feeder-Free Conditions in Chemically Defined Medium with Enzymatic Single-Cell Passaging. *Methods Mol. Biol.* **767**, 137–146 (2011).
32. Xie, Y. *et al.* Reproducible and efficient generation of functionally active neurons from human hiPSCs for preclinical disease modeling. *Stem Cell Res.* **26**, 84–94 (2018).
33. Schutte, R. J. *et al.* Astrocyte-enriched feeder layers from cryopreserved cells support differentiation of spontaneously active networks of human iPSC-derived neurons. *J. Neurosci. Methods* **294**, 91–101 (2018).
34. Paquet, D. *et al.* Efficient introduction of specific homozygous and heterozygous mutations using CRISPR/Cas9. *Nature* **533**, 125–129 (2016).
35. Martin, M. S. *et al.* Altered function of the SCN1A voltage-gated sodium channel leads to gamma-aminobutyric acid-ergic (GABAergic) interneuron abnormalities. *J. Biol. Chem.* **285**, 9823–9834 (2010).
36. Yu, F. H. *et al.* Reduced sodium current in GABAergic interneurons in a mouse model of severe myoclonic epilepsy in infancy. *Nat. Neurosci.* **9**, 1142–1149 (2006).
37. Yu, J. *et al.* Induced pluripotent stem cell lines derived from human somatic cells. *Science* **318**, 1917–1920 (2007).
38. Gautron, S. *et al.* The glial voltage-gated sodium channel: cell- and tissue-specific mRNA expression. *Proc. Natl. Acad. Sci. U. S. A.* **89**, 7272–7276 (1992).
39. Watanabe, E. *et al.* Nav2/NaG channel is involved in control of salt-intake behavior in the CNS. *J. Neurosci.* **20**, 7743–7751 (2000).
40. Kim, H. W. *et al.* Differential effects on sodium current impairments by distinct SCN1A mutations in GABAergic neurons derived from Dravet syndrome patients.

Brain Dev. **40**, 287–298 (2018).
41. Hedrich, U. B. S. *et al.* Impaired action potential initiation in GABAergic interneurons causes hyperexcitable networks in an epileptic mouse model carrying a human Na(V)1.1 mutation. *J. Neurosci.* **34**, 14874–14889 (2014).
42. Mistry, A. M. *et al.* Strain- and age-dependent hippocampal neuron sodium currents correlate with epilepsy severity in Dravet syndrome mice. *Neurobiol. Dis.* **65**, 1–11 (2014).
43. Ananiev, G., Williams, E. C., Li, H. & Chang, Q. Isogenic pairs of wild type and mutant induced pluripotent stem cell (iPSC) lines from Rett syndrome patients as in vitro disease model. *PLoS One* **6**, e25255–e25255 (2011).
44. Bellin, M. *et al.* Isogenic human pluripotent stem cell pairs reveal the role of a KCNH2 mutation in long-QT syndrome. *EMBO J.* **32**, 3161–3175 (2013).
45. Singh, N. A. *et al.* A role of SCN9A in human epilepsies, as a cause of febrile seizures and as a potential modifier of Dravet syndrome. *PLoS Genet.* **5**, e1000649 (2009).
46. Hawkins, N. A., Zachwieja, N. J., Miller, A. R., Anderson, L. L. & Kearney, J. A. Fine Mapping of a Dravet Syndrome Modifier Locus on Mouse Chromosome 5 and Candidate Gene Analysis by RNA-Seq. *PLOS Genet.* **12**, e1006398 (2016).
47. Landis, B. J. *et al.* Exome Sequencing Identifies Candidate Genetic Modifiers of Syndromic and Familial Thoracic Aortic Aneurysm Severity. *J. Cardiovasc. Transl. Res.* **10**, 423–432 (2017).
48. Burrows, C. K. *et al.* Genetic Variation, Not Cell Type of Origin, Underlies the Majority of Identifiable Regulatory Differences in iPSCs. *PLOS Genet.* **12**, e1005793 (2016).
49. Rouhani, F. *et al.* Genetic Background Drives Transcriptional Variation in Human Induced Pluripotent Stem Cells. *PLOS Genet.* **10**, e1004432 (2014).
50. Favero, M., Sotuyo, N. P., Lopez, E., Kearney, J. A. & Goldberg, E. M. A Transient Developmental Window of Fast-Spiking Interneuron Dysfunction in a Mouse Model of Dravet Syndrome. *J. Neurosci.* **38**, 7912–7927 (2018).
51. Tai, C., Abe, Y., Westenbroek, R. E., Scheuer, T. & Catterall, W. A. Impaired excitability of somatostatin- and parvalbumin-expressing cortical interneurons in a mouse model of Dravet syndrome. *Proc. Natl. Acad. Sci. U. S. A.* **111**, E3139-48 (2014).
52. Cheah, C. S. *et al.* Specific deletion of NaV1.1 sodium channels in inhibitory interneurons causes seizures and premature death in a mouse model of Dravet syndrome. *Proc. Natl. Acad. Sci. U. S. A.* **109**, 14646–14651 (2012).
53. Dutton, S. B. *et al.* Preferential inactivation of Scn1a in parvalbumin interneurons increases seizure susceptibility. *Neurobiol. Dis.* **49**, 211–220 (2013).
54. Rubinstein, M. *et al.* Dissecting the phenotypes of Dravet syndrome by gene deletion. *Brain* **138**, 2219–2233 (2015).
55. Ogiwara, I. *et al.* Nav1.1 localizes to axons of parvalbumin-positive inhibitory interneurons: a circuit basis for epileptic seizures in mice carrying an Scn1a gene mutation. *J. Neurosci.* **27**, 5903–5914 (2007).
56. Ogiwara, I. *et al.* Nav1.1 haploinsufficiency in excitatory neurons ameliorates seizure-associated sudden death in a mouse model of Dravet syndrome. *Hum. Mol. Genet.* **22**, 4784–4804 (2013).
57. Bergren, S. K., Rutter, E. D. & Kearney, J. A. Fine mapping of an epilepsy modifier gene on mouse Chromosome 19. *Mamm. Genome* **20**, 359–366 (2009).
58. Jorge, B. S. *et al.* Voltage-gated potassium channel KCNV2

(Kv8.2) contributes to epilepsy susceptibility. *Proc. Natl. Acad. Sci.* **108**, 5443 LP – 5448 (2011).
59. Kalmbach, B. E., Johnston, D. & Brager, D. H. Cell-Type Specific Channelopathies in the Prefrontal Cortex of the fmr1-/y Mouse Model of Fragile X Syndrome. *eNeuro* **2**, ENEURO.0114-15.2015 (2015).
60. Ohmori, I. *et al.* A CACNB4 mutation shows that altered Ca(v)2.1 function may be a genetic modifier of severe myoclonic epilepsy in infancy. *Neurobiol. Dis.* **32**, 349–354 (2008).
61. Ohmori, I. *et al.* CACNA1A variants may modify the epileptic phenotype of Dravet syndrome. *Neurobiol. Dis.* **50**, 209–217 (2013).
62. Colatsky, T. J. Voltage clamp measurements of sodium channel properties in rabbit cardiac Purkinje fibres. *J. Physiol.* **305**, 215–234 (1980).
63. Franciolini, F. Patch clamp technique and biophysical study of membrane channels. *Experientia* **42**, 589–594 (1986).
64. Stühmer, W., Methfessel, C., Sakmann, B., Noda, M. & Numa, S. Patch clamp characterization of sodium channels expressed from rat brain cDNA. *Eur. Biophys. J.* **14**, 131–138 (1987).
65. Shao, L.-R., Habela, C. W. & Stafstrom, C. E. Pediatric Epilepsy Mechanisms: Expanding the Paradigm of Excitation/Inhibition Imbalance. *Child. (Basel, Switzerland)* **6**, (2019).
66. Tidball, A. M. & Parent, J. M. Concise Review: Exciting Cells: Modeling Genetic Epilepsies with Patient-Derived Induced Pluripotent Stem Cells. *Stem Cells* **34**, 27–33 (2016).
67. Close, J. L. *et al.* Single-Cell Profiling of an In Vitro Model of Human Interneuron Development Reveals Temporal Dynamics of Cell Type Production and Maturation. *Neuron* **93**, 1035-1048.e5 (2017).
68. Hiyama, T. Y. *et al.* Nax channel involved in CNS sodium-level sensing. *Nat. Neurosci.* **5**, 511–512 (2002).
69. Sun, L. *et al.* A knock-in model of human epilepsy in Drosophila reveals a novel cellular mechanism associated with heat-induced seizure. *The Journal of neuroscience : the official journal of the Society for Neuroscience* **32**, 14145–14155 (2012).
70. Du, X. & Parent, J. M. Using Patient-Derived Induced Pluripotent Stem Cells to Model and Treat Epilepsies. *Current neurology and neuroscience reports* **15**, 71 (2015).
71. Odawara, A., Katoh, H., Matsuda, N. & Suzuki, I. Physiological maturation and drug responses of human induced pluripotent stem cell-derived cortical neuronal networks in long-term culture. *Sci. Rep.* **6**, 26181 (2016).
72. Parent, J. M. & Anderson, S. A. Reprogramming patient-derived cells to study the epilepsies. *Nat. Neurosci.* **18**, 360–366 (2015).

Chapter V

Summary, Future Directions and Significance

5.1 Summary

A myriad of *SCN1A* mutations are associated with epilepsies. However, how specific mutations give rise to seizures in epilepsy patients remains elusive. To detect mutation-associated alterations in electrophysiological properties of human iPSC-derived neurons, we developed reproducible and efficient differentiation protocols that generate functionally active neurons by growing them on top of mouse astroglial feeder layers. Neuronal cultures contain inhibitory and excitatory neurons that are capable of firing multiple action potentials and forming functional connections. To determine the cellular effect of a single *SCN1A* mutation, independent of genetic background, we generated dual pairs of human iPSCs using CRISPR/Cas9 editing and differentiated them into functional neurons using our optimized protocols. Comparison of electrophysiological properties of inhibitory and excitatory neurons revealed gene dosage-dependent and cell type-specific alterations in sodium currents and evoked firing, resulting in a hyper-excitable neural network. We also identified alterations associated with the genetic background and the interaction between the mutation and the background.

5.2 Future directions

5.2.1. Identify genetic modifiers using RNA sequencing

Our results identified alterations due to the genetic background, as is seen in the voltage dependence of Nav activation and inactivation in inhibitory neurons of both of the patient-derived lines when compared to both of the lines from the control. We have also found alterations due to the interatction between the mutation and the genetic background, as is seen in the voltage dependence of Nav activation and inactivation and

evoked firing frequency in excitatory neurons of the patient line. Thess suggest that genetic modifiers in the patient background alter the phenotypic expression of the *SCN1A* gene. Indeed, individuals in the multigenerational family where the K1270T *SCN1A* mutation was identified exhibit seizure phenotypes in different severity[1].

Sequencing in combination with dual isogenic pairs of human iPSCs is a promising system for identifying alterations due to the genetic background. Using a reverse genetics approach, the mechanism underlying the differences between the two pairs pinpoint the potential genetic modifiers that might be involved in regulating this property[2]. As we found genetic background-dependent alterations in the patient-derived isogenic pair, sequencing analysis in the candidate genes in the patient-derived vs the control-derived isogenic pairs can be used to identify mutations in other genes that are involved in regulating neuronal activity or network activity. For instance, missense mutations in *SCN9A* that encodes Nav1.7 has been identified in other *SCN1A*-associated epilepsy patients[3]. In addition, single-cell RNA sequencing is a powerful tool to identify genes with altered expression level that might contribute to the modification of the disease phenotypes. For example, altered expression of *Gabra2* that encodes $GABA_A$ receptor has been identified in DS mice with a *SCN1A* mutation[4]. Further pharmacological manipulation using an anti-convulsant drug with higher affinity with $GABA_A$ receptor ameliorates the susceptibility to heat-induced seizures in mice[4]. This can be applied to our current study by comparing the transcriptome in dual isogenic pairs of human iPSCs.

Inbred mice are also an excellent model system for identification of genetic modifiers based on a forward genetics approach[5]. Mutant mice that exhibit seizure phenotypes are crossed with different inbred wild-type mice. Based on the outcome in survival and seizure

phenotypes in the offspring, candidate genes can be identified using genetic mapping tools such as positional cloning or quantitative trait loci mapping, followed by sequencing and expression analysis to find out strong modifier candidates. Using this strategy, the *Kcnv2* gene that encodes voltage-gated potassium channel subfamily V member 2 have been identified as genetic modifiers in *SCN2A* epilepsy[6].

5.2.2. Screen drugs using high-throughput multi-electrode array

The prescription of drugs to epilepsy patients is largely based on an empirical approach with little understanding in the underlying mechanism of action in each individual. Two GEFS+ siblings with the same K1270T *SCN1A* mutation, exhibited different seizure phenotypes. One of these individuals was most effectively treated with valproic acid and levetiracetam, while the second responded well to ethosuximide[1]. This supports the interpretation that genetic background contributes to the variation in the efficacy of the anti-epileptic drugs (AEDs). Polymorphism in genes involved in drug metabolism has been identified to induce resistance to AEDs due to altered drug concentration and drug toxicity[7]. Therefore, it is important to develop targeted treatment for patient precision medicine based on the underlying cellular mechanism of epilepsy-causing mutations. Patient iPSC-derived neuronal cultures in combination with a new multi-electrode array (MEA) is emerging as a useful platform for mechanistic study and drug screening in a high-throughput manner[8].

MEA systems enable real-time analysis in neuronal activity by converting changes in voltages due to ion flow during action potential firing into currents[9]. MEAs have been used to evaluate spontaneous activity, bursting, synchronous network activity, toxicity of anti-

convulsant drugs, drug responses and inducing long-term potentiation and depression in human iPSC-derived neuronal cultures[10–13].

In our lab, preliminary results demonstrate that iPSC-derived neurons could be co-cultured on top of astroglial feeder layers on the MEA platform. They are capable of forming spontaneously active neural networks with burst firing and synchrony (**Figure V.1**). Based on the cellular mechanism that was identified in Chapter 3, candidates involved in future studies include $GABA_A$ agonists (clonazepam and clobazam), GABA reuptake inhibitors (sodium valproate and vigabatrin), and glutamate blockers (perampanel and topiramate). Additionally, it would be interesting to test compounds used alternatively or for other disorders but attenuating seizures effectively, such as cannabidiol and riluzole[14,15]. By evaluating the network activity and synchrony in the patient iPSC-derived neuronal cultures in response to drug treatment, it is possible to identify the candidate compound that can dampen the hyperactivity in networks for the development of patient precision medicine.

MEA systems also allow for mechanistic study on the effect of *SCN1A* mutations on the GESF+ patient iPSC-derived neurons at elevated temperature. The GEFS+ individual with the K1270T *SCN1A* mutation in our current study was diagnosed with febrile seizures that occur during fever[1]. A previous study in our lab using a knock-in *Drosophila* model with the human K1270T mutation identified alterations in the Nav function at elevated temperature as a possible mechanism that contributes to the heat-induced seizures[16]. We attempted to examine the effect of the mutation in our iPSC-derived neurons at higher temperature. However, the viability of cells rapidly decreased as the recording environment was not favorable to cells probably due to a lack of 5% CO_2 as in the

incubator. As the chamber of the MEA system is capable of maintaining at stable temperature, humidity and CO_2 concentration, it has been used to investigate the effect of Nav1.7 mutations in spontaneous firing at elevated temperatures and evaluate the efficacy of a candidate drug on attenuating the hyperactivity of neurons[17,18]. It would be interesting to assess how the K1270T mutation alters the spontaneous network activity at temperatures during which febrile seizure occur in GEFS+ patients.

Figure V.1. Spontaneous neural network activity recorded by the MEA system. Spontaneously active network activity with burst firing and synchrony in the iPSC-derived neuronal cultures. Each row represents electrical activity recorded by each electrode. Each spike represents a spontaneous firing event. Scale bar represents 10 seconds.

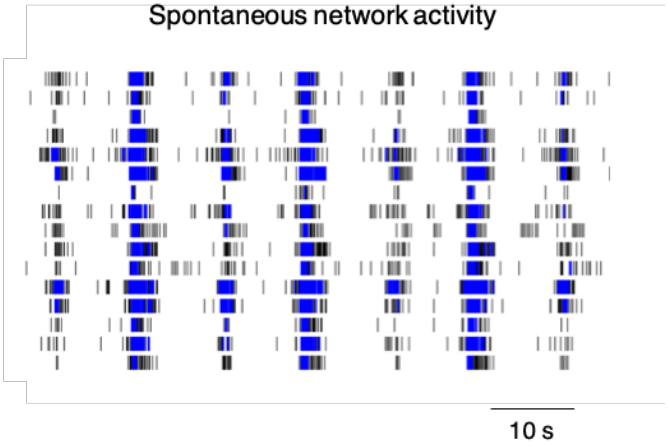

5.2.3. Determine the functional consequence of the SCN1A mutation in vivo

Due to the large diversity of hippocampal pyramidal and inhibitory neurons based on their anatomy, location and electrophysiology, understanding how different cell types contribute to dysfunctional neural circuit in epilepsy is important[19–21]. A number of studies on *SCN1A* epilepsy in mouse models have proposed an attractive interneuron hypothesis which suggests that *Scn1a* mutations did not alter the excitability of hippocampal pyramidal neurons, but the excitability of hippocampal inhibitory interneurons is impaired[22,23].

Both our *Drosophila* and iPSC models have shown the K1270T *SCN1A* mutation preferentially reduces action potential firing in inhibitory neurons but not excitatory neurons. As comparing across multiple organisms might unveil conserved mechanism, we have generated a knock-in mouse model with the human K1270T *SCN1A* mutation using CRISPR/Cas9 editing. Through collaborative efforts with Dr. Antara Das in our lab, excitability of pyramidal excitatory neurons in the CA1 of the hippocampus was recorded at P25-40. Preliminary data showed that in the firing frequency versus current step curves, the firing frequency in pyramidal neurons of the heterozygous *Scn1a*$^{KT/+}$ mice was not different from the wild-types (**Figure V.2A and B**). The two genotypes also had similar action potential threshold, amplitude, half-width and rheobase (**Figure V.2C-F**). There were no differences between *Scn1a*$^{KT/+}$ and the wild-type in the passive membrane properties including input resistance, whole-cell capacitance and rest membrane potential (**Table V.1**). Based on the interneuron hypothesis, it is expected to observe reduced activity in hippocampal parvalbumin (PV)-expressing interneurons in our mouse model. If this is not true, it is likely that the age of mice examined has passed the transient time

window of dysfunctional inhibitory neurons (P18-P21)[24]. Therefore, it will require evaluation of the effect of the mutation at multiple time points during development and the underlying mechanism of this compensatory plasticity mechanism. In addition, it will also be interesting to examine the excitability of somatostatin (SST)- and VIP (vasointestinal peptide)-expressing neurons as they are also two major interneurons in hippocampus[19].

How does altered excitability of hippocampal interneurons affect the neural circuitry in the *Scn1a* mutant mice? There are common circuit motifs of inhibition within hippocampus: feedforward and feedback inhibition[25]. Different types of interneurons have distinct roles in these motifs that modulate the neural network activity. Studies in the mouse cortex have revealed the logic of connections in distinct interneurons. Vasointestinal peptide (VIP)-expressing interneurons preferentially inhibit somatostatin (SST)-expressing interneuron that target the distal dendrites of pyramidal neurons, SST interneurons also inhibit other types of interneurons, and PV and SST neurons make monosynaptic inhibitory connection to a pyramidal neuron[26,27]. We hope to understand whether the K1270T mutation that alters the excitability of inhibitory neurons will rewire the network by changing the connectivity between interneurons and pyramidal neurons, giving rise to a hyperactive network.

Figure V.2. Unaltered excitability of hippocampal pyramidal cells in *SCN1A*$^{KT/+}$ mice. (A) Representative traces of evoked action potentials at different current injection steps in hippocampal pyramidal cells in WT vs *SCN1A*$^{KT/+}$. (B) The input-output curve of evoked action potentials. (C) Action potential threshold. (D) Action potential amplitude. (E) Action potential half-width. (F) Rheobase of evoked action potential defined as the current step when action potentials first appeared. Data reported as mean ± s.e.m with total 10-12 neurons from 6 mice in each group. Two-way ANOVA with repeated measures for B, two-tailed unpaired *t*-test for C-F.

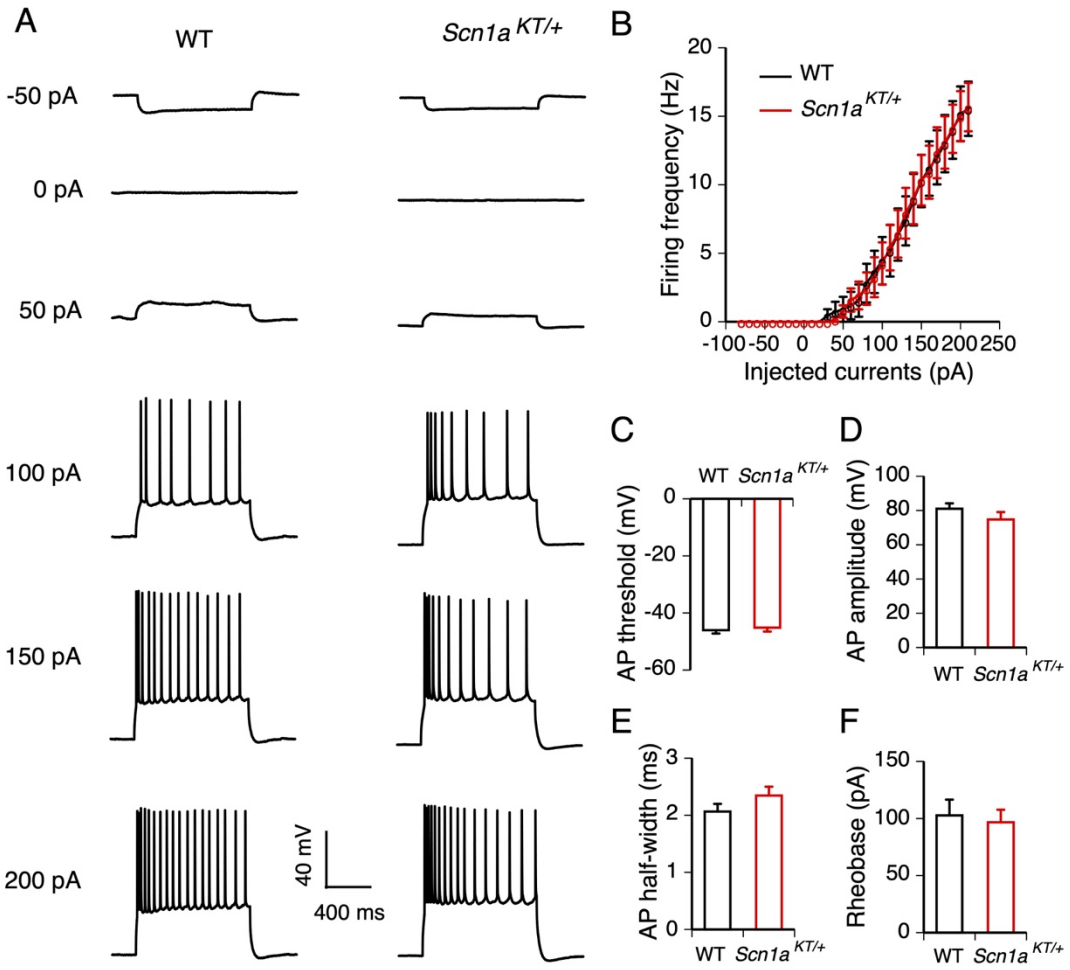

Table V.1. Passive membrane properties of pyramidal neurons

Cell type	Genotype	R_m (MΩ)	C_m (pF)	RMP (mV)
Pyramidal	WT	48.9 ± 11	34.1 ± 5.2	-66.1 ± 1.0
	Scn1a$^{KT/+}$	51.8 ± 9	32.4 ± 4.1	-65.7 ± 0.8

a. Data reported as mean ± s.e.m with total 10-12 neurons from 6 mice in each group.
b. Two-tailed Mann-Whitney U test for C_m and unpaired *t*-test for R_m and RMP.

5.3 Significance

We developed reproducible and efficient protocols that generate neuronal cultures that contain excitatory and inhibitory neurons from human iPSCs. The derived neurons are capable of firing action potentials and forming functional synaptic connections. This allows for identification of mutation-associated alterations in electrophysiological properties for neurological disease modeling.

We used CRISPR/Cas9 editing to generate dual isogenic pairs. This strategy facilitates elucidating the causality of a genetic mutation to disease phenotypes in neurological disorders. Further, it provides insight into the development of patient-specific medicine.

5.4 Bibliography

1. Abou-Khalil, B. *et al.* Partial and generalized epilepsy with febrile seizures plus and a novel SCN1A mutation. *Neurology* **57**, 2265–2272 (2001).
2. Kearney, J. A. *et al.* Severe epilepsy resulting from genetic interaction between Scn2a and Kcnq2. *Hum. Mol. Genet.* **15**, 1043–1048 (2006).
3. Singh, N. A. *et al.* A role of SCN9A in human epilepsies, as a cause of febrile seizures and as a potential modifier of Dravet syndrome. *PLoS Genet.* **5**, e1000649 (2009).
4. Hawkins, N. A., Zachwieja, N. J., Miller, A. R., Anderson, L. L. & Kearney, J. A. Fine Mapping of a Dravet Syndrome Modifier Locus on Mouse Chromosome 5 and Candidate Gene Analysis by RNA-Seq. *PLOS Genet.* **12**, e1006398 (2016).
5. Kearney, J. A. Genetic modifiers of neurological disease. *Curr. Opin. Genet. Dev.* **21**, 349–353 (2011).
6. Bergren, S. K., Rutter, E. D. & Kearney, J. A. Fine mapping of an epilepsy modifier gene on mouse Chromosome 19. *Mamm. Genome* **20**, 359–366 (2009).
7. Lopez-Garcia, M. A. *et al.* Genetic polymorphisms associated with antiepileptic metabolism. *Front. Biosci. (Elite Ed).* **6**, 377–386 (2014).
8. Tidball, A. M. & Parent, J. M. Concise Review: Exciting Cells: Modeling Genetic Epilepsies with Patient-Derived Induced Pluripotent Stem Cells. *Stem Cells* **34**, 27–33 (2016).
9. Grainger, A. I. *et al.* In vitro Models for Seizure-Liability Testing Using Induced Pluripotent Stem Cells . *Frontiers in Neuroscience* **12**, 590 (2018).
10. Odawara, A., Saitoh, Y., Alhebshi, A. H., Gotoh, M. & Suzuki, I. Long-term

electrophysiological activity and pharmacological response of a human induced pluripotent stem cell-derived neuron and astrocyte co-culture. *Biochem. Biophys. Res. Commun.* **443**, 1176–1181 (2014).
11. Odawara, A., Katoh, H., Matsuda, N. & Suzuki, I. Physiological maturation and drug responses of human induced pluripotent stem cell-derived cortical neuronal networks in long-term culture. *Sci. Rep.* **6**, 26181 (2016).
12. Odawara, A., Katoh, H., Matsuda, N. & Suzuki, I. Induction of long-term potentiation and depression phenomena in human induced pluripotent stem cell-derived cortical neurons. *Biochem. Biophys. Res. Commun.* **469**, 856–862 (2016).
13. Odawara, A., Matsuda, N., Ishibashi, Y., Yokoi, R. & Suzuki, I. Toxicological evaluation of convulsant and anticonvulsant drugs in human induced pluripotent stem cell-derived cortical neuronal networks using an MEA system. *Sci. Rep.* **8**, 10416 (2018).
14. Kaplan, J. S., Stella, N., Catterall, W. A. & Westenbroek, R. E. Cannabidiol attenuates seizures and social deficits in a mouse model of Dravet syndrome. *Proc. Natl. Acad. Sci. U. S. A.* **114**, 11229–11234 (2017).
15. Borowicz, K. K., Sekowski, A., Drelewska, E. & Czuczwar, S. J. Riluzole enhances the anti-seizure action of conventional antiepileptic drugs against pentetrazole-induced convulsions in mice. *Pol. J. Pharmacol.* **56**, 187–193 (2004).
16. Sun, L. *et al.* A knock-in model of human epilepsy in Drosophila reveals a novel cellular mechanism associated with heat-induced seizure. *The Journal of neuroscience : the official journal of the Society for Neuroscience* **32**, 14145–14155 (2012).
17. Yang, Y. *et al.* Nav1.7-A1632G Mutation from a Family with Inherited Erythromelalgia: Enhanced Firing of Dorsal Root Ganglia Neurons Evoked by Thermal Stimuli. *J. Neurosci.* **36**, 7511 LP – 7522 (2016).
18. Yang, Y. *et al.* Reverse pharmacogenomics: carbamazepine normalizes activation and attenuates thermal hyperexcitability of sensory neurons due to Nav1.7 mutation I234T. *Br. J. Pharmacol.* **175**, 2261–2271 (2018).
19. Tricoire, L. *et al.* A blueprint for the spatiotemporal origins of mouse hippocampal interneuron diversity. *J. Neurosci.* **31**, 10948–10970 (2011).
20. Cembrowski, M. S. & Spruston, N. Heterogeneity within classical cell types is the rule: lessons from hippocampal pyramidal neurons. *Nat. Rev. Neurosci.* **20**, 193–204 (2019).
21. Farrell, J. S., Nguyen, Q.-A. & Soltesz, I. Resolving the Micro-Macro Disconnect to Address Core Features of Seizure Networks. *Neuron* **101**, 1016–1028 (2019).
22. Yu, F. H. *et al.* Reduced sodium current in GABAergic interneurons in a mouse model of severe myoclonic epilepsy in infancy. *Nat. Neurosci.* **9**, 1142–1149 (2006).
23. Hedrich, U. B. S. *et al.* Impaired action potential initiation in GABAergic interneurons causes hyperexcitable networks in an epileptic mouse model carrying a human Na(V)1.1 mutation. *J. Neurosci.* **34**, 14874–14889 (2014).
24. Favero, M., Sotuyo, N. P., Lopez, E., Kearney, J. A. & Goldberg, E. M. A Transient Developmental Window of Fast-Spiking Interneuron Dysfunction in a Mouse Model of Dravet Syndrome. *J. Neurosci.* **38**, 7912–7927 (2018).
25. Pelkey, K. A. *et al.* Hippocampal GABAergic Inhibitory Interneurons. *Physiol. Rev.* **97**, 1619–1747 (2017).
26. Lee, S., Kruglikov, I., Huang, Z. J., Fishell, G. & Rudy, B. A disinhibitory circuit mediates

motor integration in the somatosensory cortex. *Nat. Neurosci.* **16**, 1662 (2013).
27. Pfeffer, C. K., Xue, M., He, M., Huang, Z. J. & Scanziani, M. Inhibition of inhibition in visual cortex: the logic of connections between molecularly distinct interneurons. *Nat. Neurosci.* **16**, 1068 (2013).